PL-TR-93-2192

INVESTIGATION OF LATERAL VARIATION IN THE SEISMIC VELOCITY STRUCTURE OF THE SHALLOW CRUST BENEATH EASTERN MASSACHUSETTS AND SOUTHERN NEW HAMPSHIRE

Susan E. D'Annolfo
Alan L. Kafka

Weston Observatory
Department of Geology and Geophysics
Boston College
Weston, MA 02193

30 September 1993

Scientific Report No. 2

Approved for public release; distribution unlimited

PHILLIPS LABORATORY
Directorate of Geophysics
AIR FORCE MATERIEL COMMAND
HANSCOM AIR FORCE BASE, MA 01731-3010

The views and conclusions contained in this document are those of the authors and should not be interpreted as representing the official policies, either expressed or implied, of the Air Force or the U.S. Government.

This technical report has been reviewed and is approved for publication.

JAMES F. LEWKOWICZ
Contract Manager
Solid Earth Geophysics Branch
Earth Sciences Division

JAMES F. LEWKOWICZ
Branch Chief
Solid Earth Geophysics Branch
Earth Sciences Division

DONALD H. ECKHARDT, Director
Earth Sciences Division

This document has been reviewed by the ESD Public Affairs Office (PA) and is releasable to the National Technical Information Service (NTIS).

Qualified requestors may obtain additional copies from the Defense Technical Information Center. All others should apply to the National Technical Information Service.

If your address has changed, or if you wish to be removed from the mailing list, or if the addressee is no longer employed by your organization, please notify PL/IMA, 29 Randolph Road, Hanscom AFB MA 01731-3010. This will assist us in maintaining a current mailing list.

Do not return copies of this report unless contractual obligations or notices on a specific document require that it be returned.

REPORT DOCUMENTATION PAGE

Form Approved
OMB No 0704-0188

1. AGENCY USE ONLY (Leave blank)	2. REPORT DATE	3. REPORT TYPE AND DATES COVERED
	30 September 1993	Scientific No. 2

4. TITLE AND SUBTITLE

Investigation of Lateral Variation in the Seismic Velocity Structure of the Shallow Crust Beneath Eastern Massachusetts and Southern New Hampshire

5. FUNDING NUMBERS

PE 62101F

PR 7600 TA 09 WU AL

Contract F19628-90-K-0035

6. AUTHOR(S)

S.E. D'Annolfo and A.L. Kafka

7. PERFORMING ORGANIZATION NAME(S) AND ADDRESS(ES)

Weston Observatory
Department of Geology and Geophysics
Boston College
Weston, MA 02193

8. PERFORMING ORGANIZATION REPORT NUMBER

9. SPONSORING / MONITORING AGENCY NAME(S) AND ADDRESS(ES)

Phillips Laboratory
29 Randolph Rd.
Hanscom AFB, MA 01731-3010
Contract Manager: James Lewkowicz/GPEH

10. SPONSORING / MONITORING AGENCY REPORT NUMBER

PL-TR-93-2192

11. SUPPLEMENTARY NOTES

12a. DISTRIBUTION / AVAILABILITY STATEMENT

Approved for public release; distribution unlimited

12b. DISTRIBUTION CODE

13 ABSTRACT *(Maximum 200 words)*

This is one of five scientific reports describing specific research projects conducted at Weston Observatory under Contract No. F19628-90-K-0035. The research conducted under this contract covers a range of topics related to seismology in general and to nuclear test monitoring in particular. This report describes a study in which group velocity dispersion was determined for short-period Rayleigh waves recorded from blasts detonated at the San-Vel quarry in Littleton, MA. Field data were recorded to complement network data in order to create a denser distribution of stations than was possible in past experiments. Group velocity dispersion was estimated for each path. The resulting dispersion curves were analyzed to investigate the relationship between group velocities and shallow crustal structure beneath eastern MA and southern NH. Our results suggest that the quarry lies in a "trough" of low group velocities, where the group velocities systematically increase toward the E and W-NW directions. This creates a "valley" of group velocities where the primary trend of the valley trough is N, and a secondary feature is a trough that trends in a NE direction. This NE trending feature is of particular interest because of a possible correlation with the trend of the Clinton-Newbury fault zone.

14 SUBJECT TERMS	15. NUMBER OF PAGES
Shallow crustal structure, Rg wave dispersion, quarry blasts, chemical explosions	104
	16. PRICE CODE

17. SECURITY CLASSIFICATION OF REPORT	18. SECURITY CLASSIFICATION OF THIS PAGE	19. SECURITY CLASSIFICATION OF ABSTRACT	20. LIMITATION OF ABSTRACT
Unclassified	Unclassified	Unclassified	SAR

CONTENTS

PREFACE

This is one of five scientific reports describing specific research projects conducted at Weston Observatory under Contract No. F19628-90-K-0035. The research conducted under this contract covers a range of topics related to seismology in general and to nuclear test monitoring in particular.

This scientific report consists of an M.S. thesis written by Susan E. D'Annolfo under the supervision of Professor Alan L. Kafka. In this study, group velocity dispersion was determined for Rayleigh waves between periods of 0.2 and 2.2 sec (Rg) recorded from blasts detonated at the San-Vel quarry in Littleton, MA. Field data were recorded to complement network data in order to create a denser distribution of stations than was possible in past experiments. Rg wave dispersion was estimated for each path. The resulting dispersion curves were analyzed to investigate the relationship between Rg wave velocities and the shallow crustal structure beneath eastern Massachusetts and southern New Hampshire.

The results of this study suggest that there is a systematic lateral variation in the structure of the shallow crust underlying eastern Massachusetts and southern New Hampshire. Lateral variation in group velocities within this area appear to depend on distance from the San-Vel quarry. Three dimensional plots of the group velocity data reveal that the San-Vel quarry appears to lie in a "trough" of particularly low group velocities, where the group velocities systematically increase toward the east and west-northwest directions. This creates a "U-shaped valley" of group velocities where the primary trend of the valley trough trends in a north-south direction, and a secondary feature is a "valley" that trends in a northeast direction. This northeast trending featureis of particular interest because of a possible correlation with the structural geology of the area, particulary the trend of the Clinton-Newbury fault zone, which forms the boundary between the Merrimack trough and the Putnam-Nashoba terrane.

INVESTIGATION OF LATERAL VARIATION IN THE SEISMIC VELOCITY STRUCTURE OF THE SHALLOW CRUST BENEATH EASTERN MASSACHUSETTS AND SOUTHERN NEW HAMPSHIRE

1. INTRODUCTION

1.1 Background and Purpose of this Study

Studies of shallow crustal structure using Rg wave dispersion have shown that the dispersion patterns in Southern New England (SNE) exhibit differences in group velocity from one area to the next (e.g. Kafka and Dollin, 1985; Kafka, 1988). Rg is a short period fundamental mode Rayleigh wave, and the dispersive properties of Rg waves are sensitive to variations in the seismic velocity structure of the shallow crust. Based on observed differences in Rg dispersion, Kafka and Skehan (1990) divided SNE into five regions of distinct Rg dispersion characteristics that they called "dispersion regions." The most clearly distinct dispersion region in SNE is the northern portion of the Hartford Rift Basin (Figure 1), where Rg group velocities are distinctly lower than they are in other parts of SNE (presumably due to the abundance of sediments and sedimentary rock in that area). On the other hand, systematic lateral variations of Rg group velocities have not been clearly delineated in crystalline basement provinces. One crystalline basement province that was thought to be characterized by distinctly higher Rg group velocities was southwestern Connecticut (Kafka & Dollin, 1985). In a more recent study however, Kafka and Bowers (1991) have shown that southwestern Connecticut is actually characterized by Rg group velocities quite similar to those of other areas where the crystalline basement rocks are at or near the surface. Thus the question remains: "What is the pattern of lateral variation of shallow crustal structure in the crystalline basement rock underlying SNE?"

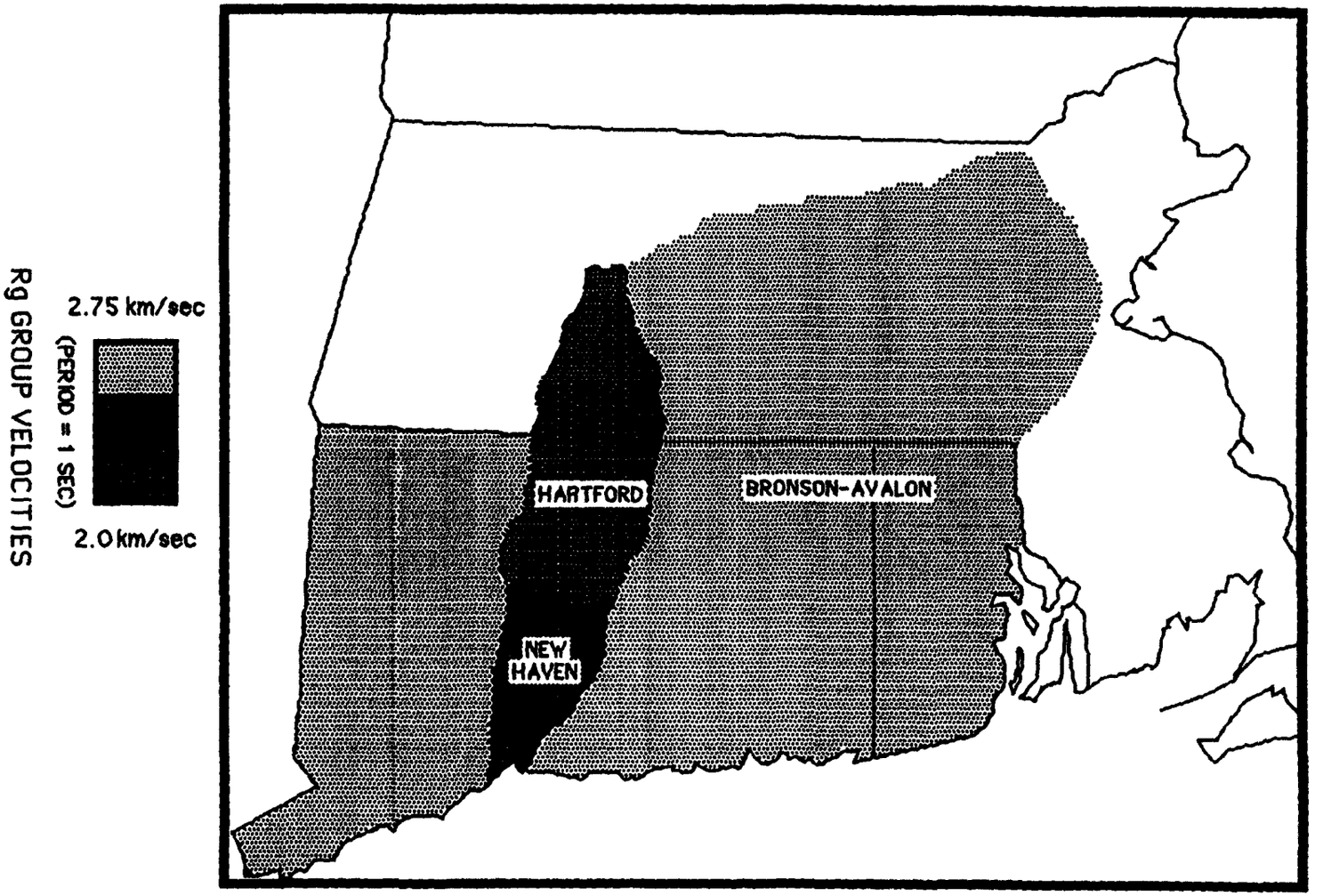

Figure 1: Map of Rg dispersion regions in Southern New England. (after Kafka and Skehan, 1990)

The Rg dispersion pattern in the rather large area that extends from the Bronson Hill Anticlinorium to the Avalonian Terrane (Figure 2) displays very little variation in group velocities. This observation suggests that the shallow crust underlying this area is laterally homogeneous (at least at the scale of features revealed by previous Rg dispersion studies).

Because of that lack of observed lateral variation, Kafka and Skehan (1990) characterized that entire area as an Rg dispersion region, which they called the Bronson Avalon Dispersion Region (BADR). Since the BADR includes a wide range of geological structures and rock types, it is surprising that this region appears to be so homogeneous. The Rg dispersion pattern seems to ignore the transition from one geological feature to the next. In contrast, there is at least one other area of New England (southeastern Maine) where significant differences in Rg dispersion have been observed that appear to correlate with the geology of the crystalline basement structures. Kafka and Reiter (1987) found evidence for lateral anisotropy in the shallow crust of southeastern Maine, where the trend of the anisotropy is parallel to the structural grain of the Appalachians. Thus the question arises: Does the seismic velocity structure of the shallow crust beneath the so called BADR really have no systematic relationship to the surface mapped geology? Alternatively, does the relationship between the surface geology and shallow crustal structure exist at a scale that is too small to be seen by the distribution of paths described in the above mentioned studies?

During the summer of 1987 an experiment was performed where portable seismic stations were set up around the San-Vel/Lonestar Quarry in Littleton, MA. Since the stations were densely distributed and the distances between source and receiver varied from a few kilometers to 71 km (Figure 3), this experiment provided an opportunity to investigate the pattern of Rg dispersion within the BADR in greater detail than previously possible. Figure 4 shows group velocities measured from six seismograms recorded during the 1987 experiment. In spite of this denser station coverage, there is still very little variation in the group

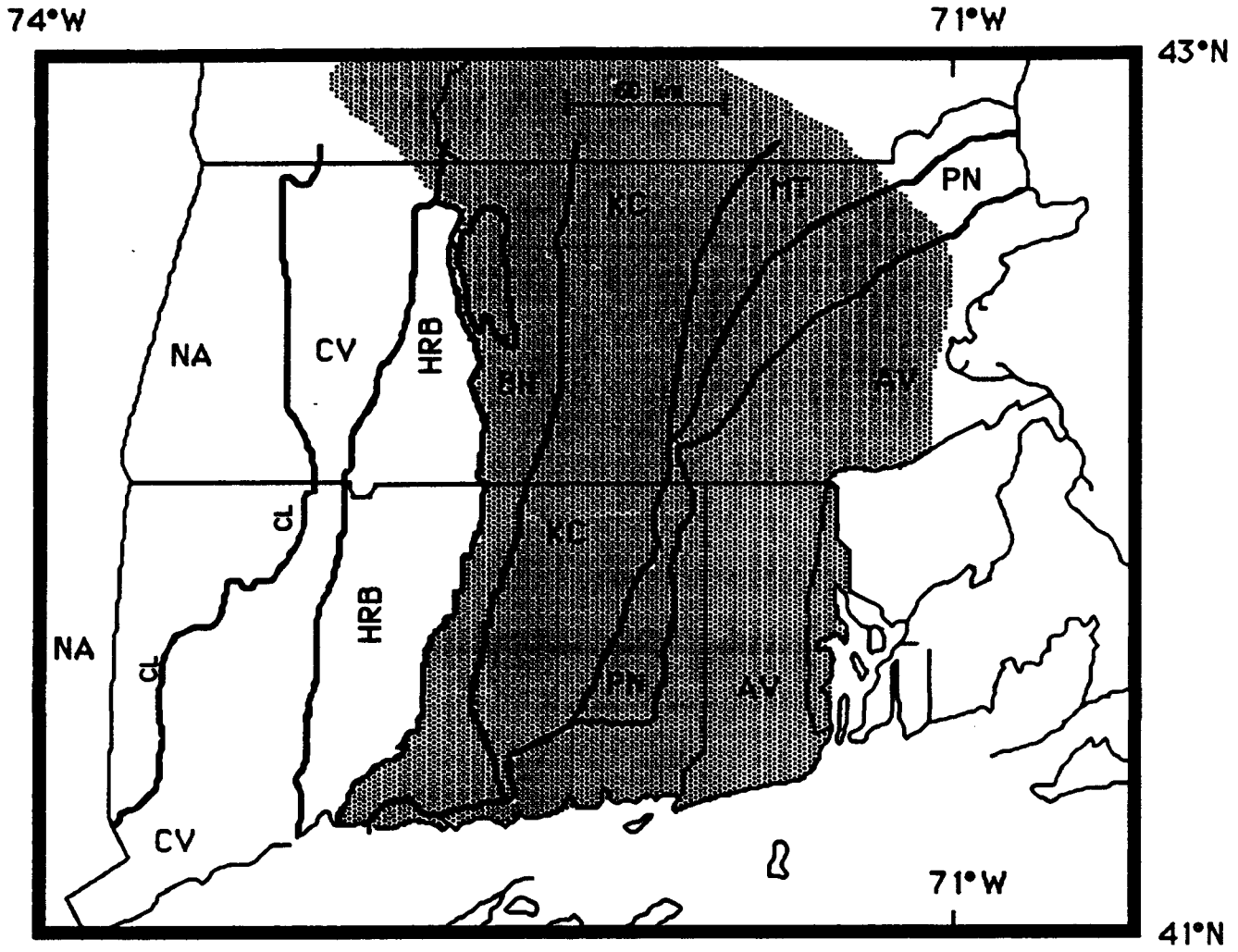

Figure 2: Map of tectonic regions in Southern New England, with the BADR shaded. (after Kafka and Skehan, 1990)

velocities. This is surprising considering that the propagation paths traverse geologically diverse areas.

It is possible that systematic velocity variations actually do exist within the BADR but are not evident because the seismic waves that have been observed there have propagated across relatively large distances. Source-to-receiver distances in previous studies have ranged from a little less than 25 km to over 100 km, and when an Rg wave travels a great distance it travels with a group velocity that reflects an average of the different types of materials it encounters.

For my thesis research, I investigated the details of lateral variations in seismic velocity structure of the shallow crust beneath eastern MA and southern NH in greater detail than has been done in the past by utilizing field data to obtain a denser station spacing. The object of this experiment is twofold: 1) to obtain paths of shorter length; and 2) to have a more dense distribution of paths. The purpose of this investigation is to determine whether or not the lack of observed variation of Rg dispersion in SNE is an artifact of the relatively sparse distribution of paths.

In this study, the following two alternative hypotheses regarding the extent of lateral variations in seismic velocity structure of the shallow crust beneath eastern MA and southern NH were tested:

(1) The crystalline basement rock underlying eastern MA and southern NH actually is homogeneous at the scale of features differentiated by Rg waves, even with the addition of the field stations.

(2) Lateral variations exist within the shallow crust underlying eastern MA and southern NH, but they exist on a scale that is too small to have been revealed by previous studies.

As will be discussed below, the results of this study suggest that there does in fact appear to be smaller scale lateral variation in the shallow crust beneath the area surrounding the San-Vel quarry.

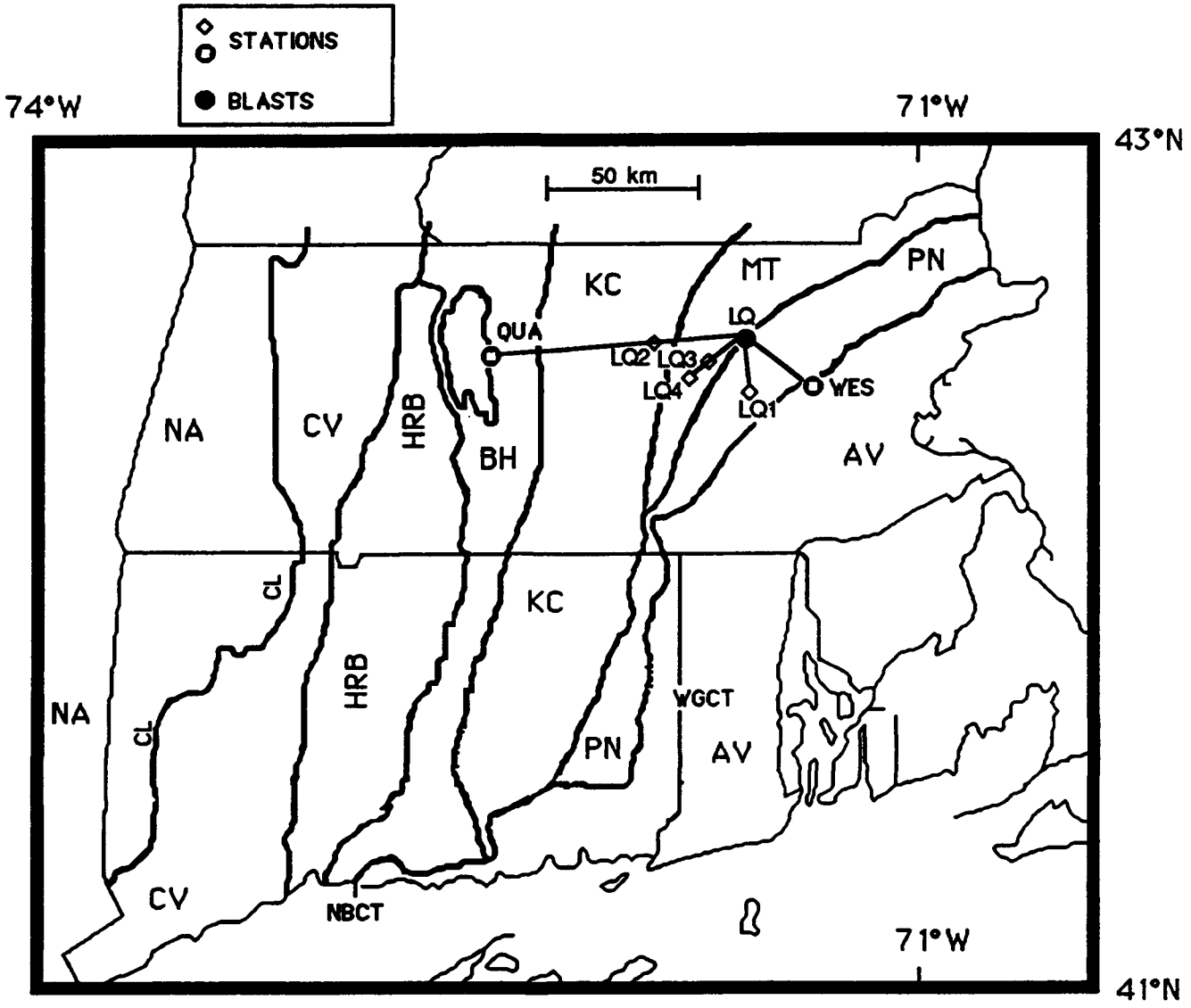

NA = Proto-North American Terrane
CV = Connecticut Valley Synclinorium
CL = Cameron's Line
HRB = Hartford Rift Basin
BH = Bronson Hill Anticlinorium
KC = Kearsarge-Central ME Synclinorium
MT = Merrimack Trough
PN = Putnam-Nashoba Terrane
AV = Avalonian Superterrane

Figure 3: Tectonic map of Southern New England showing the sites of the 1987 Littleton Quarry Blast Experiment.

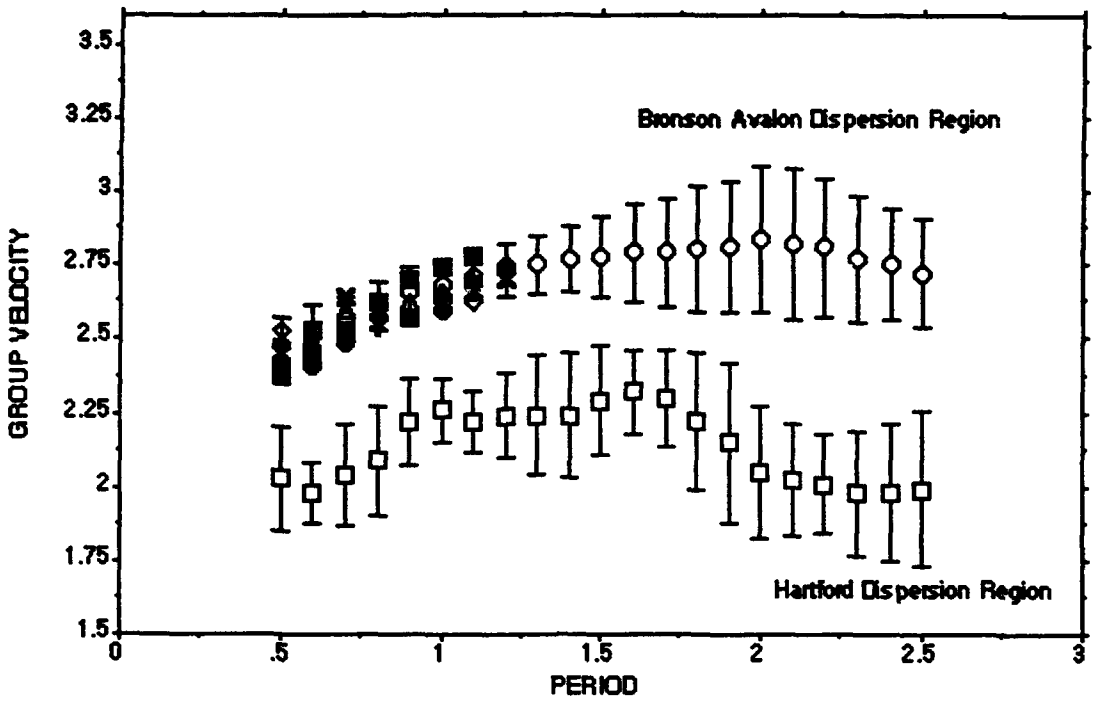

Figure 4: Average and standard deviation for paths in the BADR and HDR. Also shown are the results from the 1987 LQBE.

1.2 Data Acquisition

For this research, analysis was done on the group velocity dispersion of Rg waves recorded from quarry blasts detonated at the San-Vel/Lonestar Quarry in Littleton, MA in order to investigate the extent of lateral variation in the shallow crust beneath the area surrounding that quarry. There are many seismograms of quarry blasts and shallow focus earthquakes in the New England area that have been recorded digitally by the New England Seismic Network (NESN) operated by Weston Observatory. The Earth Resources Laboratory at the Massachusetts Institute of Technology (MIT) also operates a regional network that records seismic events in this region. Data from both of these networks were used for this study. Both networks record clear signals and prominent Rg waveforms from the San-Vel quarry. Data from several field experiments performed by the Air Force Geophysics Laboratory (AFGL) at Hanscom AFB, that were part of the 1987 field study described above are also included in this study. In addition, portable seismic stations were installed in the field to investigate whether or not a denser station spacing would reveal any lateral variations in seismic velocity structure that have yet been observed in previous studies.

As part of this study, a field experiment was designed in which portable field stations were set up to follow a straight line path that extended from the San-Vel Quarry out in a northwest direction to New Ipswich, NH. The path was approximately 35 km long. Eleven receiver stations were set up. The object was to locate the stations at intervals ranging from 2 km to 4 km along the line. Most of the stations were located on private property where permission was granted from the owners. A few of the sites fell on state or city owned property. Permission was also obtained from the proper authorities to utilize those areas. Sites were numbered in a series labeled NW01 through NW11 to delineate the line direction and station number. Of the eleven original field sites, only one (NW09) was abandoned because it was too difficult to access on short notice. Equipment was deployed at the remaining ten sites once per week during the months of July and the beginning of August, 1989. Because of technical

failures and human error, data recovery for the experiment was approximately 65% successful for the five blasts undertaken to record.

There was an attempt to include in this study a second and third line of field stations that extended out in a northeast and a southeast direction. However, time only allowed me to record a small part of the northeast line once before all of the field equipment became unavailable for the remainder of the season. Figure 5 is a map showing all of the paths used for this study and their proximity to the San-Vel Quarry (located at 42.554°N and 71.517°W). Figure 6 is a diagram of the quarry pit which encompasses approximately one square kilometer of land. Because different faces of the pit are mined at different times, an average location was chosen at the center of the quarry pit to represent the geographic location of the quarry. This means that the location of any particular blast could at worst be off by one half of a kilometer. Table 1 lists all of the stations by name with their geographical coordinates and distances from the quarry.

1.3 Seismic Sources

Quarry blasts detonated at the San-Vel Quarry were chosen to be the primary seismic sources for this research for several reasons: 1) the quarry operator was extremely cooperative and worked closely with me on the experiment, enabling me to pinpoint source location and quite accurately determine event origin times; 2) blasts from the quarry are often large and generate prominent Rg waveforms; 3) there are two to three quarry blasts per week at this quarry during summer months; and 4) there was a source of AFGL data from this quarry from the 1987 experiment that augmented this data set quite well and had not been analyzed yet.

1.4 Instrumentation

The NESN stations operated by Weston Observatory consist of 1 Hz HS-10 vertical component sensors, and the MIT network stations consist of 1 Hz Mark Products L-4C vertical component sensors. Data are telemetered to Weston and MIT by telephone line and are recorded

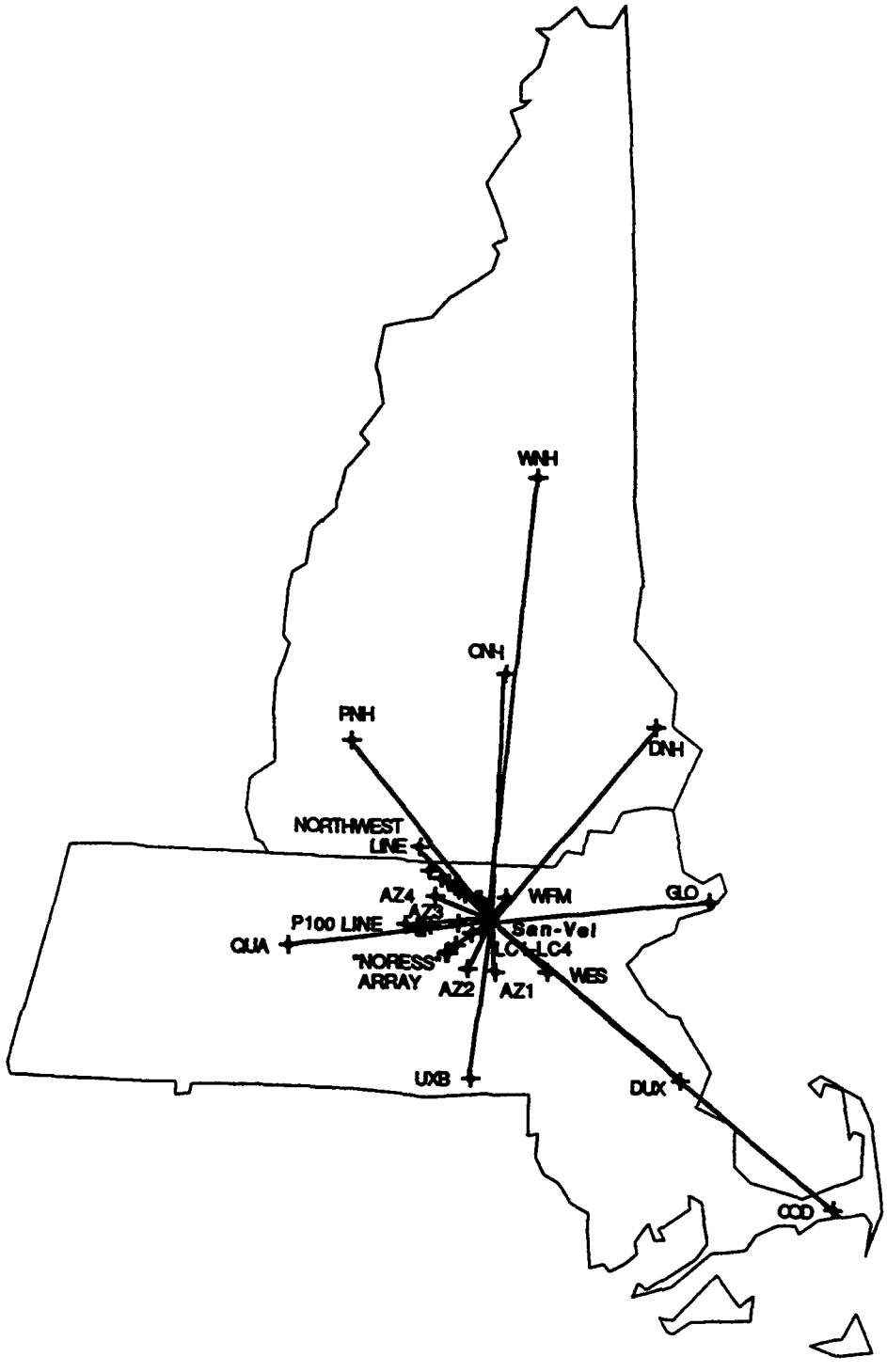

Figure 5: Map of station locations and paths used in this study.

Figure 6: Map of San-Vel Quarry mining pit. The star in the center of the map delineates the geographic location of the quarry used for data processing as described in the text.

Table 1

Station	Lat	Lon	Dist (km)	Affiliation
NW01	42.5790	-71.5800	5.9	FIELD 1989
NW02	42.5940	-71.5960	7.9	FIELD 1989
NW03	42.5950	-71.6110	9.0	FIELD 1989
NW04	42.6155	-71.6630	13.8	FIELD 1989
NW05	42.6240	-71.6830	15.7	FIELD 1989
NW06	42.6360	-71.7010	17.6	FIELD 1989
NW07	42.6520	-71.7250	20.3	FIELD 1989
NW08	42.6610	-71.7540	22.8	FIELD 1989
NW10	42.6880	-71.8880	33.9	FIELD 1989
NW11	42.7550	-71.8500	35.3	FIELD 1989
WES	42.3847	-71.3221	25.0	BC NETWORK
QUA	42.4566	-72.3738	71.0	BC NETWORK
WFM	42.6106	-71.4906	6.7	MIT NETWORK
ONH	43.2792	-71.5056	80.6	MIT NETWORK
PNH	43.0942	-72.1358	78.5	MIT NETWORK
WNH	43.8683	-71.3997	146.3	MIT NETWORK
DNH	43.1225	-70.8948	81.1	MIT NETWORK
GLO	42.6403	-70.7272	65.5	MIT NETWORK
UXB	42.0614	-71.6773	56.3	MIT NETWORK
DUX	42.0686	-70.7678	82.0	MIT NETWORK
COD	41.6858	-70.1350	149.5	MIT NETWORK
AZ1	42.3864	-71.5311	18.4	BC/MIT 1987
AZ2	42.3937	-71.6467	20.4	BC/MIT 1987
AZ3	42.5156	-71.8221	25.1	BC/MIT 1987
AZ4	42.6079	-71.7821	22.4	BC/MIT 1987
LC1	42.5312	-71.5571	3.8	BC/MIT 1987
LC2	42.5071	-71.5910	7.7	BC/MIT 1987
LC3	42.4962	-71.6267	10.7	BC/MIT 1987
LC4	42.4603	-71.6935	17.5	BC/MIT 1987
P102	42.5400	-71.5660	4.0	AFGL 1987,88
P103	42.5360	-71.5880	5.9	AFGL 1987,88
P107	42.5300	-71.6900	14.0	AFGL 1987
P110	42.5200	-71.8000	23.1	AFGL 1987
P112	42.5145	-71.8396	26.9	AFGL 1987
P113	42.5121	-71.8546	27.8	AFGL 1987
P115	42.5187	-71.9054	31.9	AFGL 1987
P201	42.5480	-71.5390	1.5	AFGL 1988
P202	42.5450	-71.5460	2.1	AFGL 1988
P203	42.5440	-71.5550	2.9	AFGL 1988
P206	42.5310	-71.5980	6.6	AFGL 1988
NSA0	42.4400	-71.7270	21.5	AFWL 1987
NSA1	42.4390	-71.7280	21.6	AFWL 1987
NSA2	42.4400	-71.7240	21.3	AFWL 1987
NSA3	42.4410	-71.7280	21.5	AFWL 1987
NSB1	42.4400	-71.7290	21.6	AFGL 1987
NSB2	42.4420	-71.7260	21.2	AFGL 1987
NSB3	42.4390	-71.7230	21.2	AFGL 1987
NSB4	42.4370	-71.7260	21.6	AFGL 1987
NSB5	42.4390	-71.7300	21.7	AFGL 1987

digitally at 50 samples per second (sps) at Weston and 100 sps at MIT, when a trigger condition is met.

Equipment for most of the field stations was supplied by the Air Force Geophysics Laboratory (AFGL) at Hanscom AFB, Bedford, MA. Each of these stations consisted of a 2 Hz, three component Sprengthenether S-6000 seismometer connected to a Terra-Technology DCS-302 digital recorder. Some of the field stations consisted of portable instruments from Weston Observatory. These stations consisted of a 2 Hz, three component Sprengthenether S-6000 seismometer connected to a Sprengthenether DR-200 digital recorder. All field recorder clocks were synchronized with a Kinemetrics satellite-synchronized clock both before deployment and upon return from the field in order to compensate for clock drift. The AFGL stations were also connected by radio antenna to WWVB.

Deployment of field stations consisted of burying the seismometer approximately one foot below the ground surface. The sensor was oriented so that the "Longitudinal" arrow pointed towards Magnetic North. The sensor was then leveled and connected to one of the digital recorders. A WWVB radio antenna was also connected to the recorder as a back-up time source. Care was taken to set up the same sensor and recorder pair at the same site and calibrations were made at each site. At the scheduled blast time, field recorders were switched on manually to record the event. Stations were manually run because most of them would either not automatically trigger on an event or else the site would be so "noisy" that too many false triggers would use up all of the tape. Also, blasting times tend to be too unpredictable to leave the recorders on trigger mode. Therefore after the recorders were turned on, the person monitoring the site would call the quarry scale house to confirm whether or not the blast had taken place.

1.5 Description of Data Set

The factors that affect the quality and success with which a seismic event is recorded are innumerable. To discuss every one of those factors in detail would stray from the focus of this thesis. However, on a most fundamental level, an investigation of this type requires that at least the following three criteria be satisfied for each seismogram: 1) accurate timing; 2) a relatively high signal-to-noise ratio; and 3) precise source and receiver locations. As straightforward as that may sound, obtaining all three of those criteria for a single seismogram can be somewhat of a challenge.

The original data set used to begin work consisted of approximately 110 seismograms that crossed about 49 different paths throughout the study area. Several paths that were part of the 1989 summer field experiment had to be eliminated immediately because of internal clock failures. For this type of investigation, data without accurate timing is useless. The remaining seismograms were plotted using a band-pass filter with a high-pass cutoff of 12.5 Hz and a low-pass cutoff of .01 Hz to filter out some of the background noise and also to enhance the event signal. At this point four more paths were eliminated because these (MIT) network stations did not adequately record the event. The reason for this could have been that the distance between source and receiver was too great, and/or that the signal-to-noise ratio was so low that the event could not be distinguished from background noise.

After analyzing the waveforms on the remaining seismograms, the data set was divided into the following four categories according to the quality of the Rg signals:

Category 1) Excellent quality. Seismogram has excellent Rg and P and/or S waveforms. High signal-to-noise ratio.

Category 2) Good quality. Seismogram has good Rg waveform, but may have a significant amount of background noise that interferes with the signal.

Category 3) Fair quality. Seismogram has average to poor waveform and a low signal-to-noise ratio.

Category 4) Poor quality. Seismogram has no apparent Rg wave. Other waveforms are of poor quality or nonexistent. Difficult to distinguish signal from background noise.

Table 2 is a list of all the data files and their corresponding categories. When processing for group velocity, it was found that those seismograms in category 4 did not yield useful measurements. Therefore, those paths were eliminated from the Rg dispersion analysis. What remained after all these inspections was a data set consisting of approximately 81 seismograms that trace 44 different paths within the study area. Of the 81 seismograms, 17 are quality 1; 22 are quality 2; 28 are quality 3; and 14 are quality 4 seismograms Figures 7 - 10 are examples of seismograms that are representative of their respective categories. The paths range in length from about 2 km to about 82 km. For a few of the paths there are more than one recording. In such cases an analysis was done on the multiple recordings separately. Multiple data was then averaged for a given path and examined that way as well. In the final analysis, it was elected to display the data as separate data files.

Table 2

Station	Category	Station	Category
LC1	2	87202-GLO	1
LC2	1	87210-ONH	3
LC3	1	87210-WFM	3
LC4	1	87210-WNH	4
AZ1	2	87210-DNH	3
AZ2	1	87210-GLO	1
AZ3	1	88089-ONH	4
AZ4	1	88089-PNH	3
NSA0	2	88089-WFM	2
NSA1	2	88089-DNH	3
NSA2	2	88089-GLO	2
NSA3	2	88089-UXB	2
NSB1	2	89177-ONH	4
NSB2	2	89177-PNH	4
NSB3	2	89177-WFM	3
NSB4	2	89177-DNH	2
NSB5	2	89177-GLO	1
P101	4	89192-ONH	4
P102	3	89192-PNH	2
P103	3	89192-WFM	2
P104	4	89192-DNH	3
P107	3	89192-GLO	3
P110	1	89192-NW01	1
P112	1	89192-NW02	3
P113	2	89192-NW06	2
P115	1	89192-NW10	1
QUA	1	89208-NW03	3
WES	1	89208-NW04	3
P201	4	89208-NW05	3
P202	4	89213-DNH	4
P203	4	89213-GLO	3
P204	4	89213-WFM	2
P205	3	89213-NW01	3
P206	3	89213-NW03	3
P301	4	89213-NW04	2
P304	3	89213-NW05	3
P305	3	89213-NW07	2
87202-ONH	4	89213-NW08	3
87202-PNH	3	89213-NW10	3
87202-WFM	1	89213-NW11	3
87202-DNH	3		

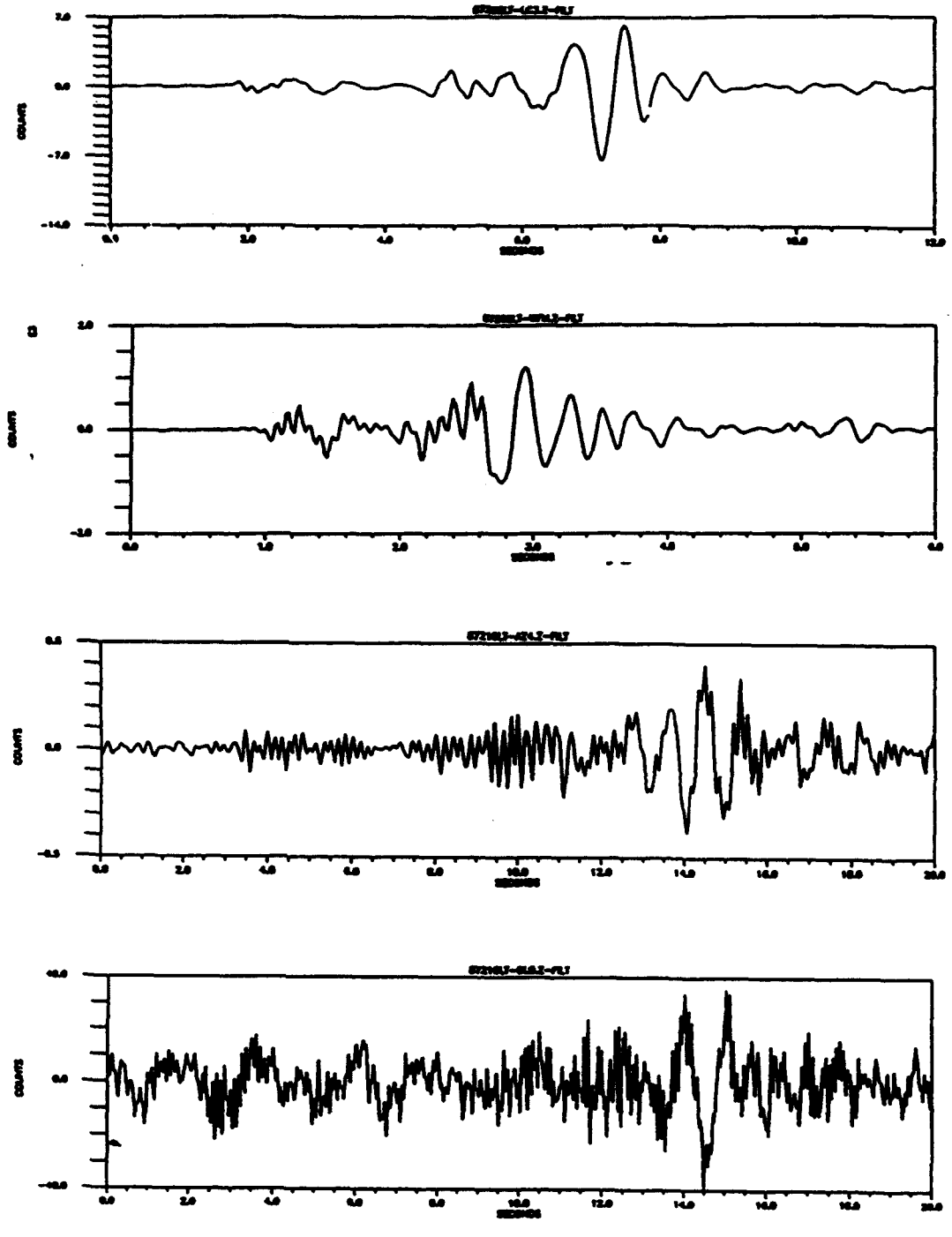

Figure 7 : Examples of quality 1 seismograms.

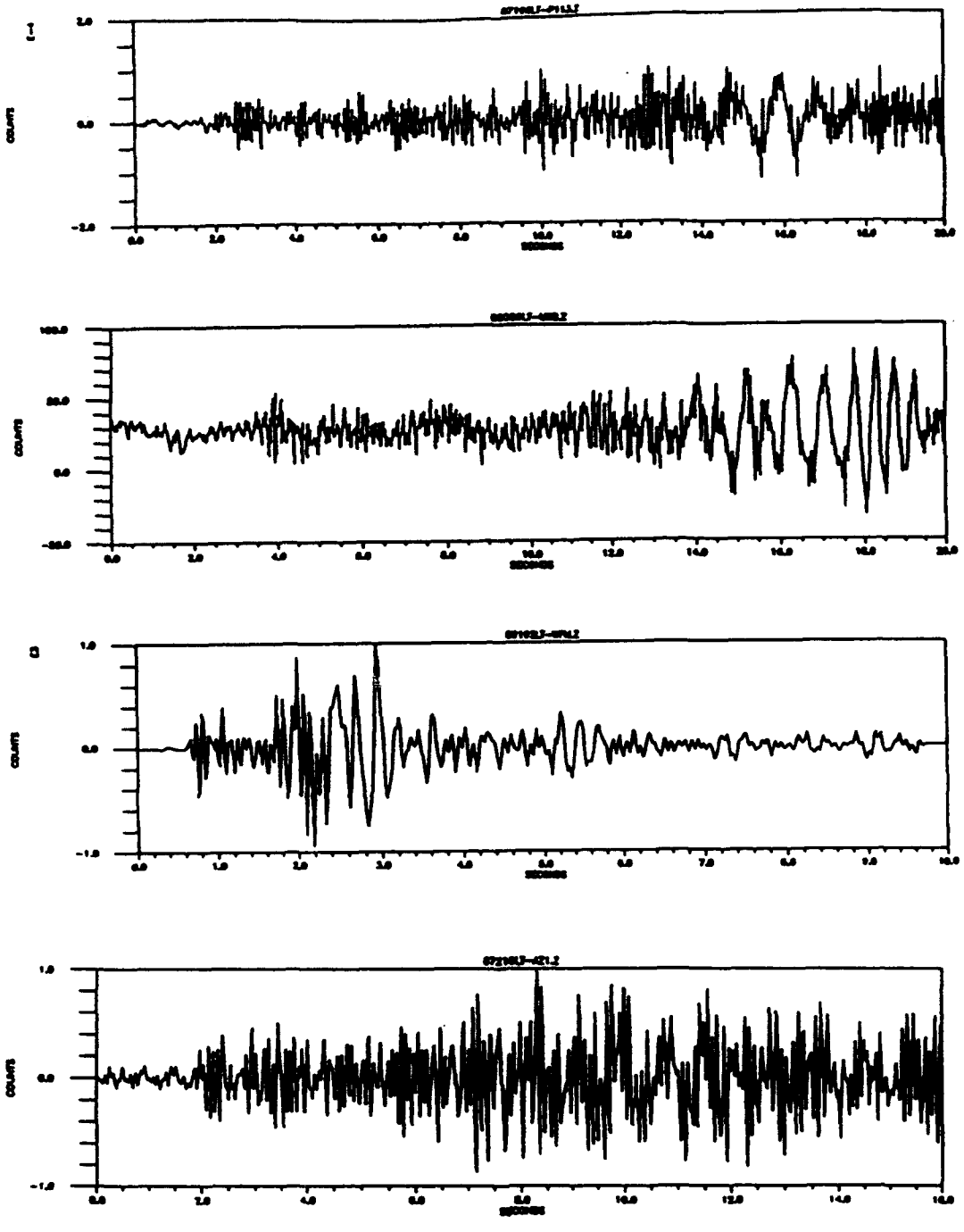

Figure 8 : Examples of quality 2 seismograms.

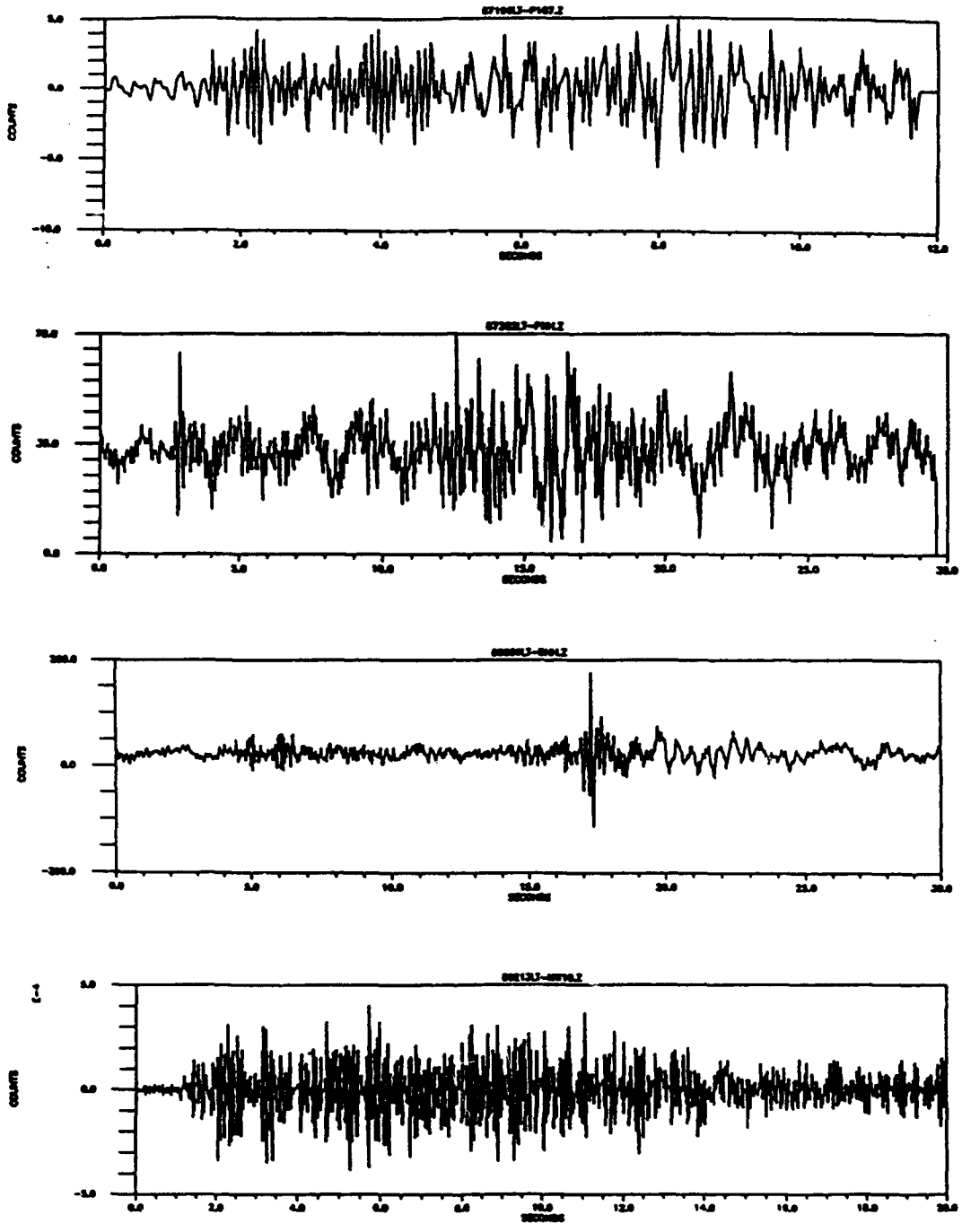

Figure 9 : Examples of quality 3 seismograms.

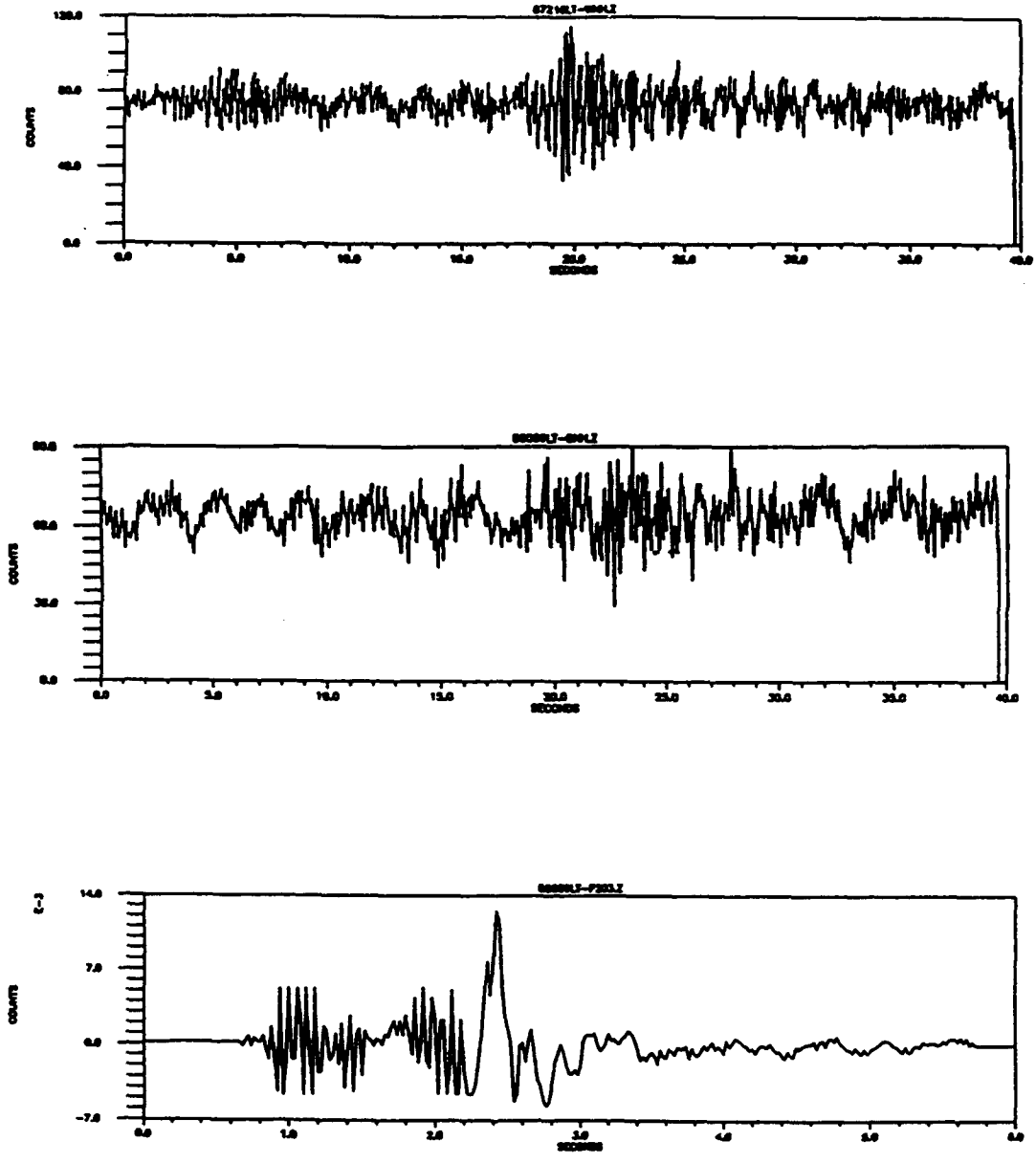

Figure 10 : Examples of quality 4 seismograms.

2. GEOLOGY AND CRUSTAL STRUCTURE OF SOUTHERN NEW ENGLAND

2.1 Geology of Southern New England

Skehan and Osberg (1979) described the Northern Appalachian Mountain Region as geologically complex and comprised of regions with distinct stratigraphy, structure and deformation. They suggested that this region is a series of "lithotectonic terranes" that have become sutured together as a result of geologic activity during the Middle Paleozoic through Mesozoic times. The terranes, which are believed to at one time have been separate and individual units, came together as a result of massive plate collisions. This created a "collage" of geologic subdivisions, each with distinct characteristics.

Figure 11 shows the terranes of SNE. They are from west to east: (1) the Proto-North American terrane (NA) which represents Late Proterozoic and Early Paleozoic rift and shelf sedimentary rocks deposited on Grenville basement; (2) the Connecticut Valley (CV) sequence of thrust slices separated from NA by Cameron's line (CL); (3) the Hartford Rift Basin (HRB) which consists of Mesozoic red bed sediments and basaltic igneous rocks covered by relatively thick Pleistocene glacial sediments; (4) the Bronson Hill (BH) Ordovician volcanic arc; (5) the Kearsarge-Central Maine Synclinorium (KC), dominantly Silurian-Devonian metasedimentary rocks intruded by Devonian plutons; (6) the Merrimac Trough (MT), metasedimentary rocks of uncertain age separated from adjacent terranes by faults ; (7) the Putnam-Nashoba terrane (PN) also bounded by faults and consisting in part of Late Proterozoic age rocks; and (8) the Avalonian terrane (AV), Late Proterozoic volcanic rocks with a cover of distinctive fossiliferous sedimentary rocks (Skehan and Kafka, 1990).

The Bronson Avalon Dispersion Region (BADR) encompasses several of these subdivisions in that it extends from the Bronson Hill Anticlinorium (BH) eastward to the Avalonian Terrane (AV). Within this area, the basement rocks are characterized by Late Precambrian gneisses and quartzose sedimentary rocks with layered gneisses and plutonic

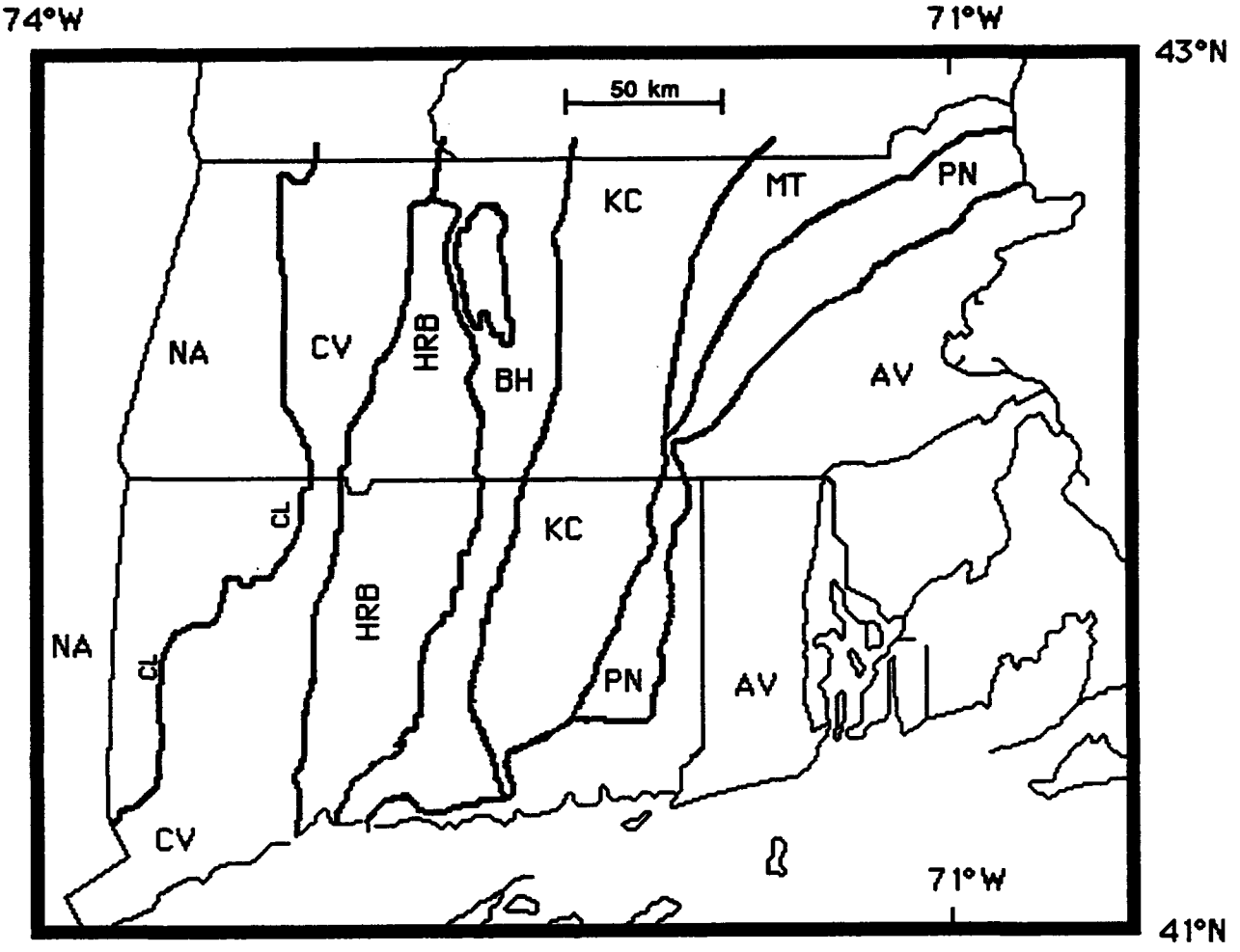

NA = Proto-North American Terrane
CV = Connecticut Valley Synclinorium
CL = Cameron's Line
HRB = Hartford Rift Basin
BH = Bronson Hill Anticlinorium
KC = Kearsarge-Central ME Synclinorium
MT = Merrimack Trough
PN = Putnam-Nashoba Terrane
AV = Avalonian Superterrane

Figure 11: Tectonic terranes of Southern New England. (from Kafka and Skehan, 1990)

gneisses that are partly Precambrian and partly Ordovician in age. Late Precambrian rocks are exposed in the cores of the Pelham dome, Clinton, Stony Creek, and Lyme domes and also in the Willimantic Dome of southeastern CT and the Milford Anticlinorium of eastern MA and RI (Hall and Robinson, 1982).

Middle Ordovician strata within the BADR lie directly on dome gneisses and consist mainly of sulfidic mica schist, although there are rocks of volcanic derivation including amphibolites and felsic gneisses that are interspersed with mica schists. The Middle Ordovician schists are mostly exposed east of the Bronson Hill Anticlinorium. Elsewhere the age of similar rocks is less certain. These rocks include metamorphosed mafic and felsic volcanics such as the Marlboro Formation in MA and the Quinebaug in CT that have been dated by Hill and others (1984) as in the range 550 to 450 million years old. The volcanics are in contrast with and possibly overlain by thick units of peltic schists and gneisses such as the Nashoba Formation in MA and the Tatnic Hill Formation in CT (Hall and Robinson, 1982).

Silurian rocks of the BADR consist of a quartz pebble type of conglomerate-quartzite called the Clough Quartzite. In northern MA this rock contains Llandovery fossils. The Fitch Formation that extends into northwestern NH also contains fossils. These fossils and the lens-like distribution of the rock suggest a marine or shoreline type depositional environment. Moving eastward, the Silurian rocks have been interpreted as thickening into a section of feldspathic calcareous granulite sulfidic schist (i.e. the Paxton Formation). The eastern limit of this Silurian basin exposure is along the Clinton-Newbury Fault in MA and the top of the Tatnic Hill Formation in CT (Hall and Robinson, 1982).

Devonian rocks in the BADR are mostly schist interlayered with quartzose marble. The western BADR is dominated by gabbro to granite plutons such as the Coys-Hill Cardigan Pluton, the Ashuelot Pluton, and parts of the Fitchburg Pluton. The eastern BADR rocks are predominantly gray-weathered graphite schists of the Littleton Formation (Hall and Robinson, 1982).

Carboniferous sedimentary rocks are exposed in three localities west of the Clinton-Newbury Fault in Central MA (Skehan, Rast, and Mosher 1986). Carboniferous to Permian plutons include the Pinewood Adamellite Pluton in southeastern CT, the Narragansett Pier Granite of RI, and the Milford Granite in southern NH (Hall and Robinson, 1982).

Within the BADR there are four structural subdivisions. They are from west to east: the Bronson Hill Anticlinorium, the Kearsarge-Central Maine Synclinorium, the Merrimack Trough, the Nashoba Terrane, and the Avalon Terrane. Within the synclinorium, the dominant structures are upright isoclinal folds, some of which have been deformed. Evidence of inverted rock sequences suggest that there has been some recumbent folding. The Bronson-Hill Anticlinorium is a complex structure distorted by domes and basins and is cut along the west margin by Late Paleozoic and Mesozoic faults (Skehan and Osberg, 1979).

The BADR is also distinguished by many well documented faults. The Clinton-Newbury Fault traces southwesterly into the Lake Char Fault near Worcester, MA. It can then be traced into the Honey Hill Fault of CT. Four faults have been mapped that splay off to the north of the Clinton Newbury Fault into NH. They are, from west to east, the Pinnacle, Hall Mountain-Campbell Hill, Silver Lake and Flint Hill Faults. The Flint Hill and Silver Lake Faults merge to the south to become the Wekepeke Fault in MA. Eventually the Wekepeke Fault joins the Clinton-Newbury Fault near Worcester, MA (Lyons et al, 1982).

2.2 Crustal Structure of Southern New England

Studies of the crustal velocity structure in the New England area are numerous. Past work using body wave or surface wave methods to determine seismic velocity structure include for example Linehan (1962), Breitling (1965), Chiburis et al. (1977), Bruenig (1980), and Taylor and Toksoz (1982). More recently, studies using group velocity dispersion of Rg waves to constrain variations in the seismic structure of the shallow crust include Kafka and

Dollin (1985), Kafka (1985), Kafka and McTigue (1985), McTigue (1986), Saikia et al. (1986), Gnewuch (1987), Kafka (1988), and Tu (1989).

Kafka and Dollin (1985) studied group velocity dispersion for Rg waves with periods between 0.5 and 2.0 sec that were recorded from quarry blasts in SNE. In that study, they identified five distinct dispersion regions. Normal dispersion was observed in the period range of 0.5-1.5 sec indicating that there must be a relatively low velocity surficial layer (about 0.5 to 1.0 km thick) in the upper crust throughout the study area. The seismic velocities in this layer displayed some lateral variation and appeared to correlate, to some extent, with the geology.

McTigue (1986) used group velocity dispersion of Rg waves between periods of 0.5 and 2.0 sec to map lateral and vertical variations in the seismic velocity structure of the crust beneath SNE. He noted the same five dispersion regions as Kafka and Skehan (1990) and obtained velocity models approximating the upper crustal structure for each region. All Rg waves analyzed in his study displayed normal dispersion at shorter periods, again indicating the presence of a low velocity layer about 0.5 to 1.0 km thick near the surface. He concluded that the Avalonian Terrane had a slightly different crustal structure than the area to the west. His velocity models suggested to him that the Avalonian extends beneath the Nashoba Terrane up to 50 km west of the westernmost exposure of the Avalonian terrane. McTigue concluded that this may represent a subsurface extension of the Douglas Woods Anticline.

Saikia et al. (1986) measured group velocities from New England quarry blasts along various paths with distances up to 180 km from the source. They inverted observed dispersion data to obtain shear wave velocity models for various areas in SNE. They also computed theoretical dispersion curves and displacement depth eigenfunctions for Rg waves using various earth models. Synthetic Rg waves were then calculated for explosion sources using those earth models from which the theoretical dispersion curves and the observed dispersion curves had the best fit.

Farther north, in southeastern Maine, Kafka and Reiter (1987) analyzed the dispersive properties of Rg waves that were recorded from blasts detonated by the U.S. Geological Survey as part of the Maine Seismic Refraction Experiment in 1984. Group velocities for the period range of 0.4 to 1.6 sec are sensitive to the velocity structure at depths ranging from near the surface to a depth of approximately 2 km. The group velocities that were observed in this study were found to be different from one path to the next. The fact that the group velocities were significantly higher for paths parallel to the grain of the Appalachians than for paths transverse to the grain, suggested to them that the shallow crustal structure beneath the Appalachians of southeastern Maine is laterally anisotropic. Rg group velocities were inverted to obtain shear wave velocity models of the upper 2.0 km of the crust. A Vp model was constructed using a Vp/Vs ratio of 1.78. Their resulting models indicated that, on average, Vp ranged from about 4.9 km/sec in the upper 0.3 km to 6.2 km/sec at a depth of about 2 km. The observed range of Rg group velocities in this study is evidence that there is a variation in shallow crustal structure that is dependent on either path location, path orientation, or both.

Kafka (1988) summarized Rg dispersion studies in SNE and concluded that although Rg dispersion varies significantly throughout SNE, there is a rather large region where the Rg dispersion is curiously uniform. That region is the BADR, which was given that name based on the findings in those studies. The Rg observations suggest that on the scale of variations delineated by these Rg studies, the shallow crust beneath this area is homogeneous. The observed variations in the shallow crustal structure across SNE is summarized by Kafka and Skehan (1990).

Tu (1989) studied quarry blasts in New Hampshire and Vermont that were recorded by the NESN, and determined group velocities for Rg waves with periods between 0.3 sec and 2.0 sec. The paths used in this study ranged from about 10 to 168 km in length. Results of this study show that group velocities in this area of New Hampshire and Vermont very much resemble those of the BADR, which suggests that the BADR extends into New Hampshire and

adjacent Vermont. However, because Kafka and Reiter (1987) discovered significant variation in seismic velocity structure in southeastern Maine, there must be a "transition zone" somewhere between southern New Hampshire and southeastern Maine where significant lateral variation begins to occur.

3. SURFACE WAVE THEORY

3.1 Rg Waves

An Rg wave is a short-period surface wave. Surface waves are a type of seismic wave that travels along the free surface of the earth. A Rayleigh wave is a type of a surface wave in which the ground displacement is in the vertical plane, with a retrograde elliptical particle motion. Fundamental mode Rayleigh waves with periods between about 0.2 sec and 2.2 sec (Rg) are very often observed on seismograms of quarry blasts and shallow-focus earthquakes. Quarry blasts and other explosions that are detonated at or just below the earth's surface usually generate strong Rg wave signals, making them ideal seismic sources for the study of Rg wave dispersion. The dispersive properties of an Rg wave are sensitive to lateral variations in the upper few kilometers of the crust.

Because the major component of Rayleigh wave particle motion is shear in the vertical plane and the minor component is compressional-dilitational in the horizontal plane, Rayleigh waves are most sensitive to variations in shear wave velocity (Dobrin et al, 1951). Panza and Calagnile (1975) calculated theoretical phase and group velocity dispersion curves for continental earth structures, and they demonstrated that Rg can be modeled as a fundamental mode Rayleigh wave. Displacement-depth eigenfunctions of fundamental mode Rayleigh waves computed for the Chiburis (1977) crustal model in the period range of 0.2 - 2.5 sec show that Rg wave particle displacement is at a maximum near the surface and decreases to essentially zero at a depth of about 10 km. It, therefore, makes sense that surface explosions such as quarry blasts and shallow-focus earthquakes are excellent sources for the generation of surface waves (see Kafka, 1990).

Observations of Rg wave propagation have shown that different frequency components of the wave travel with different velocities. This phenomenon causes the shape of the wavetrain to change with distance from the source. When this happens, the wave is said to be dispersive

(Dobrin, 1951). Because Rg waves are dispersive, two kinds of measurements for velocity can be made. The *phase velocity* of an Rg wave is the measurement of the distance traveled per unit of time by a point of constant phase, such as a peak or a trough. If you were to draw an envelope around the peak of a wave pulse and measure the speed with which the wave packet was traveling, then you would be measuring the *group velocity* of that wave. The group velocity of a wave can be defined as:

$$U = C - \lambda \frac{\partial c}{\partial \lambda} = C + \omega \frac{\partial c}{\partial \omega} \qquad (1)$$

where C = phase velocity, λ = wavelength, and ω = angular frequency.

3.2 Measuring Group Velocities

Group velocities of Rg waves are measured using a technique of narrow band pass filtering developed by Dziewonski et al (1969). This method, which has been frequently used and upgraded by seismologists at Weston Observatory, is used to study the variation of wave energy as a function of velocity and period. The signal is first Fourier transformed and then a Gaussian filter is applied in narrow frequency bands at a series of center frequencies. For each center frequency, the group arrival time is approximated by measuring the arrival time of the maximum amplitude of the envelope of the filtered signal. This process is repeated for a series of center frequencies and group velocities are estimated at each center frequency.

The result of this analysis is a contour plot of group velocity vs. period showing the log (base 10) of energy for each center frequency as a function of group velocity (Figure 12). The shape of the contour plot corresponds to the shape of the energy envelope at each center frequency (Dollin, 1984). The group velocity curve that results from the plot represents the velocities at which maximum energy arrived for each center frequency.

The example shown in Figure 12 represents the contour plot for a blast that was detonated at the San-Vel quarry and recorded at Weston Observatory's network station (WES). The lower numbers on the plot represent higher amplitudes.

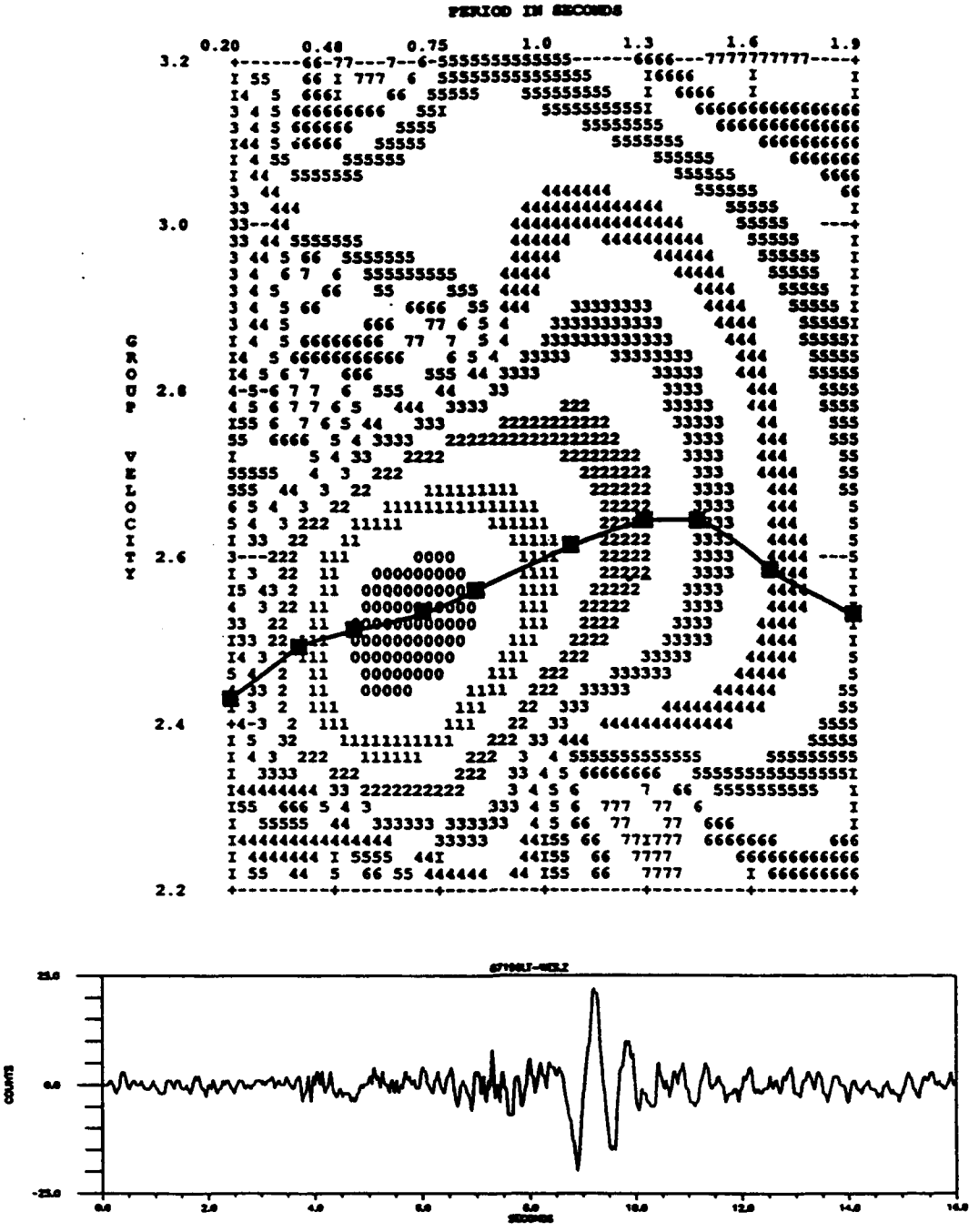

Figure 12 : Contour plot of San-Vel quarry blast recorded at station WES with group velocity curve superimposed. Below is seismogram of the event.

4. DATA PROCESSING

4.1 Origin Times

In order to analyze group velocities of Rg waves, accurate estimates of event origin times are critical. Fortunately, for this investigation all of the data gathered prior to 1989 had very accurate origin time estimates. For those events, an accelerometer was placed in the quarry as close to the shot point as possible (at a distance of approximately 100 yards). The accelerometer, which was connected to a digital recorder like all of the other field sites, recorded the shot on tape. Because of the close proximity of the sensor to the event, we were able to estimate the origin time to within a few hundredths of a second by measuring the arrival time of the first motion on the record. Table 3 lists the 1987-1988 events with their origin times.

Origin times for the 1989 field data and events thereafter were estimated to within about 0.1 to 0.2 sec of the actual origin time using a statistical method based on all of the data from events with known origin times. To do this, travel times (TT) were calculated for all pre-1989 seismograms by subtracting the event origin time (OT) from the P-wave arrival time (P-AT). These calculations were entered into the StatView SE+Graphics statistical software package designed by Abacus Concepts, Inc. for the Macintosh computer. Using this program, the travel times were plotted as a function of distance (Figure 13). A linear regression performed on these data yielded an equation for travel time:

$$TT = .171(x) + .151, \qquad (2)$$

where x = distance from source to receiver. Using this equation, theoretical travel times could be calculated for all of the seismograms with unknown origin times. Origin times for these events were then estimated by subtracting the theoretical travel time from the actual P-wave arrival time (picked directly off of the seismogram). The final estimated origin time used for the processing of this data was determined by averaging all of individual origin time estimates

Table 3

EVENTS WITH KNOWN ORIGIN TIME

EVENT LOCATION	LAT	LON
SAN-VEL/LONESTAR QUARRY	42.554N	-71.517W

YEAR	JULIAN DAY	ORIGIN TIME
1987	202	16:58:14.97
1987	210	18:13:56.17
1988	089	18:01:50.31

TABLE 4

ESTIMATING ORIGIN TIMES

USING THE EQUATION: TT = .171 (X) + .151 (from figure 4.1.1)

JULIAN DAY:

STATION	DIST. (km)	P-AT	TT	OT (est.)
DAY 177				
NW02	7.86	18:28:56.72	1.50	18:28:55.22
WFM	6.65	18:28:56.54	1.29	18:28:55.25
WES	24.71	18:28:59.84	4.38	18:28:55.46
		Average estimated origin time:		18:28:55.36
DAY 192				
NW01	5.87	19:33:55.88	1.15	19:33:54:73
NW02	7.86	19:33:56.30	1.50	19:33:54.80
NW06	17.64	19:33:58:05	3.17	19:33:54.88
		Average estimated origin time:		19:33:54.80
DAY 208				
NW03	8.96	17:29:49.83	1.68	17:29:48.15
NW04	13.80	17:29:50.60	2.51	17:29:48:09
NW05	15.69	17:29:51.12	2.83	17:29:48.29
		Average estimated origin time:		17:29:48:18
DAY 213				
NW01	5.87	19:29:26.91	1.15	19:29:25.76
NW03	8.96	19:29:27.52	1.68	19:29:25.84
NW04	13.80	19:29:28.26	2.51	19:29:25.75
NW05	15.69	19:29:28.88	2.83	19:29:26.05
NW07	20.25	19:29:29.62	3.61	19:29:26.01
NW08	22.79	19:29:29.98	4.05	19:29:25.93
		Average estimated origin time:		19:29:25.89

Table 5

EVENT (YRDAY)	ORIGIN TIME
87202	16:58:14.97
87210	18:13:56.17
88089	18:01:50.31
89177	18:28:55.31
89192	19:33:54.80
89208	17:29:48.18
89213	19:29:25.89

Table 6

Event	tt (sec)	P-vel (km/sec)	ttheo (sec)	Δtt (sec)
89177-NW02	1.36	5.78	1.50	.14
89192-NW01	1.08	5.44	1.15	.07
89192-NW02	1.51	5.21	1.50	.01
89192-NW06	3.25	5.43	3.17	.08
89208-NW03	1.65	5.43	1.68	.03
89208-NW04	2.42	5.70	2.51	.09
89208-NW05	2.94	5.34	2.83	.11
89213-NW01	1.02	5.76	1.15	.13
89213-NW03	1.63	5.50	1.68	.05
89213-NW04	2.37	5.82	2.51	.14
89213-NW07	3.73	5.43	3.61	.12
89213-NW08	4.09	5.57	4.05	.04

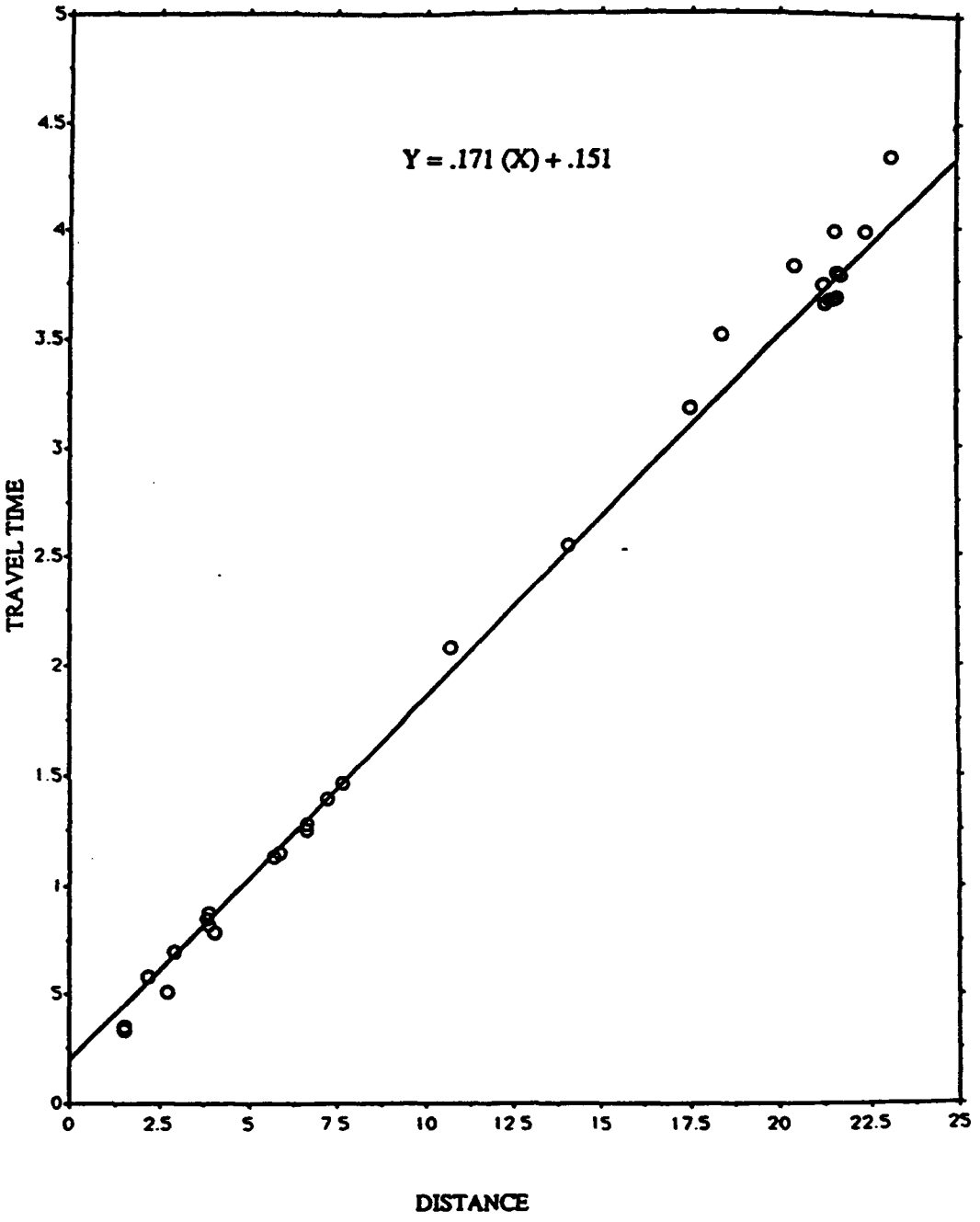

Figure 13 : Travel time plotted as a function of distance.

for each event. Table 4 shows examples of events where origin time was estimated using this procedure.

Using this method, origin times were estimated for all of the summer field events. Table 5 is a list of all seven events recorded in the field between 1987 and 1989 with their respective origin times. The effect of origin time errors on group velocity measurements is discussed in Section 4.2.

When using a statistical method to estimate any measurement there is bound to be some margin of error. As mentioned above, accurate origin times are critical when processing a seismogram for group velocity. One thing that must be considered is, "What is the margin of error in estimating origin times?" To test the accuracy of the statistical method described above, the same method was applied to estimate the origin times for events with known origin times. When these estimated origin times were compared with the actual origin times, the method was found to be accurate to within .1 to .2 sec, whereas the 1987 and 1988 events are probably accurate to within a few hundredths of a second. Also, if you calculate travel times for the data using the estimated origin times and the actual origin times and compare the travel times for both groups, you can see that the difference in travel time (Δ tt) for each event is within +/- .14 sec. Table 6 lists the events, their actual travel times (tt), P-wave velocity (P-vel), their theoretical travel times (ttheo) and the difference between the two (Δ tt).

4.2 Effect of Origin Time Errors On Group Velocity Measurements

It is important to note that errors in origin time are going to have a greater effect on paths of shorter length than on those that are longer. This is demonstrated in the following example. Consider a station whose distance from the source (x) is 30 km. Assuming an Rg wave velocity (U) of 2.5 km/sec, the Rg wave travel time would be 12 sec. If we add an error of 0.1 sec to the arrival time, we would measure a travel time of 12.1 sec. This in turn would yield an Rg velocity of U' = 2.48 km/sec. The differences between the two velocity measurements would be Δ U = 0.02 km/sec. If we set x = 60 km, then U' = 2.49 km/sec and Δ U would be equal to

0.01 km/sec. For the same 0.1 sec error, the differences or errors in velocity measurements are cut in half as we increased the distance from source to receiver by two. If we continued to increase the distance (x), then the errors in velocity would become less and less significant. Conversely, as distance decreases the origin time errors have a greater effect on the accuracy of the group velocity measurements. The graph in Figure 14 shows the change in group velocity with increasing distance for three different error measurements.

As discussed above, timing is essential to the study of seismic velocities. Great care is taken to synchronize very sensitive time keeping devices in all instruments used in a seismic experiment. Curiously, when processing this data set some very suspicious group velocity measurements were found from what appear to be some very good seismograms. Because there was no obvious explanation for these suspicious measurements, the first step I taken to investigate this problem was to ensure that the file was processed correctly. In doing so, a check was made of the timing of the event. The NESN and MIT networks are set up so that every time an event is recorded, a time file is generated that contains the time that is read off of a satellite clock and is then correlated to the event trace. The program that generates the time file calculates at what time the first data point arrives and lines the trace up with the time from there. If the program does not accurately calculate the time of the first data point on the trace, then the timing for the entire event will be off. When I plotted the time files for the above mentioned events, I found that indeed the second and minute marks did not line up precisely, as they should. Each event was offset by a small amount which I have noted in Table 7. I processed each file again, having corrected for the time discrepancies. As a result of the corrections, each seismogram has yielded usable data.

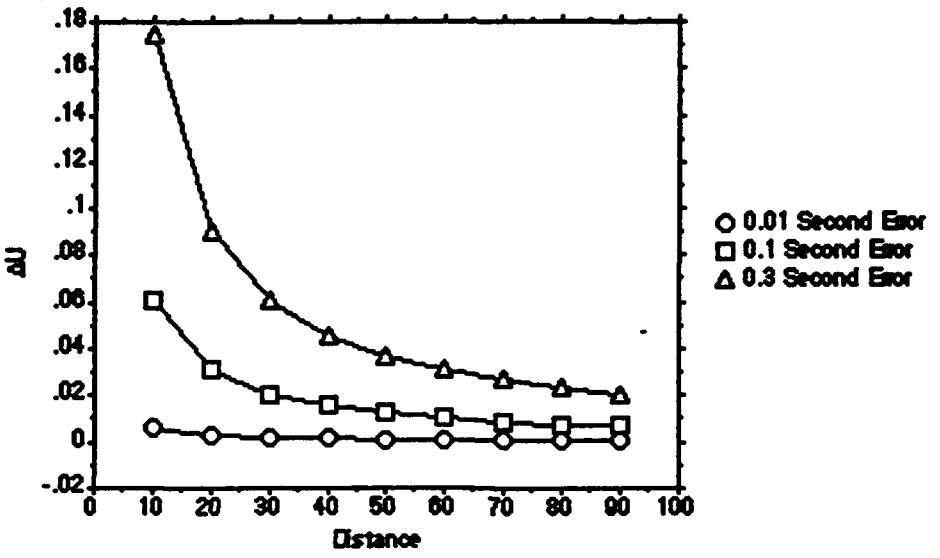

Figure 14 : Change in group velocity with increasing distance for examples of different origin time errors.

Table 7

Year	Day	Clock Error	Station Affiliation
1987	202	.04 sec (slow)	MIT
1987	210	.15 sec (slow)	MIT
1988	089	.71 sec (fast)	MIT
1989	177	.30 sec (slow)	MIT
1989	192	.30 sec (slow)	MIT
1989	213	.30 sec (slow)	MIT

5. RESULTS

5.1 Summary of Results from Previous Studies of SNE

As a result of this study, observed Rg group velocities in eastern MA and southern NH range between 2.00 to 3.29 km/sec for a period range of 0.2 to 2.2 sec. Compared with the results of previous investigations of Rg wave group velocity dispersion (Table 8), it was found that the range of group velocities from this study is most similar to that observed by Kafka and Dollin (1985) for paths in Southern New England (2.0 to 3.3 km/sec).

Originally, the results of Kafka and Dollin (1985) revealed lateral variations in group velocity dispersion curves that scattered around three distinguishable ranges of group velocities. Group velocities for paths that crossed southwestern Connecticut were noticeably higher than those paths that traversed eastern Connecticut. Both of those groups of paths were faster than paths that crossed the Hartford Rift Basin. As a result, Kafka & Dollin designated each area as a distinct dispersion region. More recently, however, Kafka and Bowers (1991) discovered that in the Kafka & Dollin (1985) study an incorrect source to receiver distance was applied in processing paths that extended from the various quarries to station BCT (Brookfield, CT). The error was a result of a misprint in the latitude and longitude file of Weston Observatory's event location program which resulted in an inaccurate geographical placement of station BCT on the map. The erroneous source to receiver distance value yielded group velocities that were significantly higher than those from the other two regions and resulted in what became known as the Waterbury Dispersion Region (WDR), a region of anomalously high group velocity.

After the discovery of this error, Kafka & Bowers (1991) reprocessed all data from paths that crossed the WDR using the correct source to receiver distance. Results of this correction indicate that Rg group velocities in the WDR are not anomalously high, but are on average consistent with the average group velocities for the BADR. For this reason, the area

Table 8

Authors	Period(sec)	G.V.(km/sec)	Region
Press & Ewing (1954)	8.0-12.0	3.05	N. America
Bath (1954)	3.0-14.0	3.07	Europe/Asia
McEvilly & Stauder (1965)	0.5-5.0	1.5-3.0	Illinois Basin/Ozark Uplift
Anderson & Dorman (1973)	0.2-1.5	1.2-3.1	Southern NY/Northern NJ
Bath (1975)	0.5-1.8	2.5-3.0	Sweden
Kafka & Dollin (1985)	0.5-2.0	2.0-3.3	Southern New England
McTigue (1986)	0.5-2.0	2.1-2.9	MA and RI
Kafka & Reiter (1987)	0.4-1.6	2.4-3.3	Southeastern Maine
Tu (1989)	0.3-2.0	2.3-2.9	NH and Vermont
this study	0.2-2.2	2.0-3.29	MA and Southern NH

that was designated as the WDR has since been merged with the quite extensive BADR, and it is probably no longer appropriate to use either name to refer to this dispersion region. (Note: Figure 1 reflects the changes made post Kafka & Bowers (1991). However , the results of this study show that lateral variation can be observed in the shallow crust beneath SNE and southern NH when a denser station spacing is used.

5.2 Results of This Study

The variation of group velocities observed in this study suggests that there is indeed systematic lateral variation in the structure of the upper crust underlying SNE. Various ways of displaying the results shows that: 1) lateral variations in group velocities within the study area appear to be a function of distance from the San-Vel quarry, yet are so subtle that they can only be observed on a small scale and are most easily observed when the data are plotted in three dimensions. The denser station spacing reveals more detail than what has previously been observed; 2) group velocity variations do not appear to be a function of azimuth, therefore, there does not seem to be any evidence of lateral anisotropy in the shallow crust underlying the study area or any paths that could be considered anomalously fast or slow (excluding path NW10 which exhibits very high group velocities, however this cannot be readily explained by the geology or the geophysics).

Figure 15 is a graph of the group velocity curves for all of the paths considered in this study. What is most striking about this graph is that the majority of the data falls within such a small range of group velocities. However, one path (NW10) exhibits higher group velocities. This is strange because the path NW10 does not cross particular geologic structures nor terminate in any particular rock type that would make it distinct from the paths that surround it, especially NW08 and NW11 which happen to exhibit group velocities that are typical of the rest of the study area.

A few of the group velocity curves appear to be anomalously slow. These paths, NW03, WFM, and UXB don't appear to have anything in common with each other that is obvious enough to suggest any reason why they exhibit slower group velocities than the rest of the group.

Figure 16 shows the average group velocity curve for the BADR from Kafka (1988), as well as the average and standard deviation for the BADR including all post 1987 data. The most interesting thing about this picture is the similarity between the two curves. Figure 17 is a graph that shows only the group velocity curves for data that fell into categories 1 and 2 (i.e. the best data). This data was graphed to show that even by weeding out the poor quality data we still see the same grouping of the curves as we did when we included all of the data (Figure 15). This would suggest to me that data quality has only a limited effect on the actual data interpretation. In other words we can, in most cases, glean the same information from a seismogram of fair recording quality as one of superior recording quality.

In order to test for anisotropy,plots were made of group velocity vs. azimuth for periods between .5 sec and 1.2 sec. Figure 18 shows the results. The diagrams in the left-hand column include all of the data used in the study. The right-hand column represents only the best quality data (quality 1 and 2 seismograms). A third order regression line was fitted to the data. It is apparent in these graphs that there is very little change in the data amongst the different periods and/or between the different quality data. The variation of the regression curves is very slight and is mainly driven by the three or four anomalous paths (NW10, NW03, UXB, and WFM) that I discussed above. If I were to remove these few paths, the regression line would be virtually flat. In either case, the plots in this figure demonstrate that differences in azimuth do not appear to have a significant effect on group velocity. Therefore we do not observe any evidence of lateral anisotropy in the shallow crust beneath the study area.

Figure 19 shows the group velocity results as a function of distance. As in Figure 18, this figure displays each period separately and also divides the data into two groups. The entire data set is plotted in the left-hand column and quality 1 and 2 data are shown in the right-

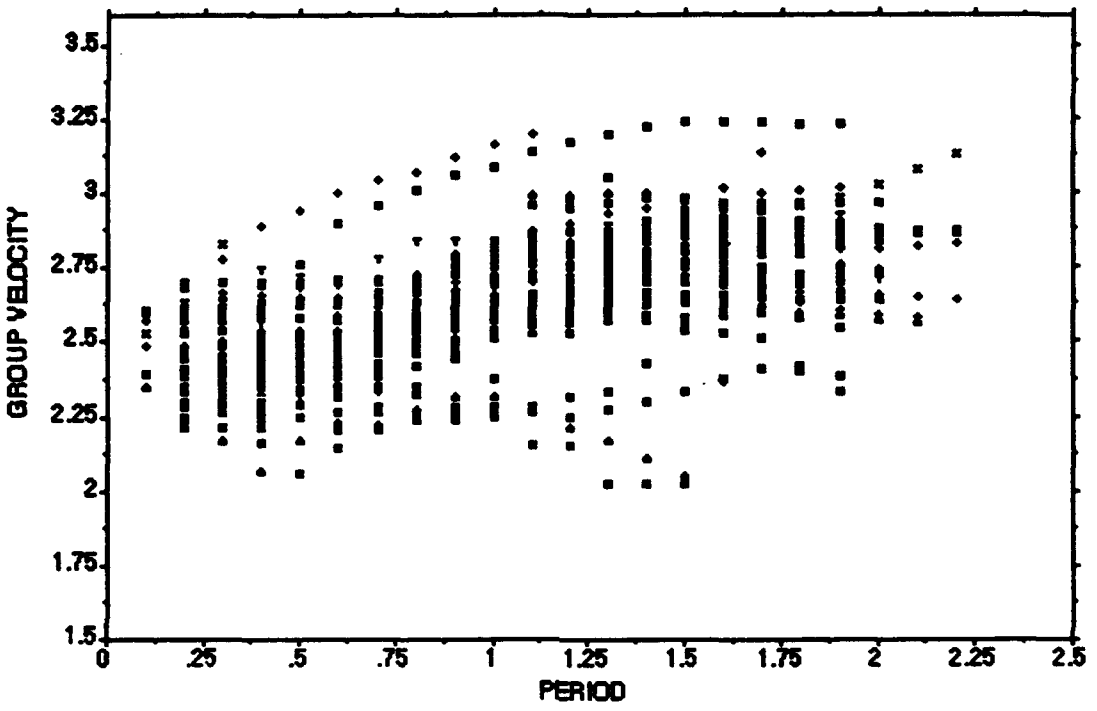

Figure 15 : Group velocity curves for all paths.

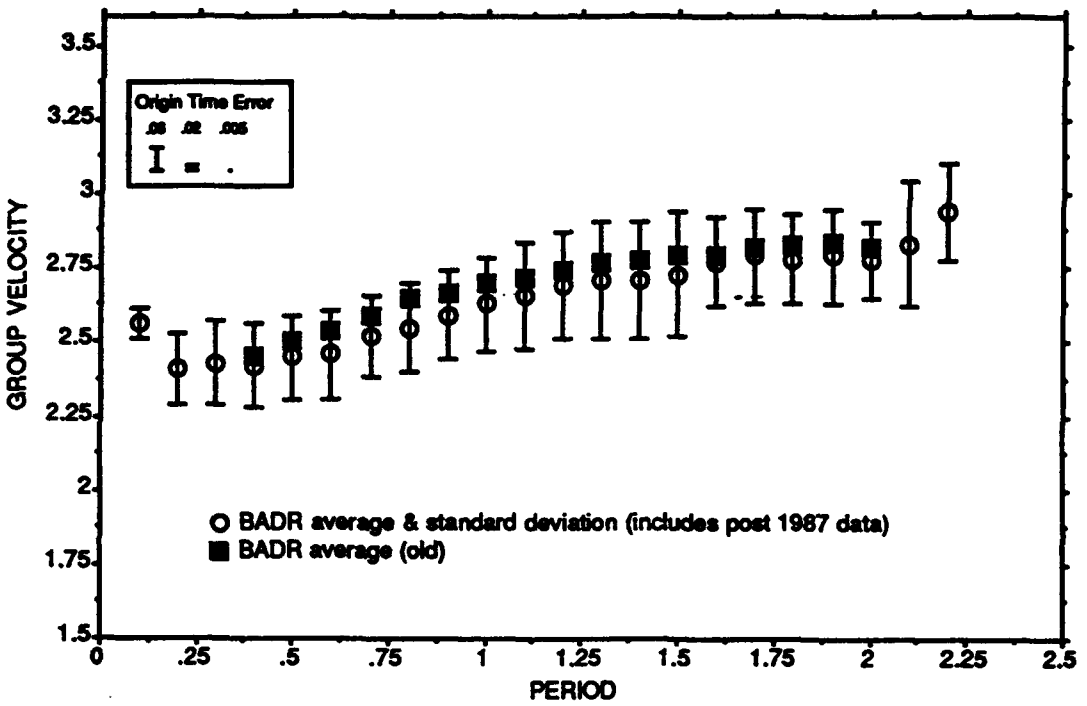

Figure 16: Group Velocity averages and standard deviations for pre- and post- 1987 data sets. Inset: Origin time errors calculated from Figure 14.

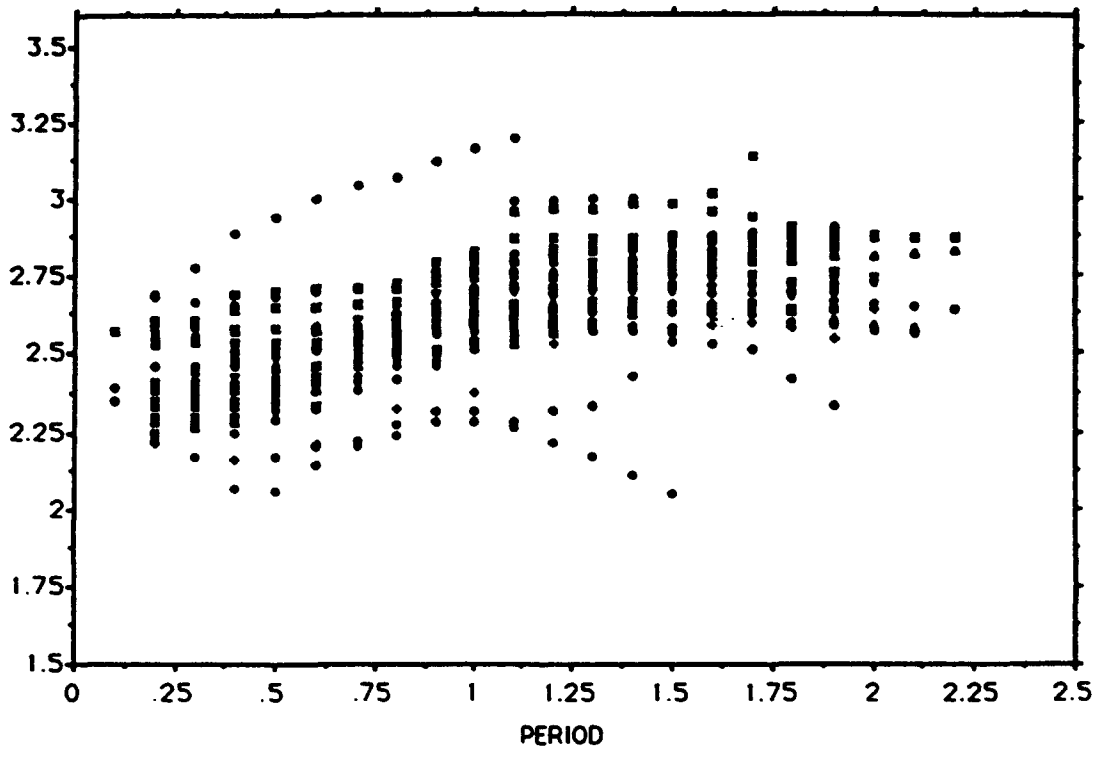

Figure 17: Group velocity curves of quality 1 and quality 2 seismograms.

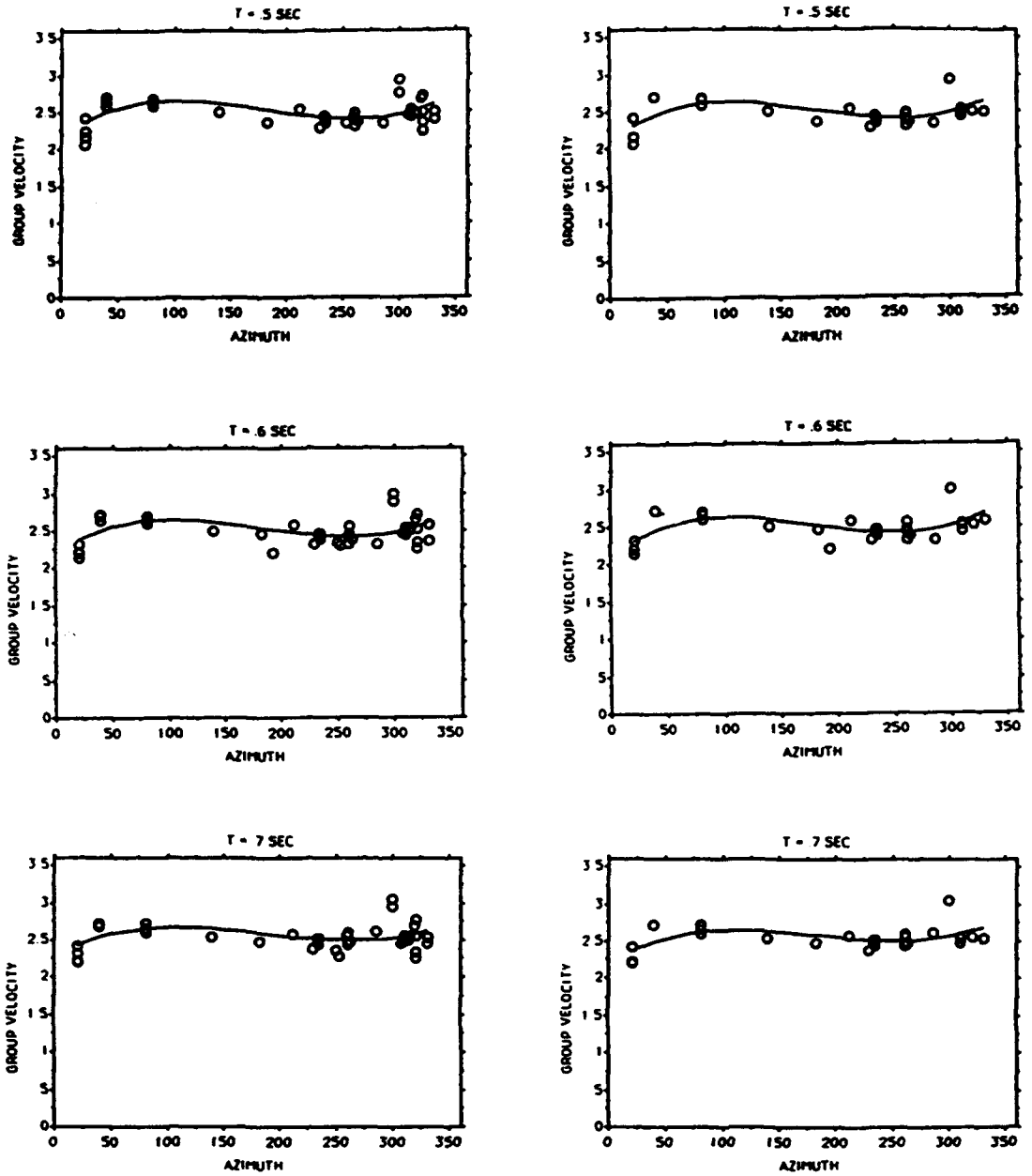

Figure 18 : Group velocity plotted as a function of azimuth.

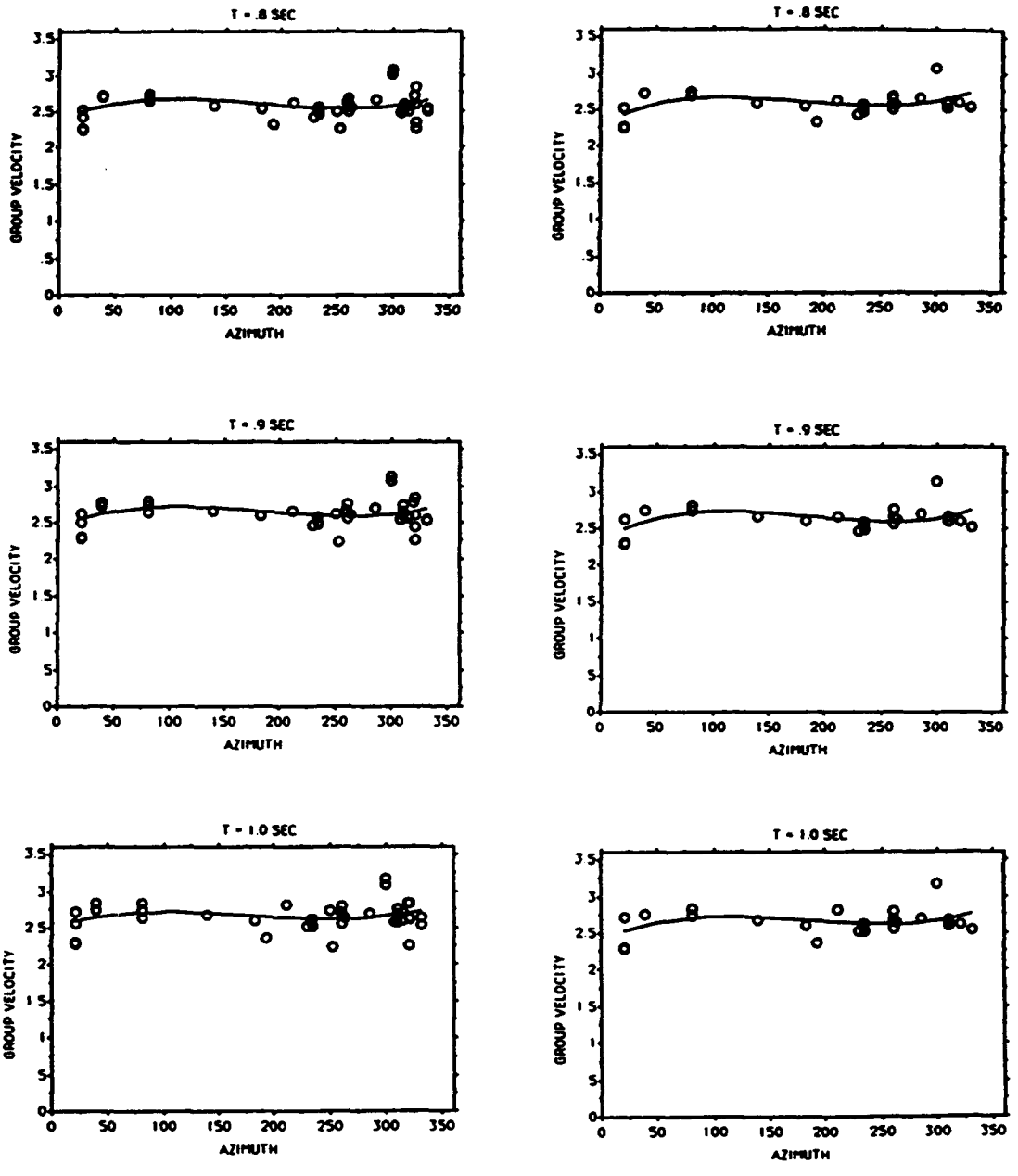

Figure 18 continued.

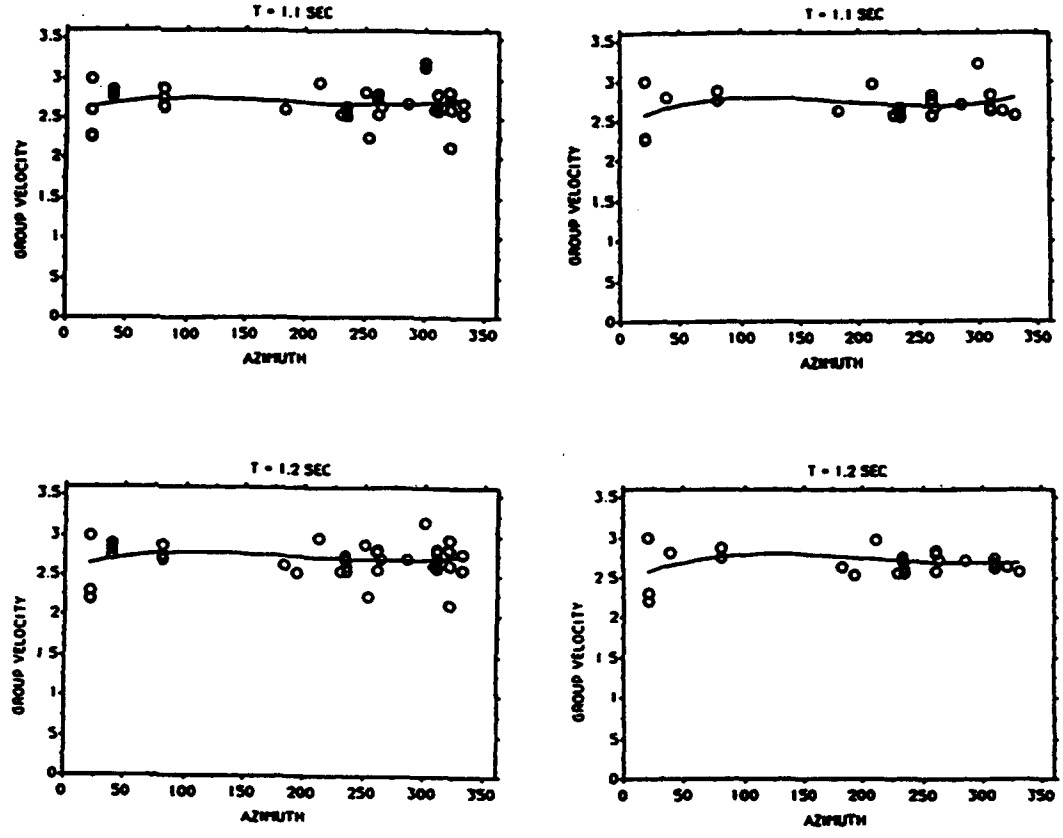

Figure 18 continued.

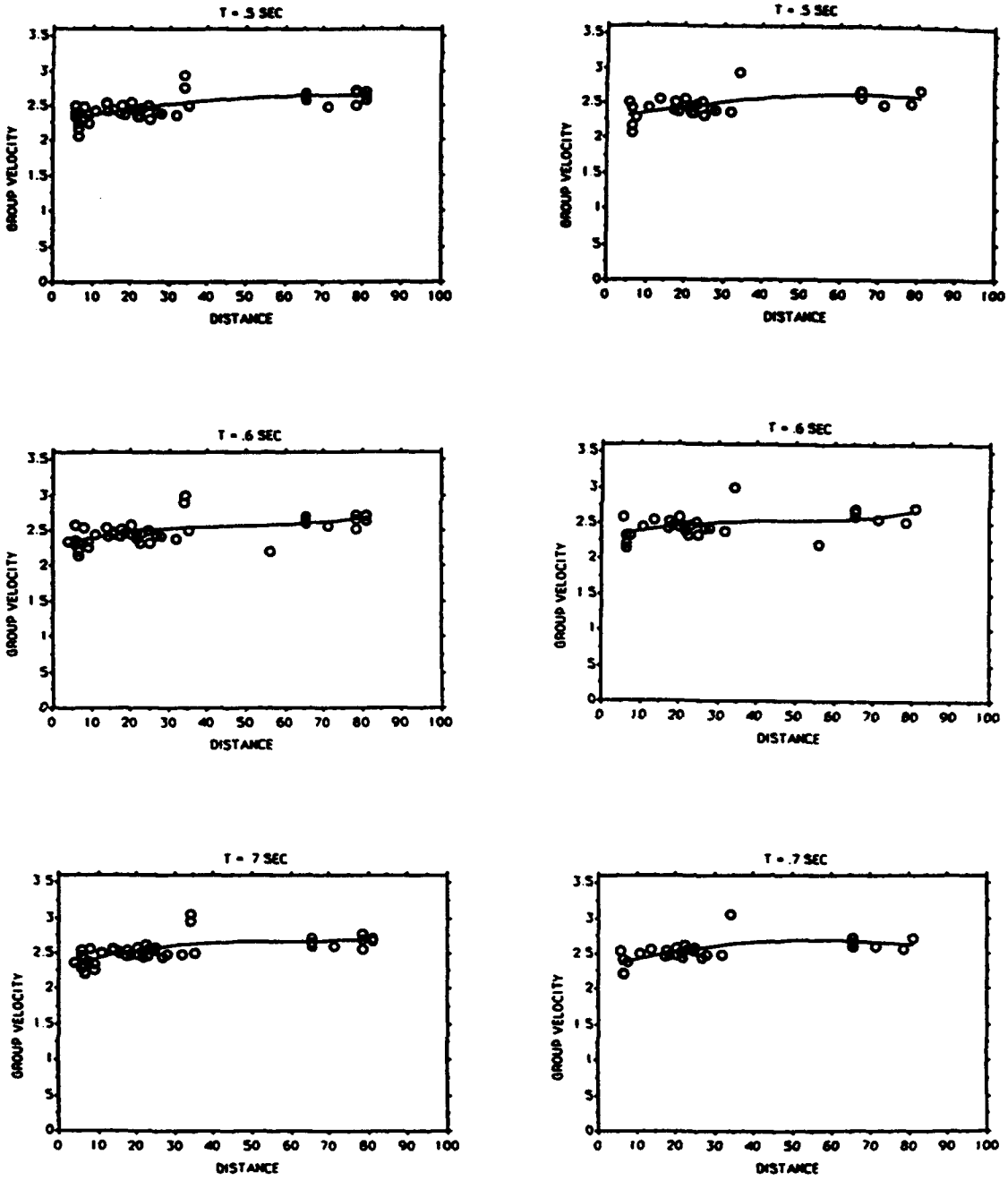

Figure 19 : Group velocity plotted as a function of distance.

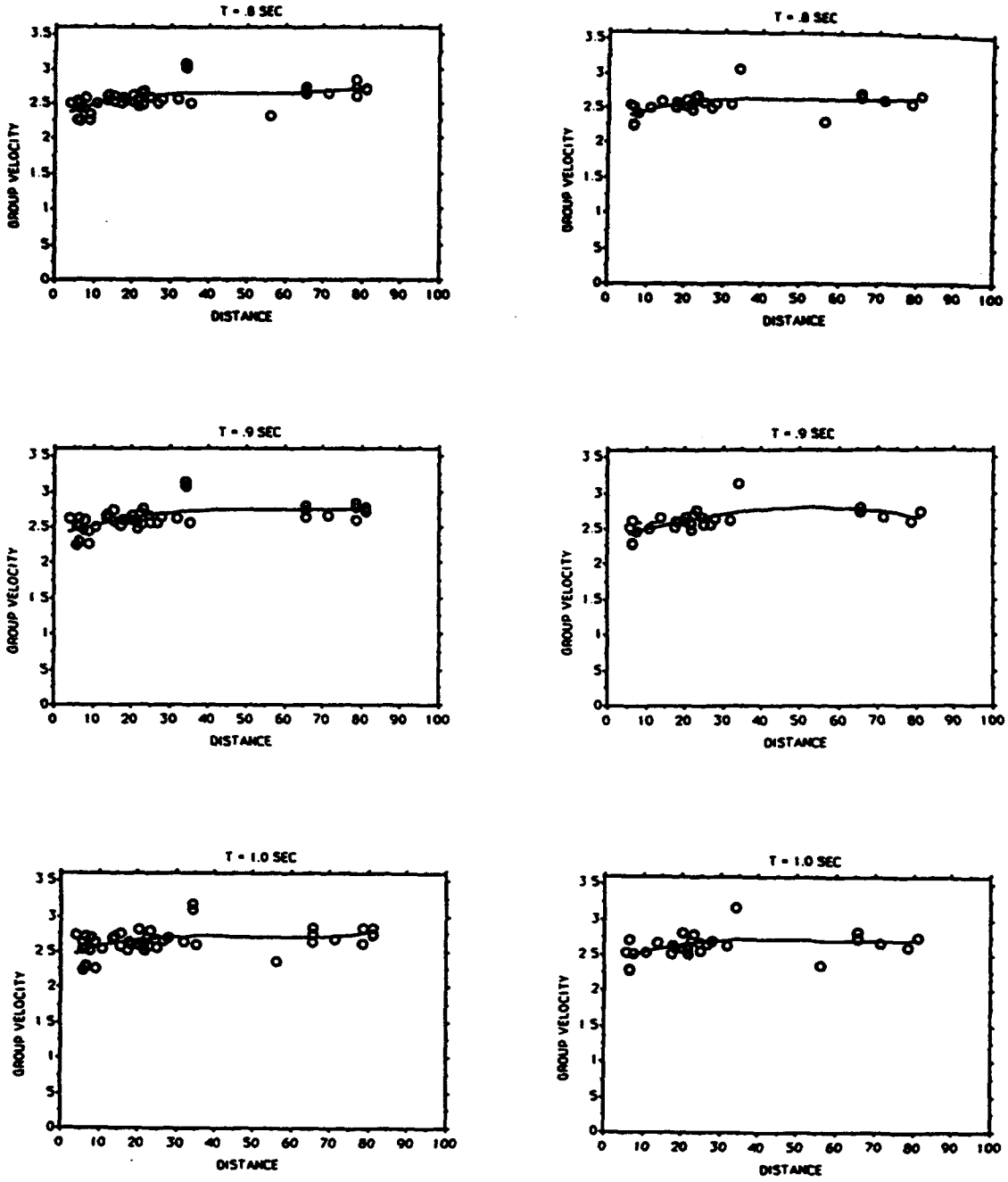

Figure 19 continued.

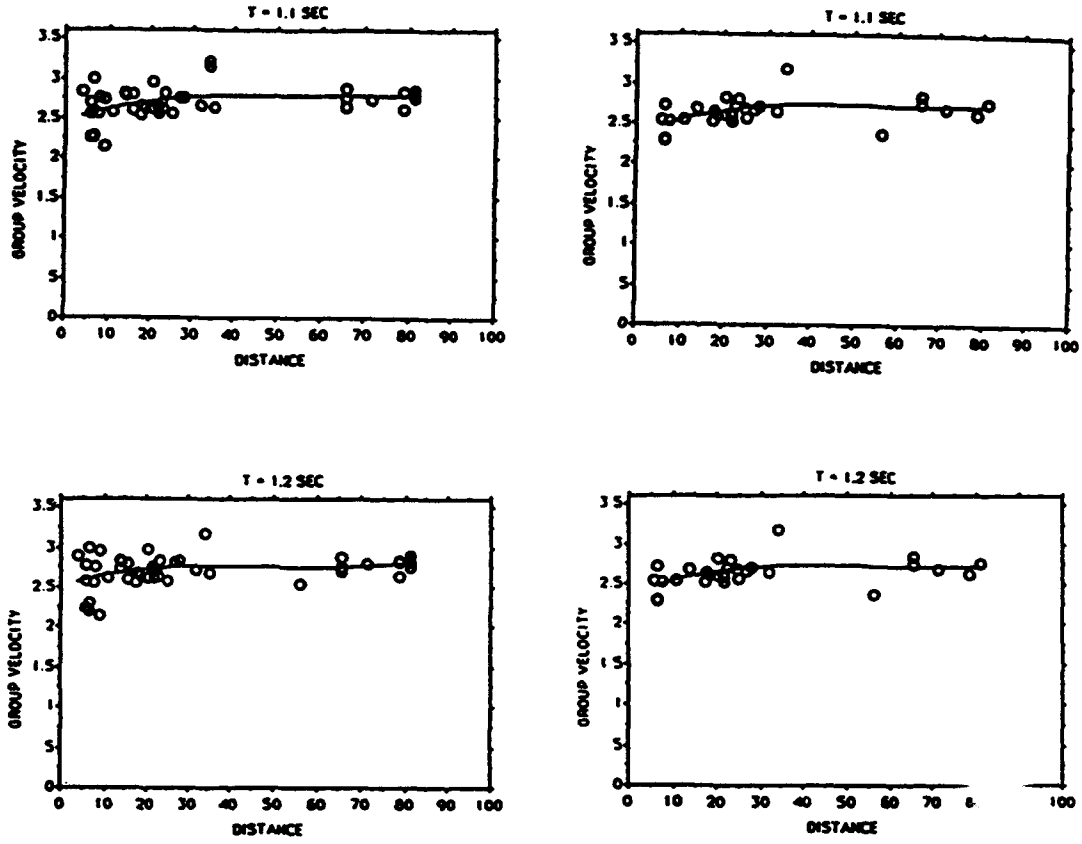

Figure 19 continued.

handed column. Again, a third order regression line was fitted to the data, and as in the case of azimuth, the regression line is virtually flat. The data show no obvious changes at different periods or between the different quality data. Plotted in this manner, it appears that the group velocity does not strongly depend on distance. However, there is some slight indication of velocity increasing with distance, and when the same data are plotted in map view, we can see that the group velocities in the area surrounding the San-Vel quarry are noticeably slower than those farther away. This strongly suggests that there actually are small scale variations in group velocity. Figures 20a,b, and c are map view plots of the group velocity for three different periods. The group velocities are divided into four ranges and each range is represented by a different symbol.

Figures 21a,b, and c are three-dimensional plots of the same data shown in Figures 20a, b and c. These figures also include a contour map of the same data (with the station array superimposed) for the same periods. These figures were plotted using the "Surfer" three-dimensional plotting program published by Golden Software Inc., Golden CO. "Grid", a module within Surfer, creates a regularly spaced grid from irregularly spaced data. An inverse distance interpolation method was used to estimate the values of group velocity for the grid points. The output from the Grid module was used to create the three dimensional and contour plots.

What is most striking about these plots is that with the data plotted in three dimensions you can see subtle undulations in the group velocities that are less than obvious when using other ways of displaying the data (i.e. Figures 18- 20). Points of interest in Figure 21 are: 1) the obvious spike at station NW10. Again, there doesn't seem to be an obvious explanation for the anomalously high group velocities here. 2) The quarry seems to lie in a "trough" (i.e. an area of particularly low group velocities). With increasing distance from the quarry, group velocities systematically increase toward the east and towards the west-northwest, creating a "U-shaped valley" of group

velocities where the trough of the valley appears to strike in a northeast direction. This is particularly interesting because the trend of this trough correlates well with the Clinton-Newbury Fault Zone. One possible explanation of this result is that group velocities within a fractured and faulted area are likely to be slower than group velocities for Rg waves that travel through solid (unfractured) bedrock.

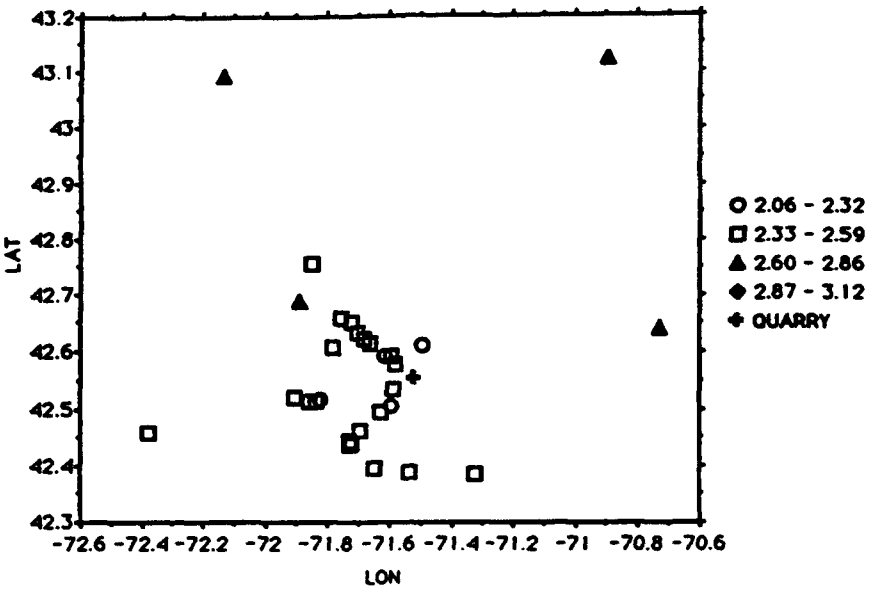

For Data With Known Origin Times

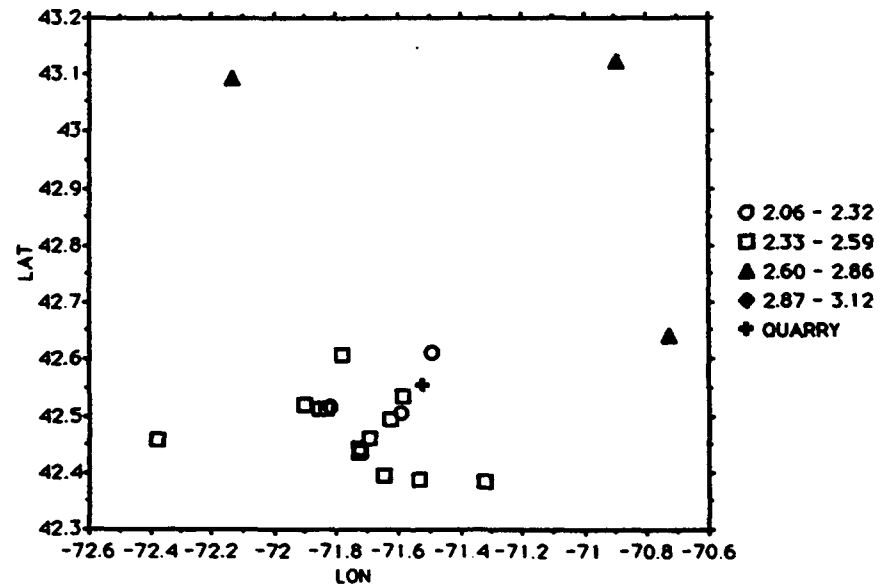

Figure 20 (a): Group velocities for Rg waves with a period of 0.5 seconds. Top figure includes all data. Bottom figure includes only seismograms with known origin times.

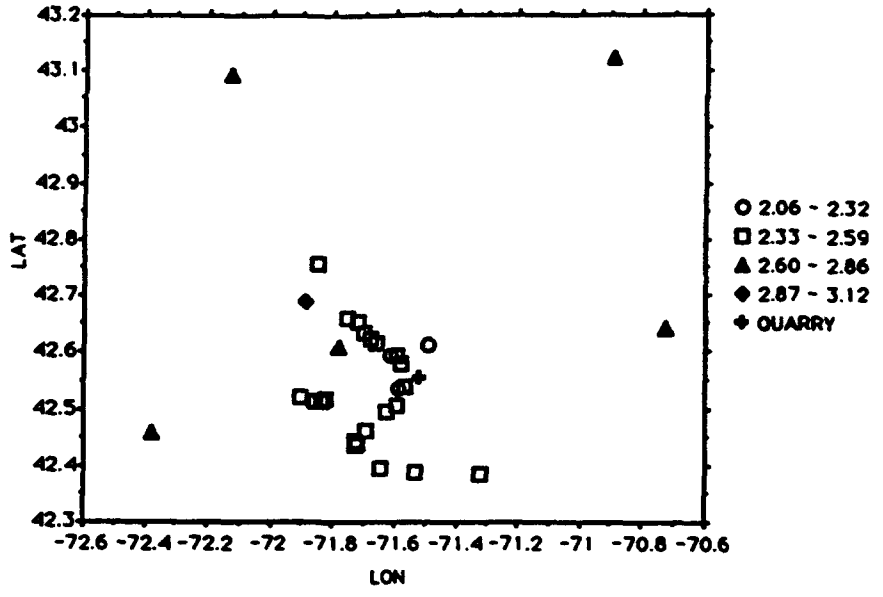

For Data With Known Origin Times

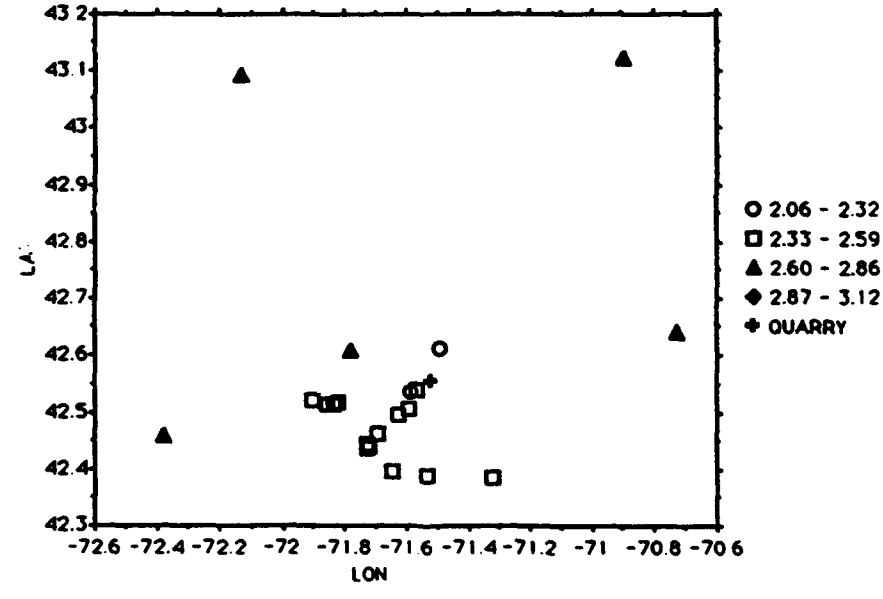

Figure 20 (b): Group velocities for Rg waves with a period of 0.7 seconds. Top figure includes all data. Bottom figure includes only seismograms with known origin times.

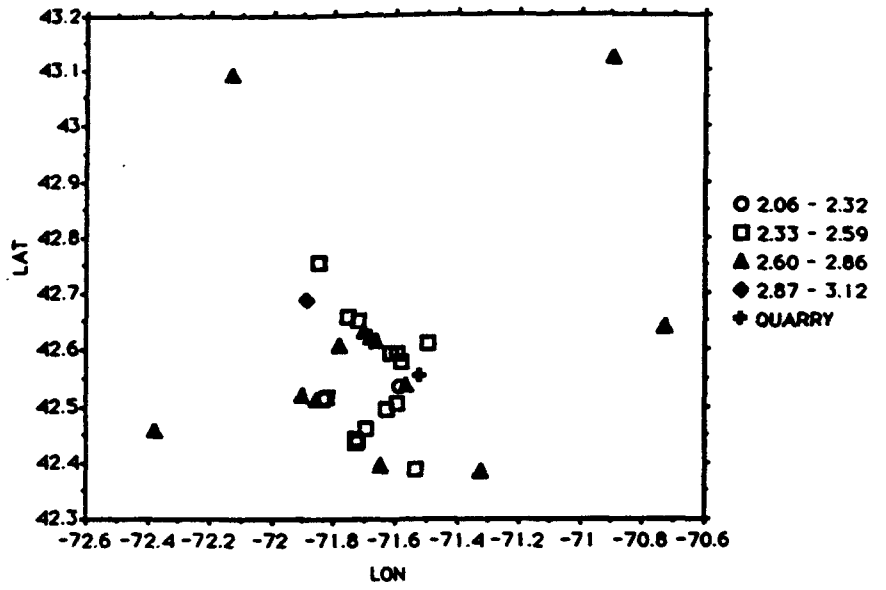

For Data With Known Origin Times

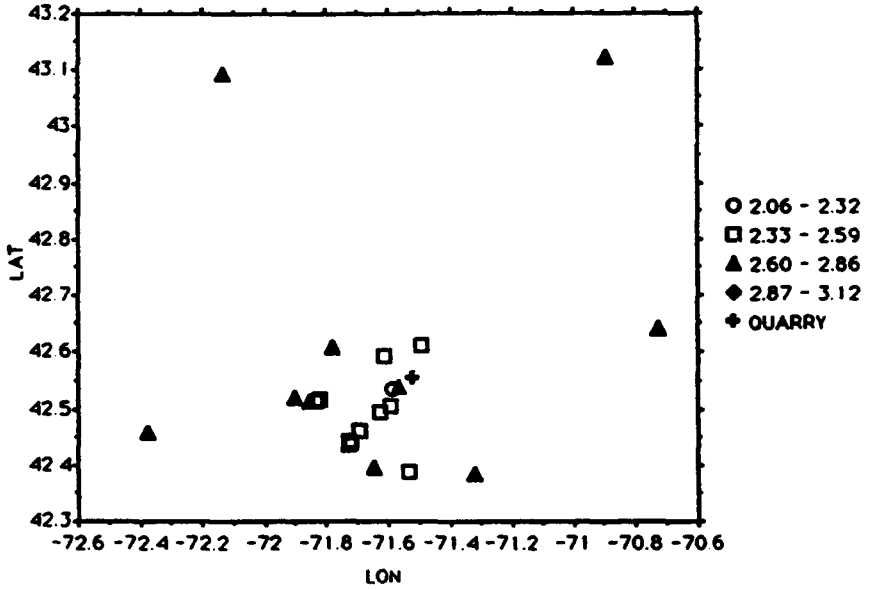

Figure 20 (c): Group velocities for Rg waves with a period of 0.9 seconds. Top figure includes all data. Bottom figure includes only seismograms with known origin times.

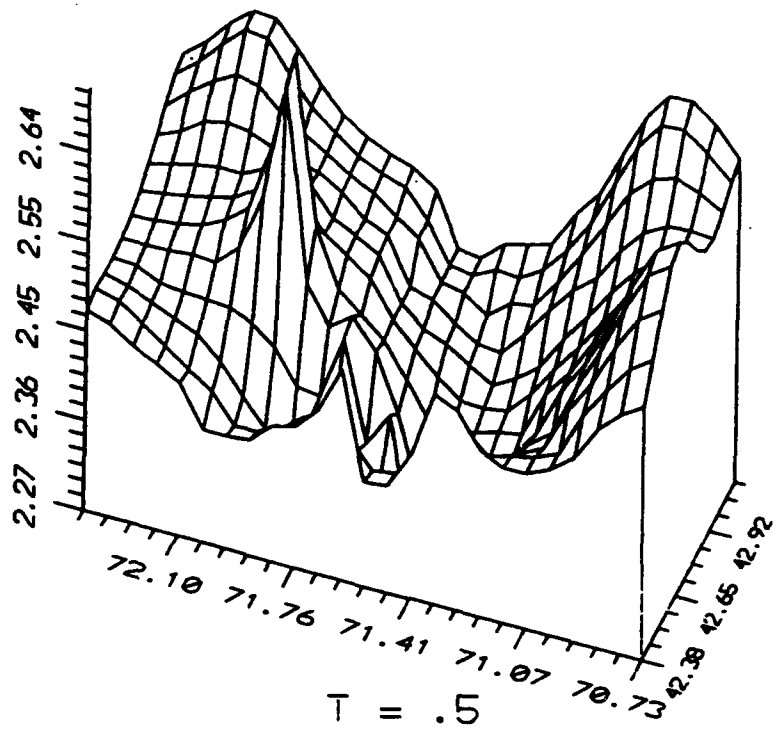

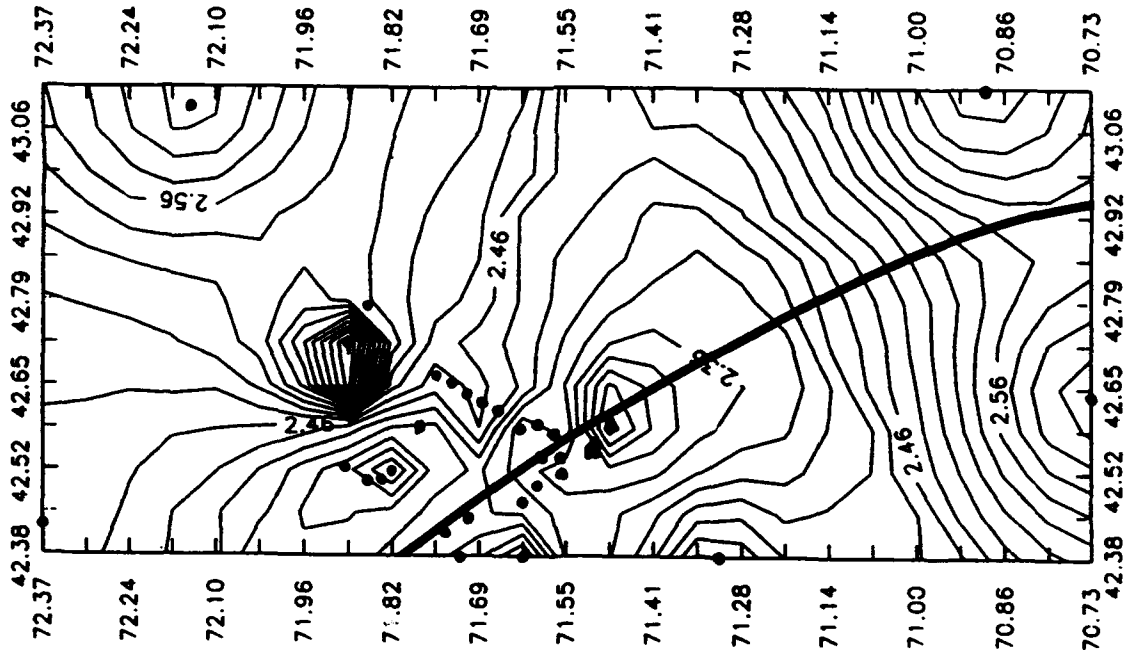

Figure 21 (a): Three dimensional plot and contour map of group velocity for Rg waves with a period of 0.5 seconds for the study area. The station array (dots) and the Clinton-Newbury fault (solid line) are superimposed on the contour map

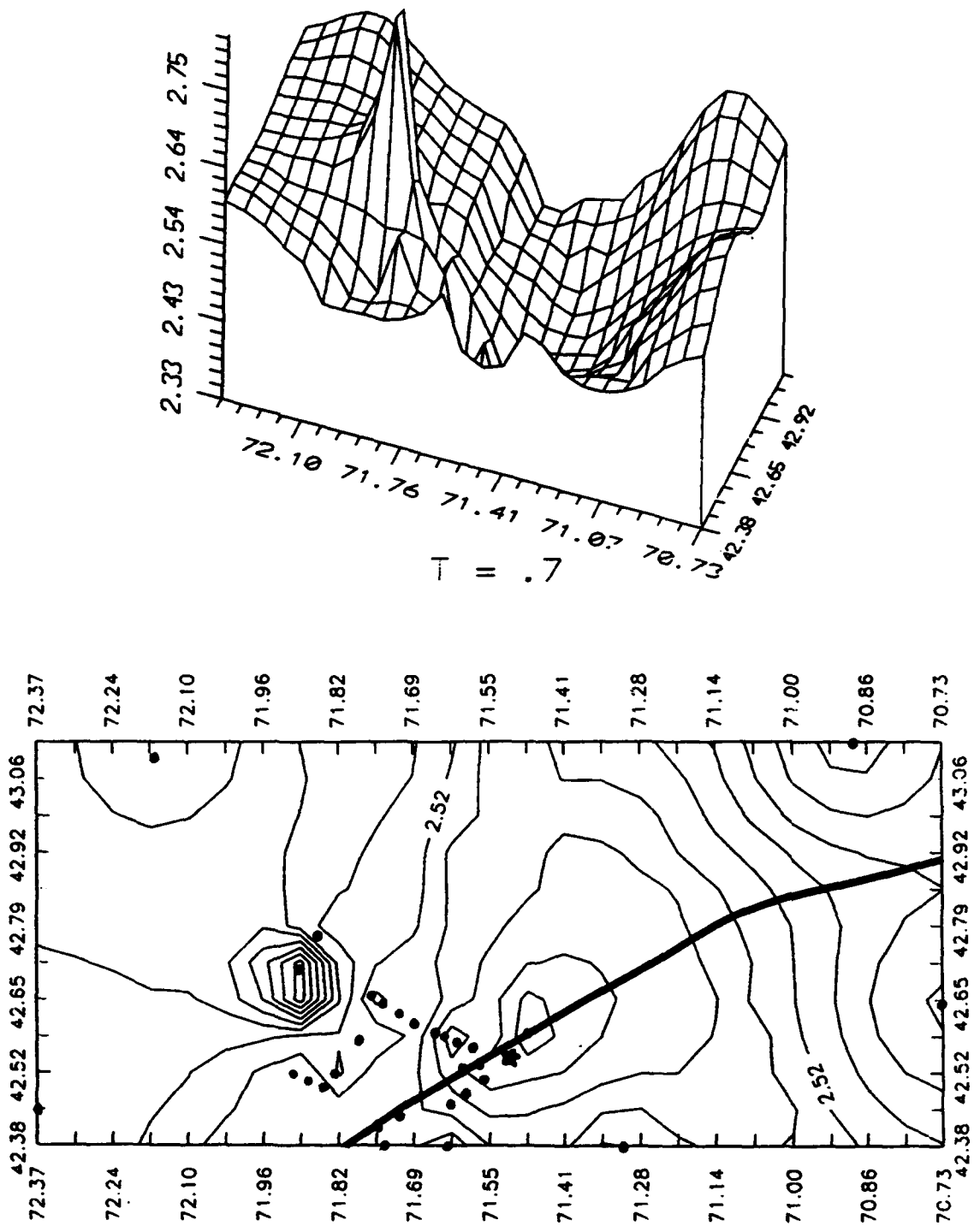

Figure 21 (b): Three dimensional plot and contour map of group velocity for Rg waves with a period of 0.7 seconds for the study area. The station array (dots) and the Clinton-Newbury fault (solid line) are superimposed on the contour map

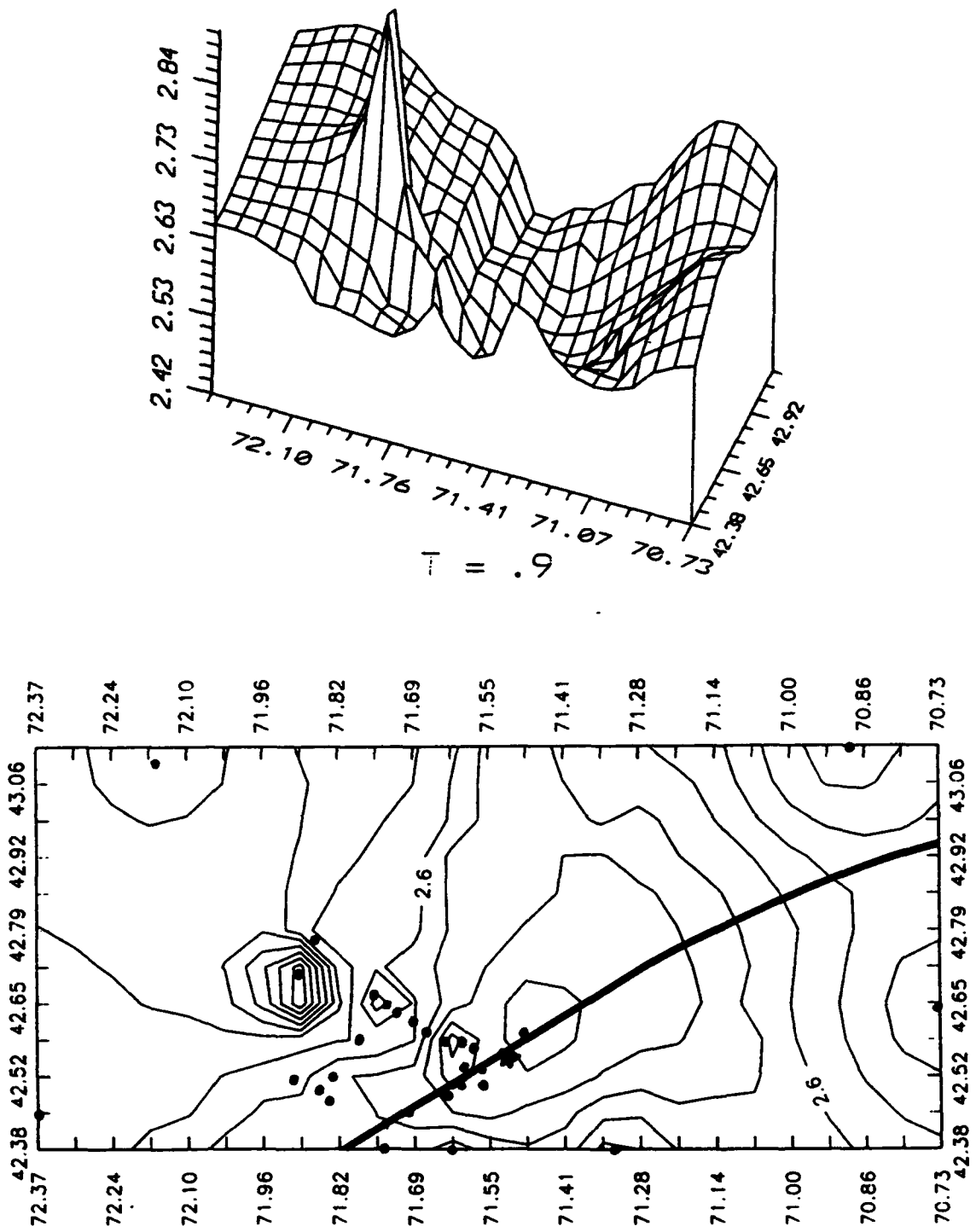

Figure 21 (c): Three dimensional plot and contour map of group velocity for Rg waves with a period of 0.9 seconds for the study area. The station array (dots) and the Clinton-Newbury fault (solid line) are superimposed on the contour map

6. DISCUSSION AND CONCLUSIONS

Figure 22 is a map of the study area showing the station array superimposed on the regional geology. It is significant to note that the general trend of the regional geologic structure as well as the trend of the Clinton-Newbury Fault Zone roughly parallels the trend of the lower group velocity zone that surrounds the San-Vel quarry. This figure shows which paths lie within this complex fault zone and which paths travel across solid bedrock. Comparing Figure 22 with Figure 20 shows that the area immediately surrounding the San-Vel quarry appears to be characterized by slower group velocities, probably because the bedrock is highly faulted and fractured. Group velocities seem to systematically increase with increasing distance from the fault zone, probably because the Rg waves spend more time traveling through solid bedrock than fractured bedrock. Therefore,it is concluded that based on the results of this study, the shallow crust beneath SNE and southern NH does indeed exhibit lateral variations in group velocity and those variations seem to correlate to some extent with the complex geologic structures of that area. A denser station spacing and/or shorter paths has successfully revealed more detail in lateral variation than has been observed from previous studies.

As long as there is an observable Rg wave on the seismogram, the quality with which a seismic event is recorded seems to have very little effect on the accuracy with which group velocities can be measured. This is most easily seen in Figures 18 and 19. It seems that if an Rg wave has been recorded, then a poor signal-to-noise ratio will not affect the group velocity curve that is extracted from the seismogram. However, it comes as no suprise that if Rg energy is absent from the seismogram to begin with, then all the filtering in the world will not produce a good group velocity curve.

Finally, the shallow crust beneath SNE and southern NH does not display significant lateral anisotropy as does the shallow crust in southeastern Maine.

References

Dollin, M (1985). The Use O Rg Waves To Constrain Crustal Velocity Structure In Connecticut, Master's Thesis, Dept. of Geology and Geophysics, Boston College, Chestnut Hill, Ma.

Dziewonski, A.M., S. Bloch and M.Landisman, (1969). A Technique for the analysis of transient seismic signals, Bull. Seis. Soc. Am., 59, pp. 427-444.

Gnewuch, S.C. (1987). Investigation of velocity and anelastic attenuation structures of the shallow crust in New England by time domain modeling of Rg waves, Master's Thesis, Dept. of Geology and Geophysics, Boston College, Chestnut Hill, Ma.

Hall, L M. and Robinson,P (1982). Stratigraphic-Tectonic Subdivisions of Southern New England, Major Structural Zones and Faults of the Northern Appalachians, Geological Association of Canada Special Paper 24, 1982.

Kafka, A.L. (1988) Earthquakes, Geology and Crustal Features in Southern New England, Seismological Research Letters, 59(4), 173 - 181.

Kafka, A.L. (1990). Rg as a Depth Discriminant for Earthquakes and Explosions: A Case Study in New England, Bull. Seis. Soc. Am., 80(2), 373 - 394.

Kafka, A.L. (1985). Source and path properties of Rg waves in New England (Abstract), Earthquake Notes, 56 (3), pp.73.

Kafka, A.L. and M.F. Dollin (1985). Constraints on lateral variation in upper crustal structure beneath southern New England from the dispersion of Rg waves, Geophys. Res. Lett., 12, pp.235-238.

Kafka, A.L. and J.W. McTigue (1985). The Avalonian Terrane and Merrimack Trough in southern New England: Similarities and differences in upper crustal structure determined from dispersion of Rg waves (Abstract), EOS Trans. Am. Geophys. Un.,66, pp.987.

Kafka A.L. and E. C. Reiter (1987) Dispersion of Rg waves in southeastern Maine : Evidence for lateral anisotropy in the shallow crust, Bull. Seis. Soc. Am., 77, pp. 925-941.

Lyons, J. B. (1982) The Avalonian and Gander Zones In Central Eastern New England,Major Structural Zones and Faults of the Northern Appalachians, Geological Association of Canada Special Paper 24,1982.

McEvilly, T.V. and Stauder , W. (1965). Effect of sedimentary thickness on short period Rayleigh wave dispersion, Geophysics, vol.30 (2),pp.198-203.

McTigue, J.W. (1986). Modeling upper crustal structure in southern New England using short period Rg waves, Master's Thesis, Dept. Geology and Geophysics, Boston College, Chestnut Hill, Ma.

Saikia, C.K., Kafka, A.L., and McTigue, J.W. (1986). Comparison between the synthesized and observed short-period Rg waves from quarry blasts (Abstract), EOS, Trans. Am. Geophys. Un., 67, pp. 313.

Saito, M. (1967), Excitation of free oscillations and surface waves by a point source in a vertically heterogeneous earth, J. Geophys. Res., vol.72,pp.3689-3699.

Skehan,S.J., J.W., Rast,N., and Mosher, S., (1986), Paleoenvironmental and Tectonic Controls of Sedimentation in Coal-Forming Basins of Southeastern New England, Geological Society of America Special Paper 210.

Skehan, S.J., J.W., and A.L. Kafka (1987). Correlations between geological terranes and shallow crustal structure in southern New England, International Geological Correlation Program (project 233, Terranes in the Circum-Atlantic Paleozoic Orogens), Nouakchott, Mauritania, December 8-11.

Skehan, S.J., J.W., and P.H. Osberg (1979). The Caledonides in the U.S.A., Internat. Geol. Corr. Prog. (IGCP), Project 27, Caledonide Orogen, Weston Observatory.

Taylor, S.R. and Toksoz, M.N. (1979). Three-dimensional crust and upper mantle structure of the northeastern United States, J. Geophys. Res., 84, pp. 7627-7644.

Tu, Zhiping (1990). A Study of Rg Wave Dispersion in New Hampshire and Vermont, Master's Thesis, Dept. Geology and Geophysics, Boston College, Chestnut Hill, MA.

Appendix A

Group Velocity Data

PERIOD	LC2	LC3	LC4	NSA1	NSA2	NSA3	NSB1	NSB2	NSB3	NSB4	NSB5
0.1	•	•	•	•	•	•	•	•	•	•	•
0.2	•	2.25	2.3	2.41	2.35	2.35	2.3	2.28	2.38	2.35	2.35
0.3	•	2.28	2.33	2.41	2.36	2.37	2.3	2.33	2.38	2.36	2.36
0.4	2.25	2.3	2.35	2.41	2.38	2.38	2.3	2.38	2.38	2.38	2.38
0.5	2.29	2.41	2.38	2.44	2.42	2.42	2.34	2.42	2.42	2.41	2.41
0.6	2.33	2.43	2.41	2.46	2.46	2.46	2.38	2.46	2.46	2.43	2.43
0.7	2.38	2.49	2.46	2.51	2.51	2.51	2.43	2.51	2.51	2.5	2.51
0.8	2.42	2.5	2.49	2.54	2.54	2.55	2.46	2.54	2.55	2.53	2.54
0.9	2.46	2.5	2.51	2.57	2.58	2.58	2.48	2.57	2.58	2.56	2.58
1	2.51	2.54	2.52	2.61	2.61	2.61	2.52	2.61	2.62	2.58	2.62
1.1	2.56	2.57	2.53	2.64	2.64	2.64	2.56	2.64	2.65	2.6	2.65
1.2	2.56	2.61	2.56	2.69	2.69	2.7	2.61	2.69	2.76	2.71	2.69
1.3	2.57	2.67	2.59	2.72	2.73	2.72	2.63	2.72	2.78	2.73	2.71
1.4	2.57	2.67	2.62	2.72	2.73	2.74	2.65	2.75	2.81	2.76	2.73
1.5	2.58	2.72	2.65	2.76	2.76	2.76	2.66	2.77	2.83	2.79	2.75
1.6	2.64	2.78	2.7	2.8	2.8	2.8	2.69	2.83	2.83	2.82	2.79
1.7	2.69	2.84	2.75	2.84	2.84	2.84	2.72	2.88	2.84	2.84	2.82
1.8	2.72	2.86	2.79	2.85	2.85	2.85	2.73	2.89	2.84	2.84	2.82
1.9	2.74	2.87	2.82	2.86	2.86	2.86	2.74	2.9	2.84	2.84	2.83
2	•	•	•	•	•	•	•	•	•	•	•
2.1	•	•	•	•	•	•	•	•	•	•	•
2.2	•	•	•	•	•	•	•	•	•	•	•
2.3	•	•	•	•	•	•	•	•	•	•	•
2.4	•	•	•	•	•	•	•	•	•	•	•

PERIOD	AZ1	AZ2	AZ3	AZ4	P102	P103	P107	P110	P112	P113	P115
0.1	•	•	•	•	•	•	•	•	•	•	•
0.2	2.25	2.39	2.3	2.41	•	2.41	2.38	2.46	2.38	2.33	2.23
0.3	2.26	2.44	2.3	2.38	•	2.4	2.4	2.46	2.38	2.35	2.28
0.4	2.28	2.48	2.3	2.35	•	2.37	2.41	2.46	2.38	2.38	2.33
0.5	2.37	2.53	2.31	2.34	•	2.34	2.41	2.46	2.4	2.39	2.36
0.6	2.46	2.57	2.33	2.33	2.34	2.31	2.41	2.46	2.41	2.41	2.38
0.7	2.48	2.58	2.58	2.61	2.36	2.28	2.56	2.56	2.43	2.48	2.48
0.8	2.54	2.62	2.57	2.65	2.49	2.26	2.62	2.67	2.5	2.56	2.55
0.9	2.59	2.66	2.56	2.69	2.62	2.24	2.67	2.75	2.56	2.64	2.61
1	2.6	2.81	2.56	2.69	2.73	2.25	2.72	2.79	2.66	2.7	2.64
1.1	2.61	2.96	2.56	2.7	2.83	2.26	2.77	2.82	2.76	2.76	2.66
1.2	2.64	2.97	2.58	2.71	2.9	2.25	2.82	2.84	2.82	2.84	2.71
1.3	2.64	2.97	2.6	2.72	2.93	2.27	2.84	2.85	2.84	2.84	2.73
1.4	2.65	2.98	2.62	2.73	2.95	2.3	2.87	2.86	2.85	2.85	2.74
1.5	2.65	2.98	2.64	2.74	2.97	2.33	2.89	2.87	2.87	2.86	2.76
1.6	2.65	2.96	2.65	2.74	2.96	2.37	2.88	2.83	2.88	2.86	2.79
1.7	2.65	2.94	2.66	2.75	3	2.41	2.87	2.79	2.89	2.87	2.82
1.8	2.64	2.91	2.68	2.73	3.01	2.4	2.86	2.73	2.9	2.87	2.82
1.9	2.64	2.88	2.69	2.72	3.02	2.38	2.84	2.67	2.91	2.87	2.82
2	•	•	•	•	•	•	•	•	•	•	•
2.1	•	•	•	•	•	•	•	•	•	•	•
2.2	•	•	•	•	•	•	•	•	•	•	•
2.3	•	•	•	•	•	•	•	•	•	•	•
2.4	•	•	•	•	•	•	•	•	•	•	•

PERIOD	CLIA	WES	87202-GLO	87210-GLO	88089-GLO	87202-DNH	87210-DNH	88089-DNH
0.1	.	.	.	.	.	.	.	.
0.2	2.35	2.33	2.58	2.69	2.61	2.7	2.46	2.56
0.3	2.44	2.42	2.61	2.67	2.59	2.7	2.49	2.56
0.4	2.53	2.51	2.64	2.66	2.58	2.7	2.51	2.56
0.5	2.53	2.51	2.65	2.68	2.58	2.7	2.58	2.63
0.6	2.53	2.51	2.65	2.7	2.58	2.7	2.64	2.69
0.7	2.55	2.53	2.66	2.71	2.58	2.7	2.67	2.7
0.8	2.56	2.54	2.73	2.72	2.67	2.7	2.69	2.71
0.9	2.56	2.56	2.79	2.74	2.76	2.73	2.77	2.72
1	2.57	2.58	2.83	2.75	2.78	2.76	2.84	2.74
1.1	2.58	2.61	2.87	2.76	2.79	2.76	2.85	2.82
1.2	2.58	2.64	2.87	2.76	2.79	2.76	2.87	2.89
1.3	2.57	2.64	2.87	2.75	2.79	2.84	2.87	2.89
1.4	2.57	2.64	2.87	2.75	2.79	2.91	2.87	2.89
1.5	2.56	2.64	2.87	2.75	2.81	2.94	2.87	2.9
1.6	2.53	2.62	2.87	2.74	2.82	2.97	2.87	2.9
1.7	2.51	2.6	2.87	2.73	2.82	2.97	2.86	2.91
1.8	2.42	2.58	2.87	2.7	2.83	2.97	2.85	2.91
1.9	2.33	2.55	2.87	2.69	2.84	2.97	2.84	2.92
2	.	.	2.87	2.66	2.87	2.97	2.84	2.82
2.1	.	.	2.87	2.65	2.87	.	.	.
2.2	.	.	2.87	2.64	2.87	.	.	.
2.3	.	.	.	.	.	.	.	.
2.4	.	.	.	.	.	.	.	.

PERIOD	88089-PNH	38089-UXB	QUA	WES	WFM-202	WFM-089
0.1	•	•	•	•	2.39	2.35
0.2	2.53	2.21	•	2.57	2.46	2.35
0.3	2.64	•	•	2.41	2.54	2.39
0.4	2.74	2.16	•	2.49	2.3	2.4
0.5	2.72	•	2.48	2.49	2.06	2.41
0.6	2.71	2.21	2.55	2.49	2.14	2.32
0.7	2.78	•	2.6	2.53	2.2	2.41
0.8	2.84	2.32	2.63	2.57	2.24	2.52
0.9	2.84	•	2.65	2.66	2.28	2.62
1	2.84	2.37	2.68	2.68	2.28	2.71
1.1	2.83	•	2.74	•	2.28	2.99
1.2	2.82	2.53	2.79	•	2.31	2.99
1.3	2.79	•	2.8	•	2.33	3
1.4	2.76	2.59	2.74	•	2.43	3
1.5	2.75	•	2.73	•	2.54	•
1.6	2.74	2.59	2.72	•	2.72	•
1.7	2.73	•	2.75	•	2.89	•
1.8	2.72	2.64	2.62	•	•	•
1.9	2.72	•	2.62	•	•	•
2	2.71	2.64	•	•	•	•
2.1	•	•	•	•	•	•
2.2	•	•	•	•	•	•
2.3	•	•	•	•	•	•
2.4	•	•	•	•	•	•

PERIOD	NW01-192	NW01-213	NW02-192	NW03-208	NW03-213	NW04-208
0.1	2.57	2.49	2.53	2.61	2.60	
0.2	2.55	2.46	2.68	2.39	2.41	2.49
0.3	2.54	2.46	2.83	2.31	2.21	2.50
0.4	2.54	2.42	2.42	2.23	2.21	2.50
0.5	2.50	2.40	2.48	2.37	2.25	2.51
0.6	2.57	2.37	2.53	2.35	2.26	2.53
0.7	2.54	2.46	2.55	2.35	2.26	2.54
0.8	2.54	2.49	2.58	2.35	2.26	2.54
0.9	2.51	2.54	2.59	2.44	2.26	2.62
1	2.54	2.64	2.69	2.63	2.26	2.70
1.1	2.55	2.70	2.76	2.73	2.15	2.79
1.2	2.58	2.77	2.76	2.95	2.15	2.83
1.3	2.60	2.81	2.76	3.05	2.02	2.87
1.4	2.74	2.78	2.77	•	2.02	2.90
1.5	2.88	2.75	2.81	•	2.02	2.92
1.6	3.02	2.70	2.84	•	•	2.90
1.7	3.14	2.67	2.85	•	•	2.87
1.8	•	•	•	•	•	2.81
1.9	•	•	•	•	•	2.71
2	•	•	•	•	•	2.65
2.1	•	•	•	•	•	•
2.2	•	•	•	•	•	•
2.3	•	•	•	•	•	•
2.4	•	•	•	•	•	•

PERIOD	NW04-213	NW05-208	NW05-213	NW06-192	NW07-213	NW08-213
0.1						
0.2	2.54	2.44			2.41	2.41
0.3	2.54	2.44			2.41	2.42
0.4	2.54	2.44		2.46	2.43	2.44
0.5	2.54	2.44		2.49	2.44	2.45
0.6	2.54	2.44	2.48	2.51	2.43	2.45
0.7	2.56	2.52	2.49	2.54	2.48	2.46
0.8	2.60	2.60	2.51	2.57	2.52	2.48
0.9	2.65	2.74	2.57	2.60	2.59	2.53
1	2.68	2.76	2.58	2.63	2.60	2.58
1.1	2.72	2.80	2.60	2.66	2.62	2.61
1.2	2.74	2.80	2.60	2.68	2.62	2.63
1.3	2.75	2.80	2.62	2.70	2.64	2.64
1.4	2.78	2.75	2.64	2.70	2.64	2.64
1.5	2.79	2.72	2.65	2.70	2.64	2.64
1.6	2.80	2.61	2.66	2.75	2.64	2.64
1.7	2.81	2.51	2.67	2.80	2.66	2.64
1.8	2.80	•	2.69	2.83	2.69	2.66
1.9	2.76	•	2.71	2.86	2.71	2.67
2	2.74	•	2.73	2.88	2.73	•
2.1	•	•	•	•	•	•
2.2	•	•	•	•	•	•
2.3	•	•	•	•	•	•
2.4	•	•	•	•	•	•

PERIOD	NW10-192	NW10-213	NW11-213	WFM-213	WFM-177	GLO-177
0.1						
0.2	2.68	2.53	2.59	2.24		2.56
0.3	2.78	2.58	2.54	2.17	2.38	2.56
0.4	2.89	2.61	2.49	2.07	2.26	2.57
0.5	2.94	2.76	2.49	2.17	2.25	2.58
0.6	3.00	2.90	2.49	2.20	2.23	2.59
0.7	3.04	2.96	2.49	2.22	2.33	2.60
0.8	3.07	3.01	2.49	2.27	2.42	2.67
0.9	3.12	3.06	2.55	2.31	2.50	2.73
1	3.16	3.09	2.60	2.31	2.55	2.74
1.1	3.20	3.14	2.64	2.26	2.59	2.75
1.2	•	3.17	2.67	2.21	•	2.76
1.3	•	3.20	2.69	2.17	•	2.77
1.4	•	3.22	2.71	2.11	•	2.78
1.5	•	3.24	2.72	2.05	•	2.78
1.6	•	3.24	2.73	•	•	2.78
1.7	•	3.24	2.74	•	•	2.79
1.8	•	3.23	2.73	•	•	2.80
1.9	•	3.23	•	•	•	2.81
2	•	•	•	•	•	2.81
2.1	•	•	•	•	•	2.82
2.2	•	•	•	•	•	2.83
2.3	•	•	•	•	•	•
2.4	•	•	•	•	•	•

PERIOD	GLO-192	GLO-213	DNH-177	PNH-192
0.1				
0.2	2.63	2.61	2.53	2.28
0.3	2.63	2.61	2.61	2.39
0.4	2.63	2.61	2.69	2.49
0.5	2.63	2.62	2.70	2.50
0.6	2.63	2.62	2.71	2.51
0.7	2.63	2.63	2.71	2.55
0.8	2.63	2.63	2.71	2.59
0.9	2.63	2.63	2.74	2.60
1	2.63	2.64	2.76	2.61
1.1	2.63	2.66	2.79	2.62
1.2	2.69	2.72	2.82	2.63
1.3	2.75	2.79	2.83	2.63
1.4	2.85	2.91	2.84	2.63
1.5	2.89	2.91	2.85	2.63
1.6	2.93	2.91	2.86	2.63
1.7	2.94	2.90	2.86	2.62
1.8	2.96	2.88	2.87	2.60
1.9	2.98	2.87	2.88	2.59
2	3.03	2.86	2.88	2.57
2.1	3.08	2.86	•	2.56
2.2	3.13	2.86	•	•
2.3	•	•	•	•
2.4	•	•	•	•

Appendix B

Group Velocity Curves

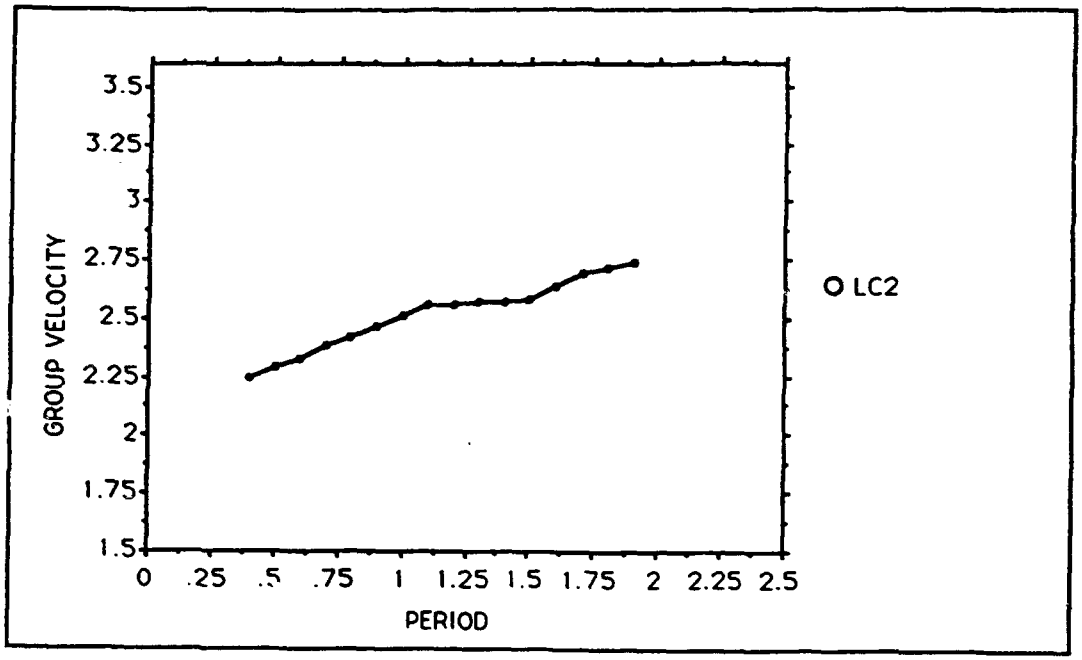
GROUP VELOCITY
3.5
3.25
3
2.75
2.5
2.25
2
1.75
1.5
0 .25 .5 .75 1 1.25 1.5 1.75 2 2.25 2.5
PERIOD
O LC2

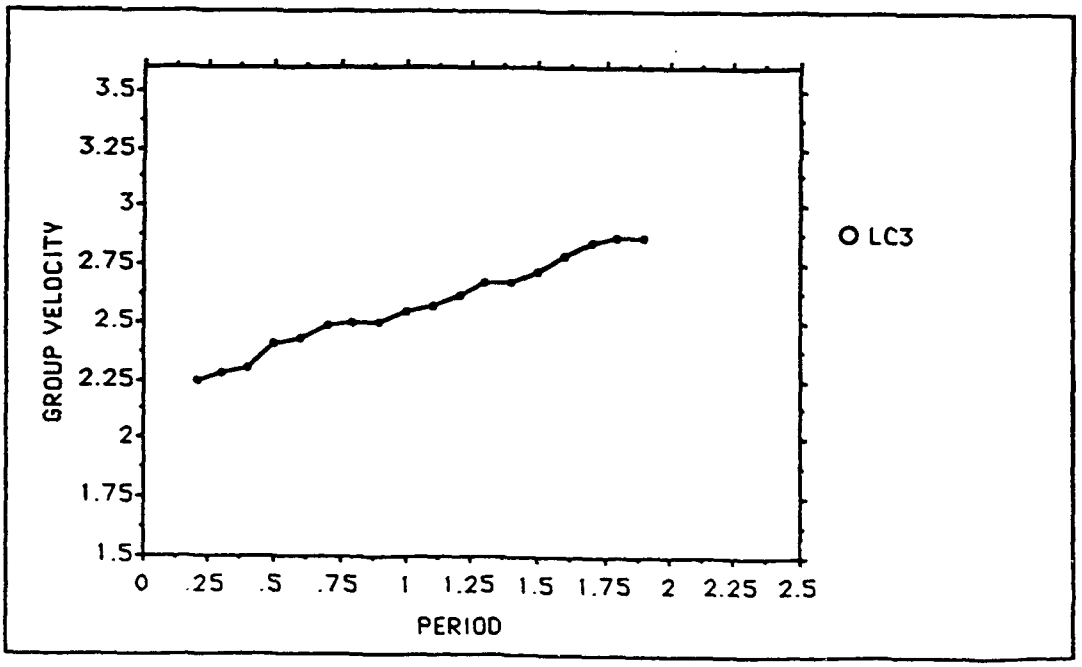
GROUP VELOCITY
3.5
3.25
3
2.75
2.5
2.25
2
1.75
1.5
0 .25 .5 .75 1 1.25 1.5 1.75 2 2.25 2.5
PERIOD
O LC3

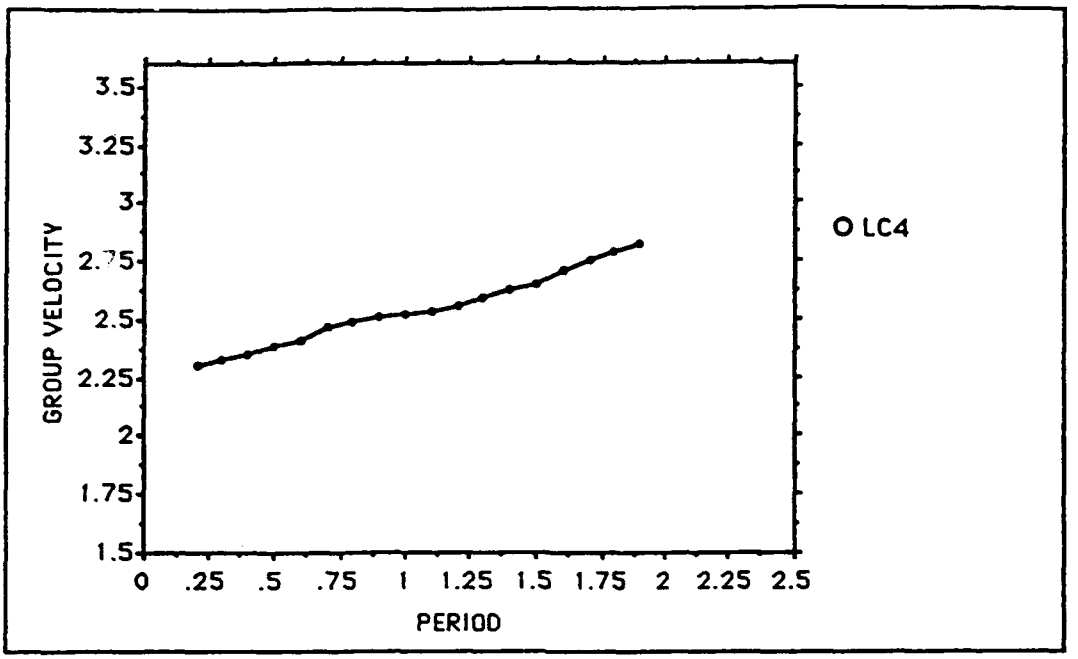
GROUP VELOCITY
3.5
3.25
3
2.75
2.5
2.25
2
1.75
1.5
0 .25 .5 .75 1 1.25 1.5 1.75 2 2.25 2.5
PERIOD
O LC4

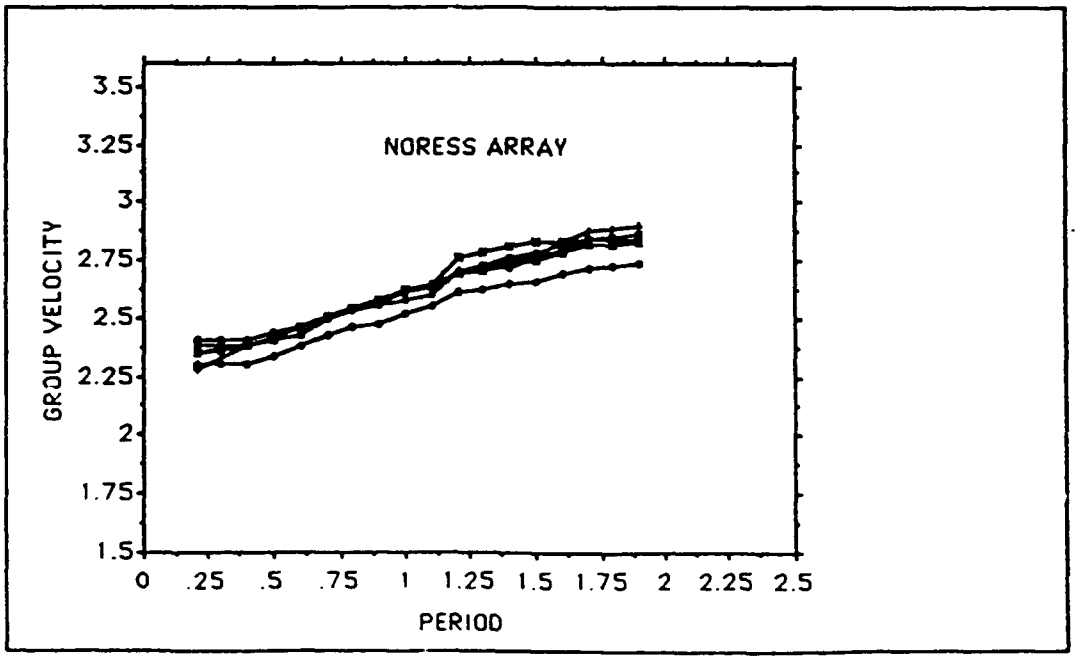
NORESS ARRAY
GROUP VELOCITY
3.5
3.25
3
2.75
2.5
2.25
2
1.75
1.5
0 .25 .5 .75 1 1.25 1.5 1.75 2 2.25 2.5
PERIOD

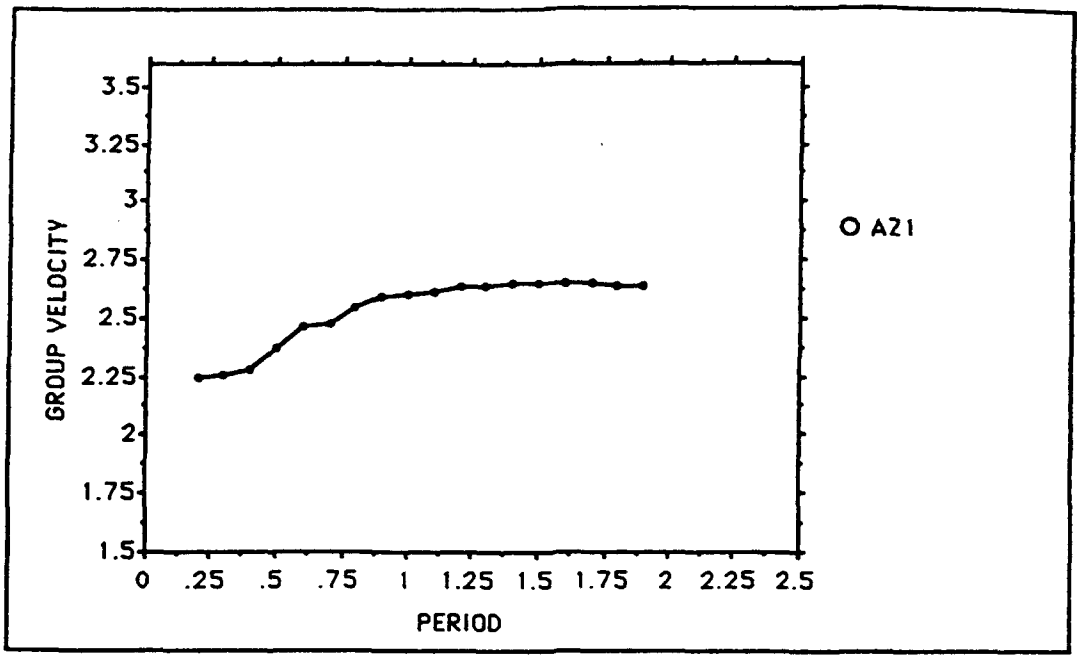
GROUP VELOCITY
3.5
3.25
3
2.75
2.5
2.25
2
1.75
1.5
0 .25 .5 .75 1 1.25 1.5 1.75 2 2.25 2.5
PERIOD
O AZ1

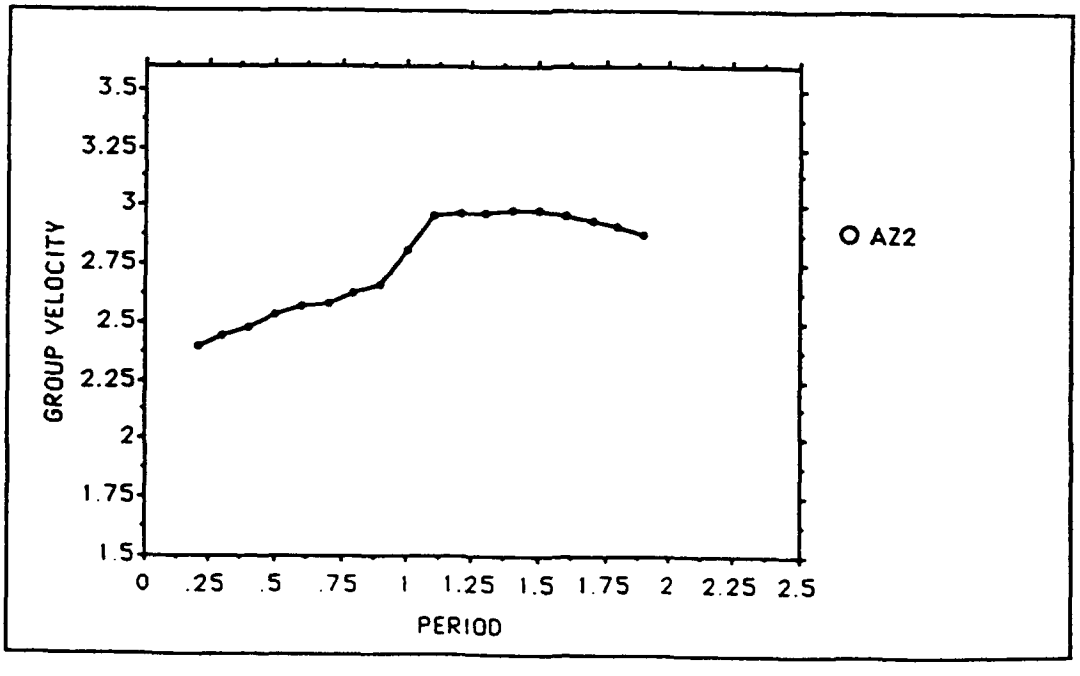
GROUP VELOCITY
3.5
3.25
3
2.75
2.5
2.25
2
1.75
1.5
0 .25 .5 .75 1 1.25 1.5 1.75 2 2.25 2.5
PERIOD
O AZ2

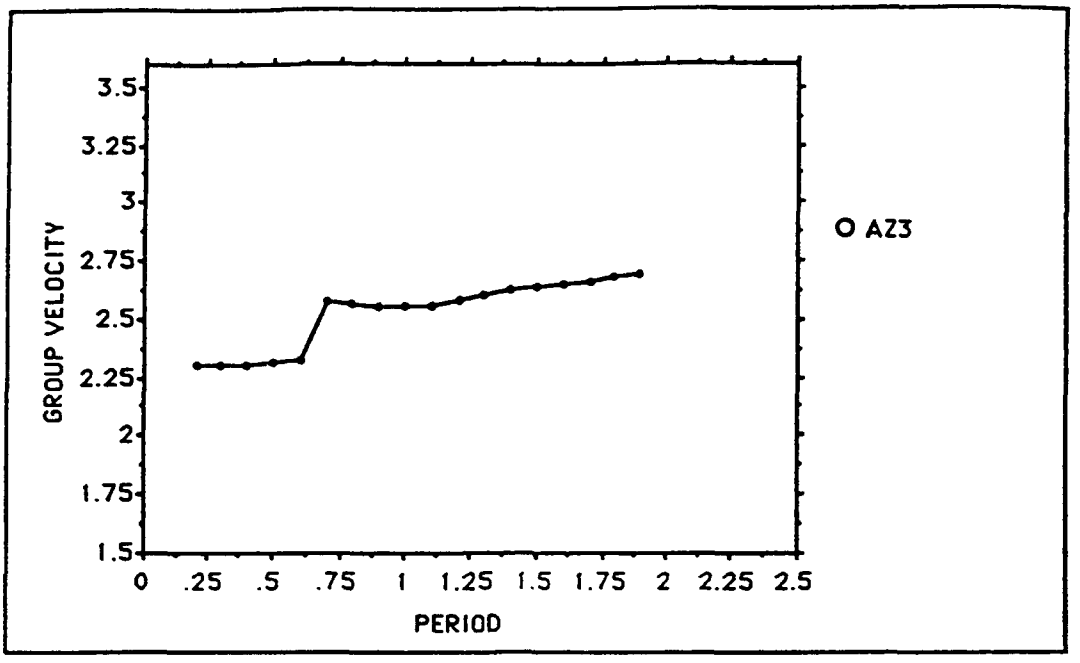
GROUP VELOCITY
3.5
3.25
3
2.75
2.5
2.25
2
1.75
1.5
0 .25 .5 .75 1 1.25 1.5 1.75 2 2.25 2.5
PERIOD
O AZ3

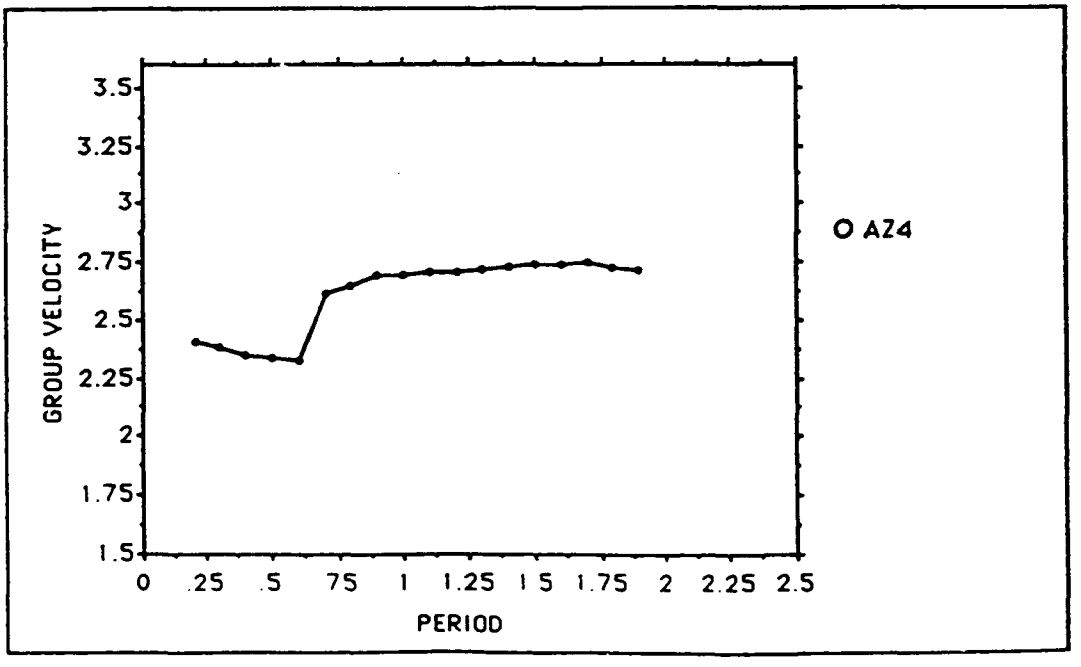
GROUP VELOCITY
3.5
3.25
3
2.75
2.5
2.25
2
1.75
1.5
0 .25 .5 75 1 1.25 1 5 1.75 2 2.25 2.5
PERIOD
O AZ4

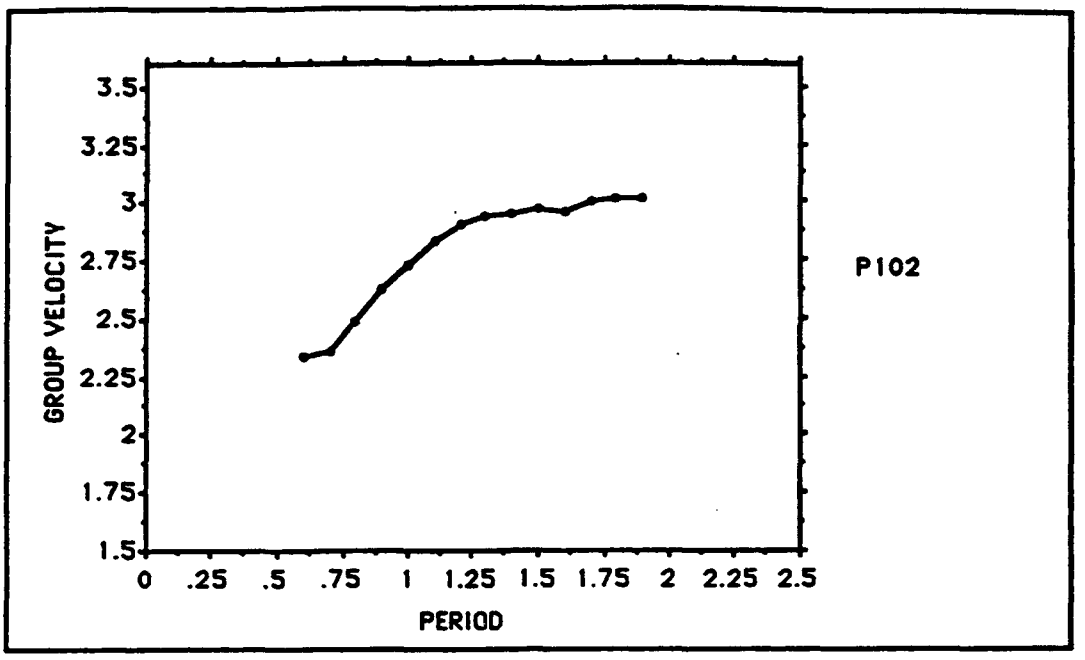
GROUP VELOCITY
3.5
3.25
3
2.75
2.5
2.25
2
1.75
1.5
0 .25 .5 .75 1 1.25 1.5 1.75 2 2.25 2.5
PERIOD
P102

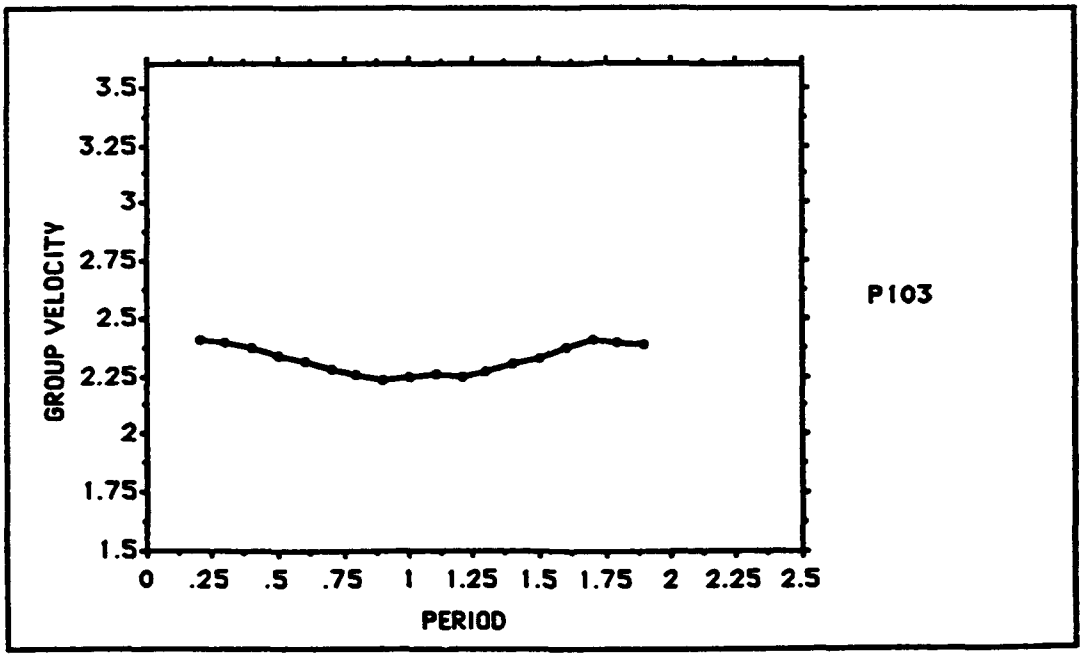
GROUP VELOCITY
3.5
3.25
3
2.75
2.5
2.25
2
1.75
1.5
0 .25 .5 .75 1 1.25 1.5 1.75 2 2.25 2.5
PERIOD
P103

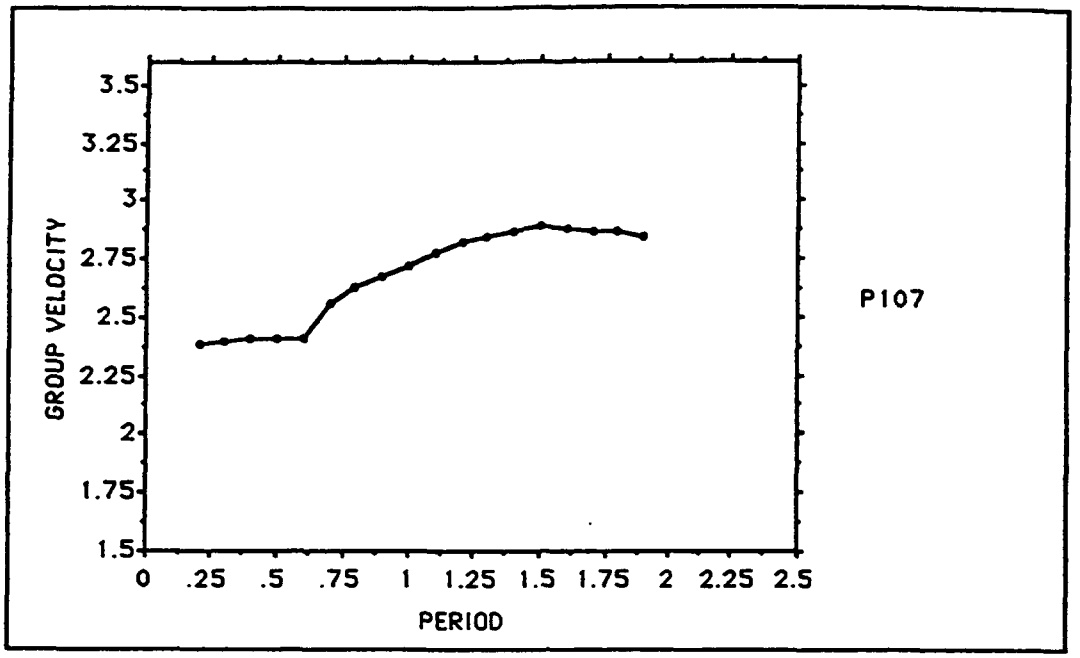
GROUP VELOCITY
3.5
3.25
3
2.75
2.5
2.25
2
1.75
1.5
0 .25 .5 .75 1 1.25 1.5 1.75 2 2.25 2.5
PERIOD
P107

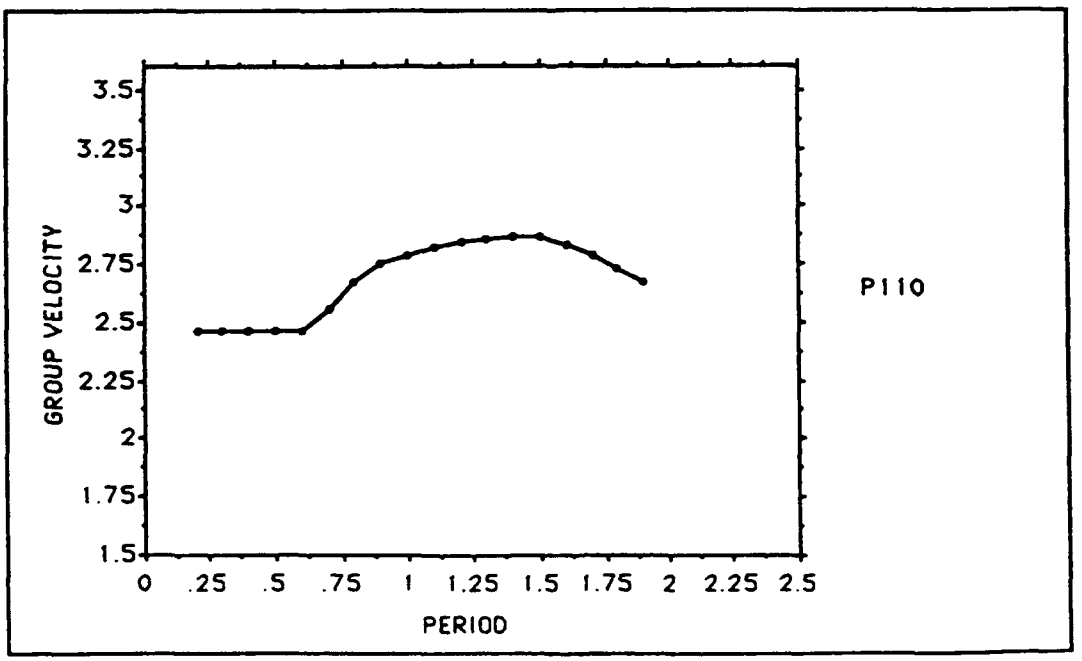
GROUP VELOCITY
3.5
3.25
3
2.75
2.5
2.25
2
1.75
1.5
0 .25 .5 .75 1 1.25 1.5 1.75 2 2.25 2.5
PERIOD
P110

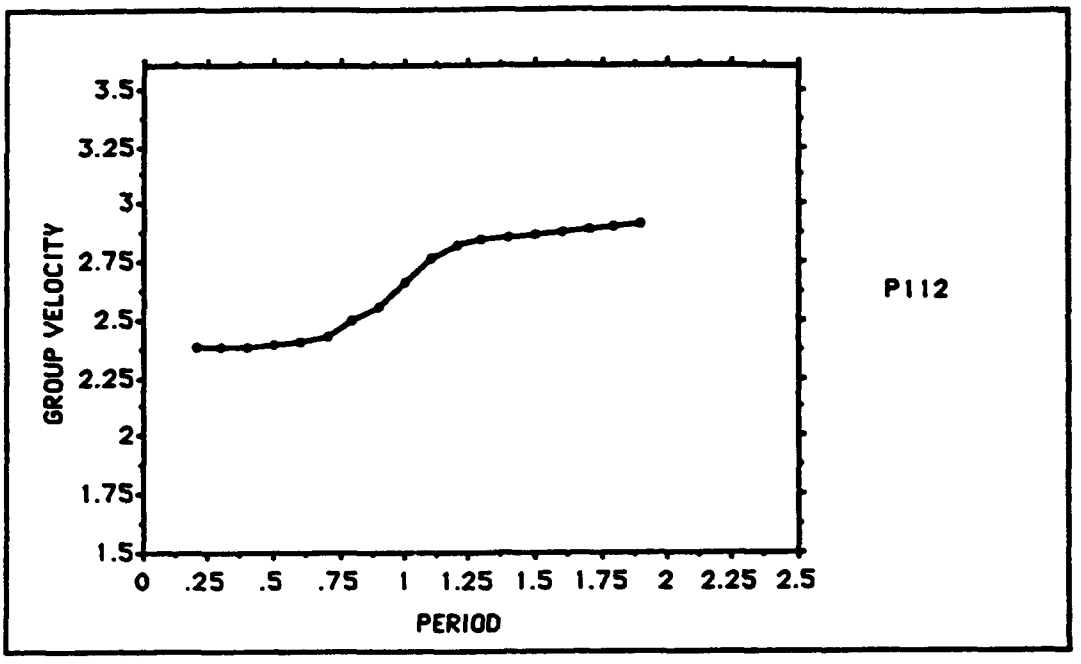
GROUP VELOCITY
3.5
3.25
3
2.75
2.5
2.25
2
1.75
1.5
0 .25 .5 .75 1 1.25 1.5 1.75 2 2.25 2.5
PERIOD
P112

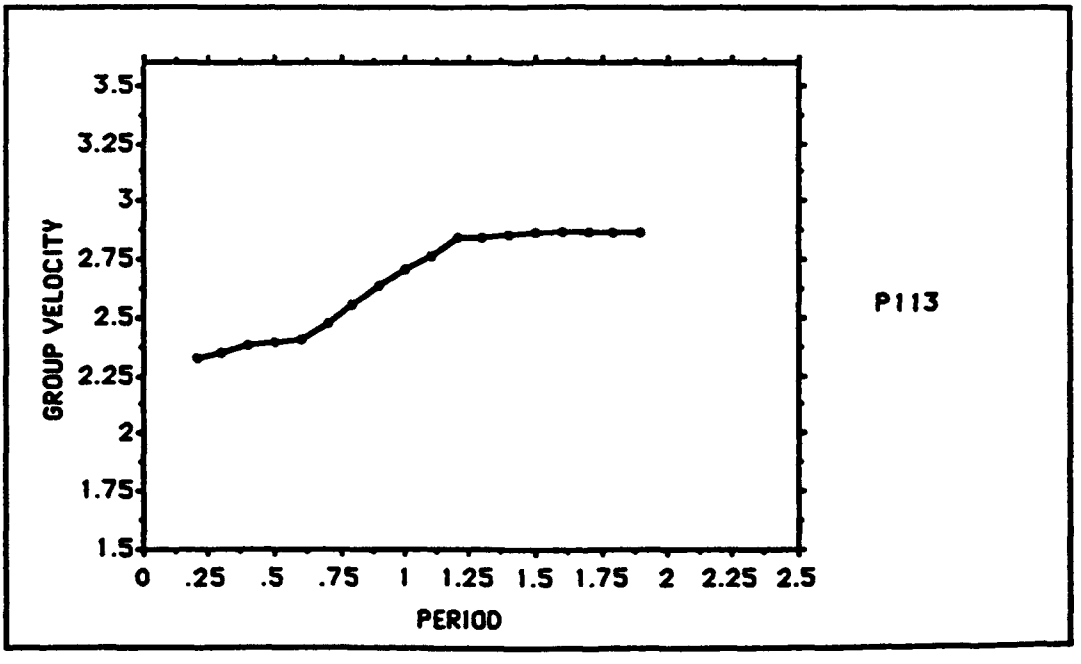
GROUP VELOCITY
3.5
3.25
3
2.75
2.5
2.25
2
1.75
1.5
0 .25 .5 .75 1 1.25 1.5 1.75 2 2.25 2.5
PERIOD
P113

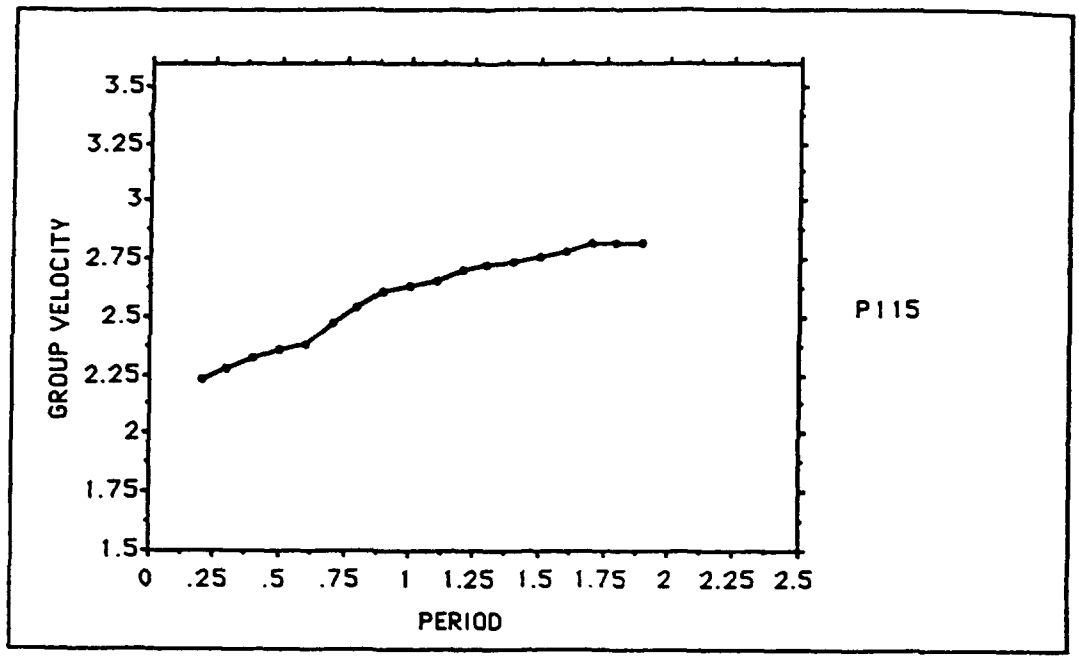
GROUP VELOCITY
3.5
3.25
3
2.75
2.5
2.25
2
1.75
1.5
0 .25 .5 .75 1 1.25 1.5 1.75 2 2.25 2.5
PERIOD
P115

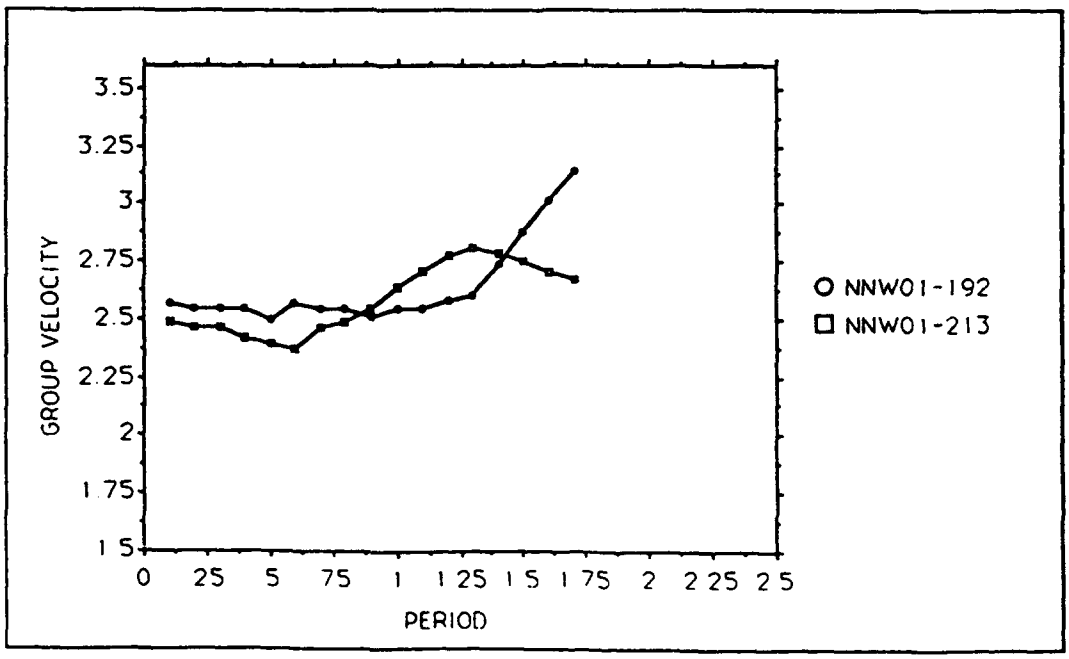
GROUP VELOCITY
3.5
3.25
3
2.75
2.5
2.25
2
1.75
1.5
0 25 5 75 1 1 25 1 5 1 75 2 2 25 2 5
PERIOD
O NNW01-192
□ NNW01-213

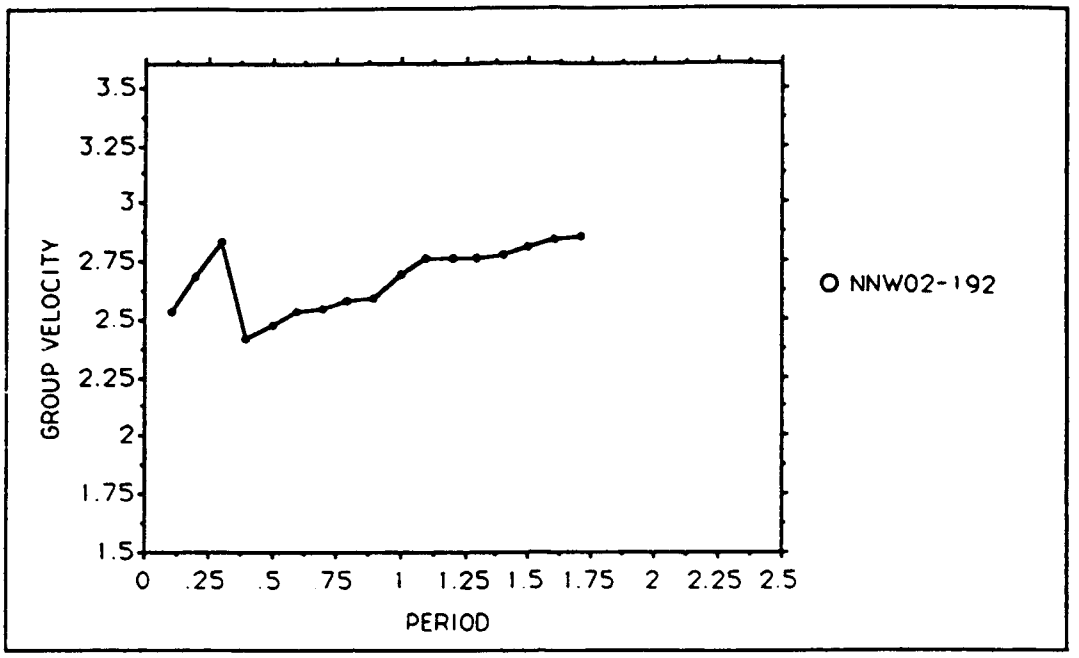
GROUP VELOCITY
3.5
3.25
3
2.75
2.5
2.25
2
1.75
1.5
0 .25 .5 .75 1 1.25 1.5 1.75 2 2.25 2.5
PERIOD
O NNW02-192

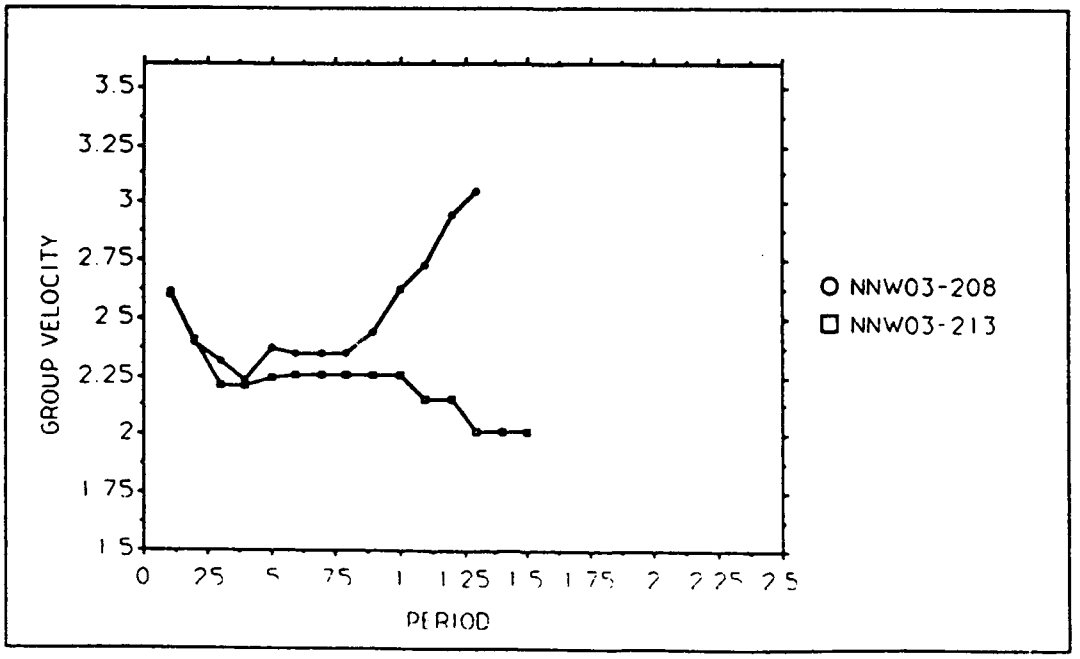
GROUP VELOCITY
3.5
3.25
3
2.75
2.5
2.25
2
1.75
1.5
PERIOD
O NNW03-208
□ NNW03-213

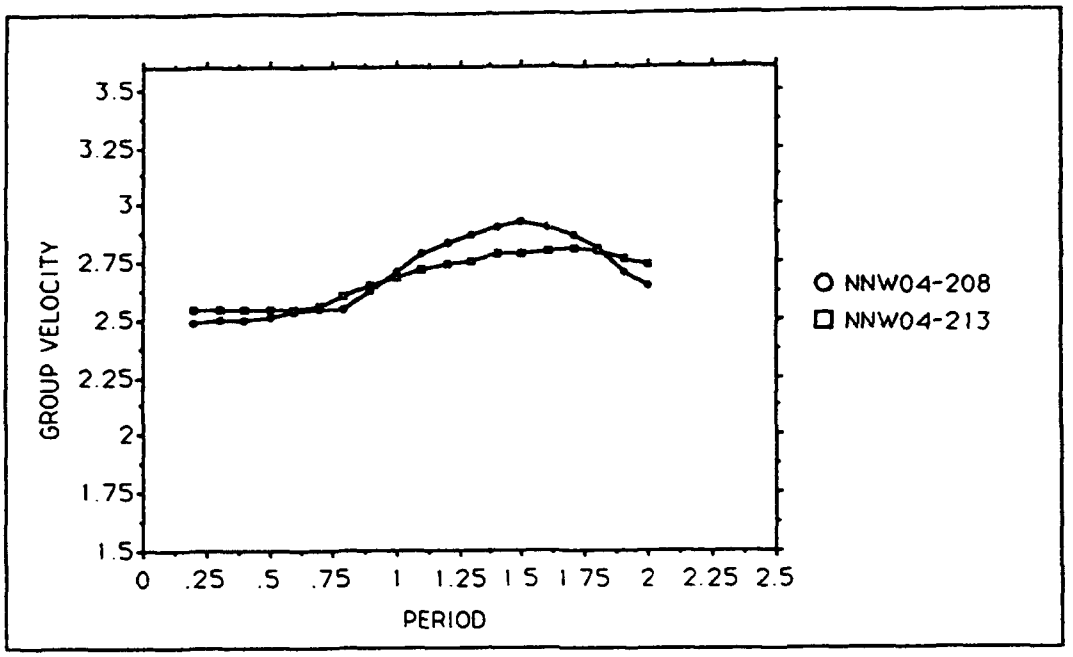
GROUP VELOCITY
3.5
3.25
3
2.75
2.5
2.25
2
1.75
1.5
0 .25 .5 .75 1 1.25 1.5 1.75 2 2.25 2.5
PERIOD
O NNW04-208
□ NNW04-213

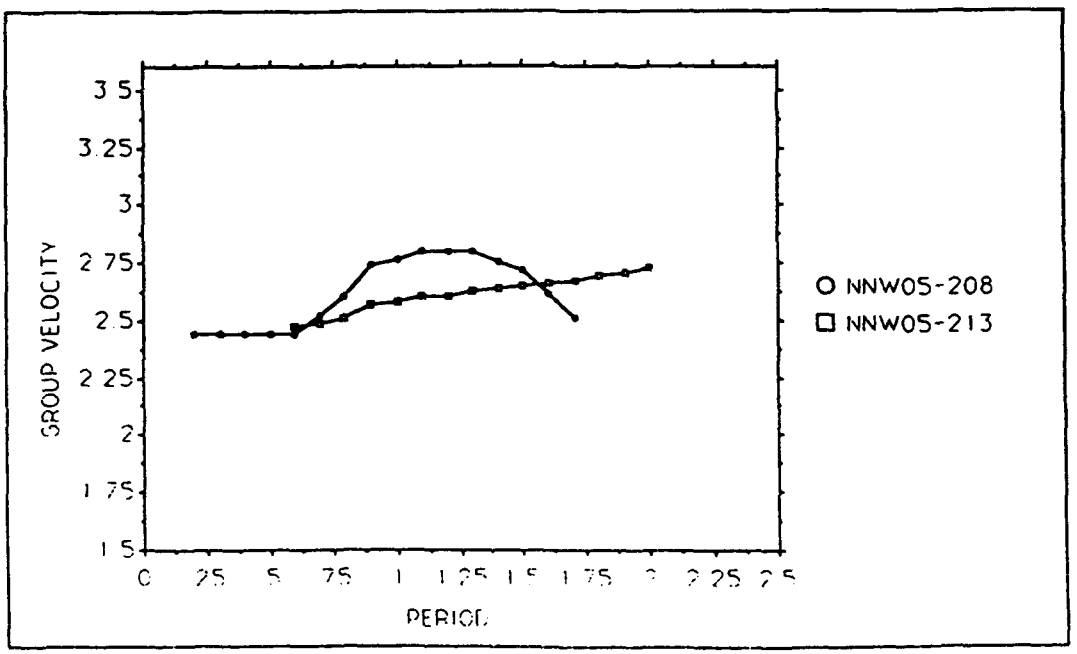
GROUP VELOCITY
3.5
3.25
3
2.75
2.5
2.25
2
1.75
1.5
PERIOD
O NNW05-208
□ NNW05-213

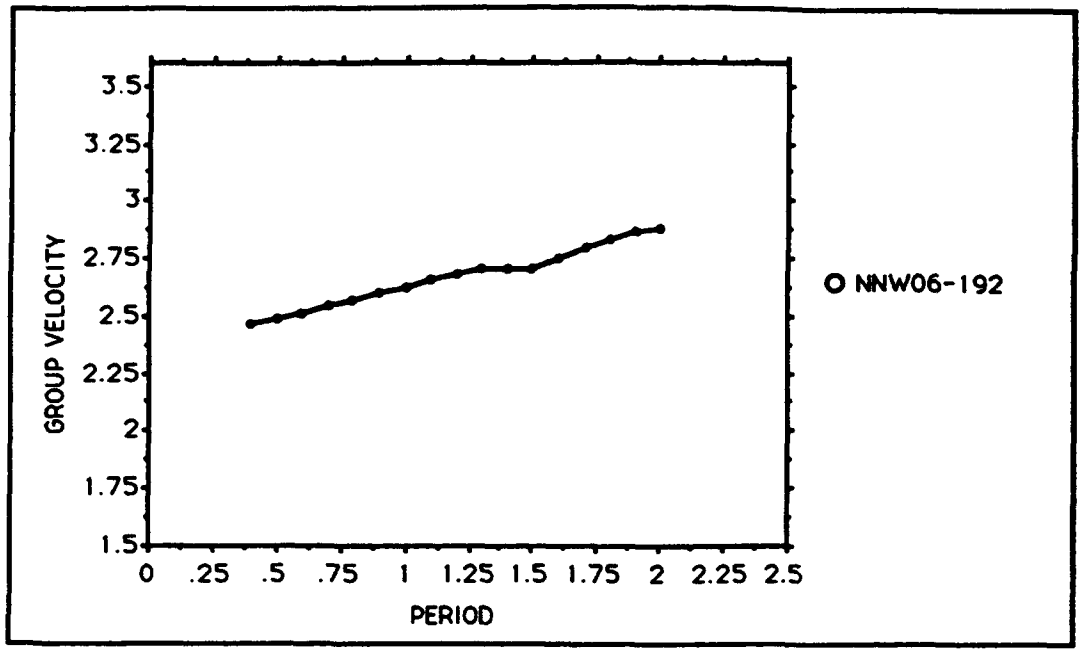
GROUP VELOCITY
3.5
3.25
3
2.75
2.5
2.25
2
1.75
1.5
0 .25 .5 .75 1 1.25 1.5 1.75 2 2.25 2.5
PERIOD
O NNW06-192

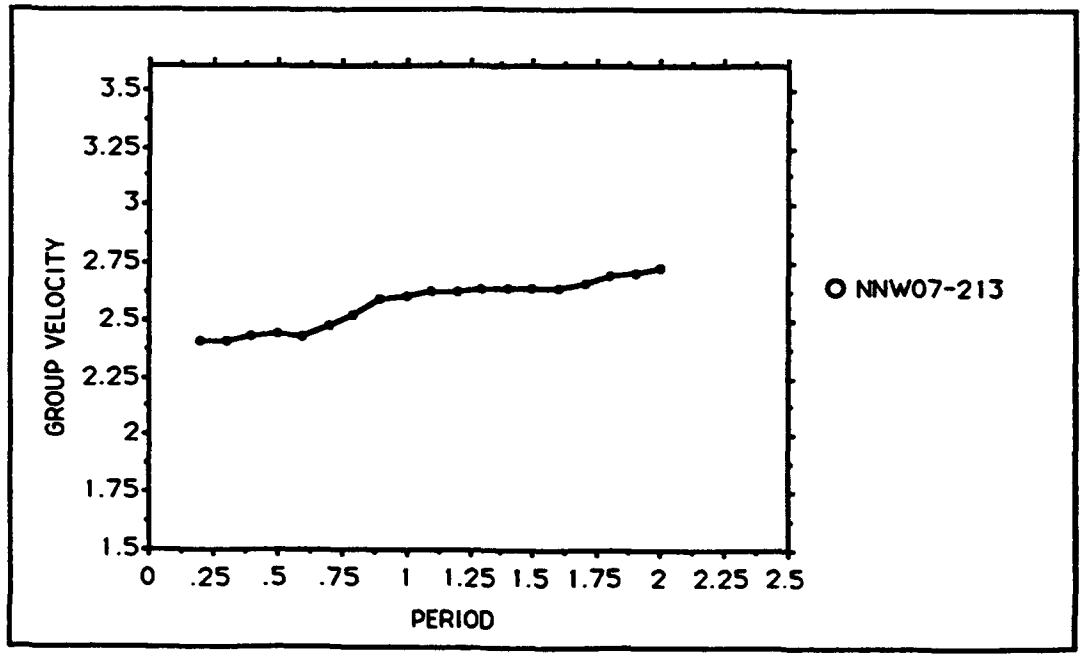
GROUP VELOCITY
3.5
3.25
3
2.75
2.5
2.25
2
1.75
1.5
0 .25 .5 .75 1 1.25 1.5 1.75 2 2.25 2.5
PERIOD
O NNW07-213

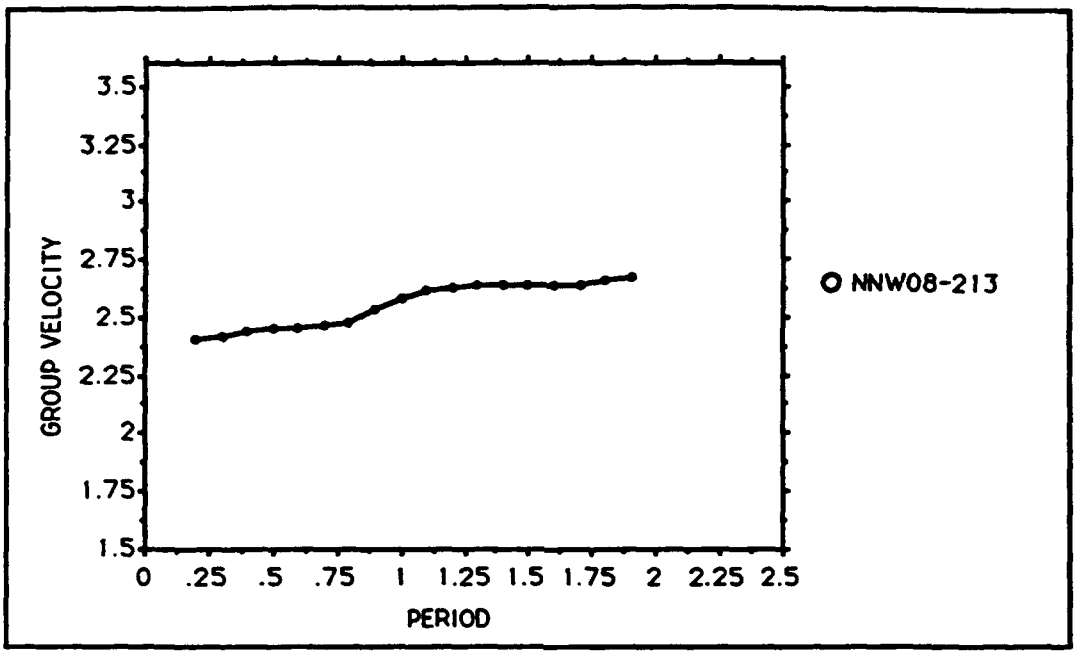
GROUP VELOCITY
3.5
3.25
3
2.75
2.5
2.25
2
1.75
1.5
0 .25 .5 .75 1 1.25 1.5 1.75 2 2.25 2.5
PERIOD
O NNW08-213

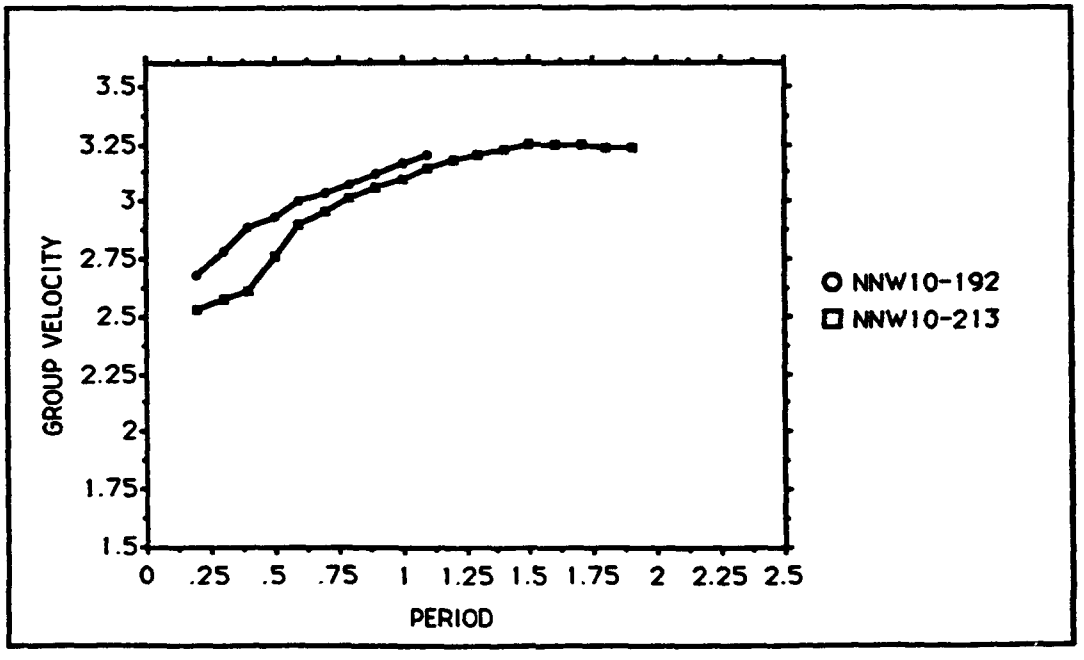
GROUP VELOCITY
3.5
3.25
3
2.75
2.5
2.25
2
1.75
1.5
0 .25 .5 .75 1 1.25 1.5 1.75 2 2.25 2.5
PERIOD
O NNW10-192
□ NNW10-213

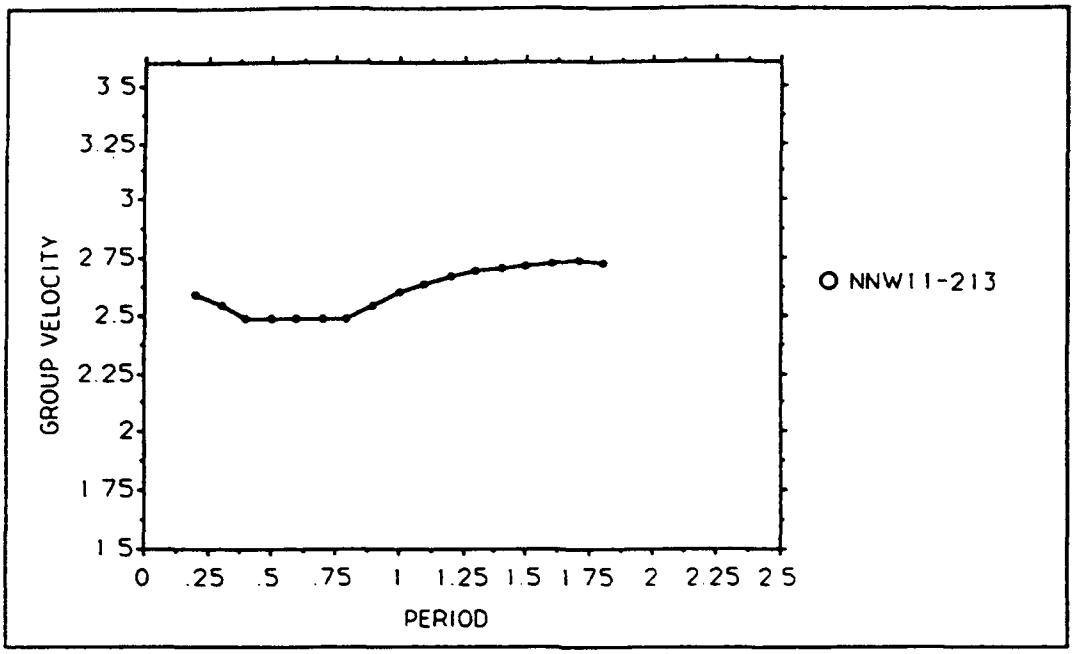
GROUP VELOCITY
3 5
3.25
3
2 75
2.5
2.25
2
1 75
1 5
0 .25 .5 .75 1 1.25 1.5 1 75 2 2.25 2 5
PERIOD
O NNW11-213

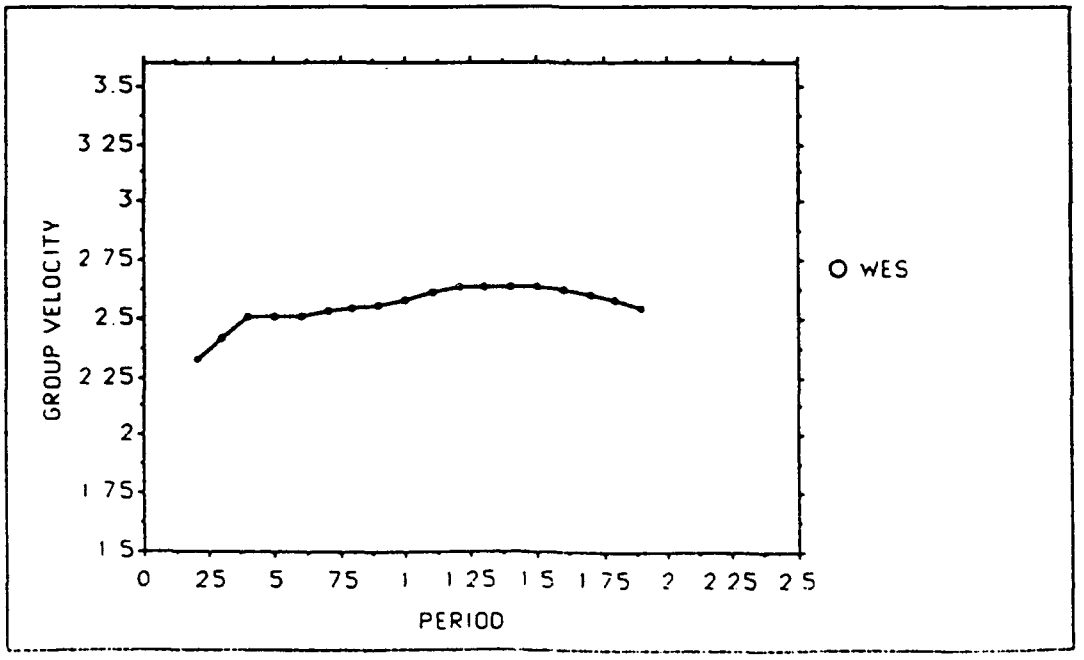
GROUP VELOCITY
3.5
3 25
3
2 75
2.5
2 25
2
1 75
1 5
0 25 5 75 1 1 25 1 5 1 75 2 2 25 2 5
PERIOD
O WES

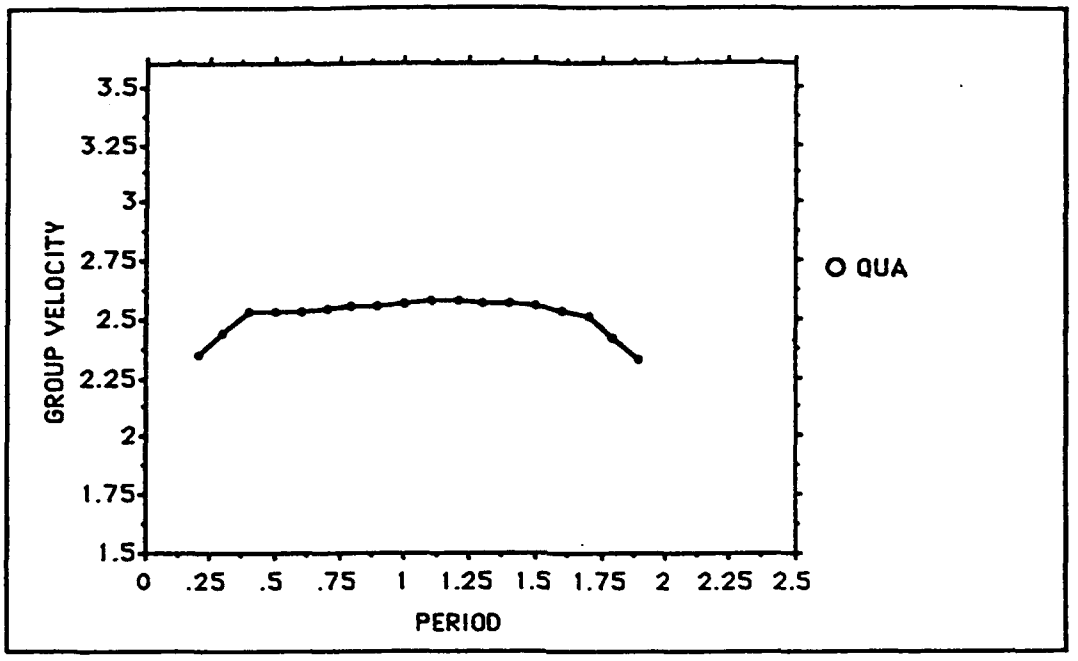
GROUP VELOCITY
3.5
3.25
3
2.75
2.5
2.25
2
1.75
1.5
0 .25 .5 .75 1 1.25 1.5 1.75 2 2.25 2.5
PERIOD
O QUA

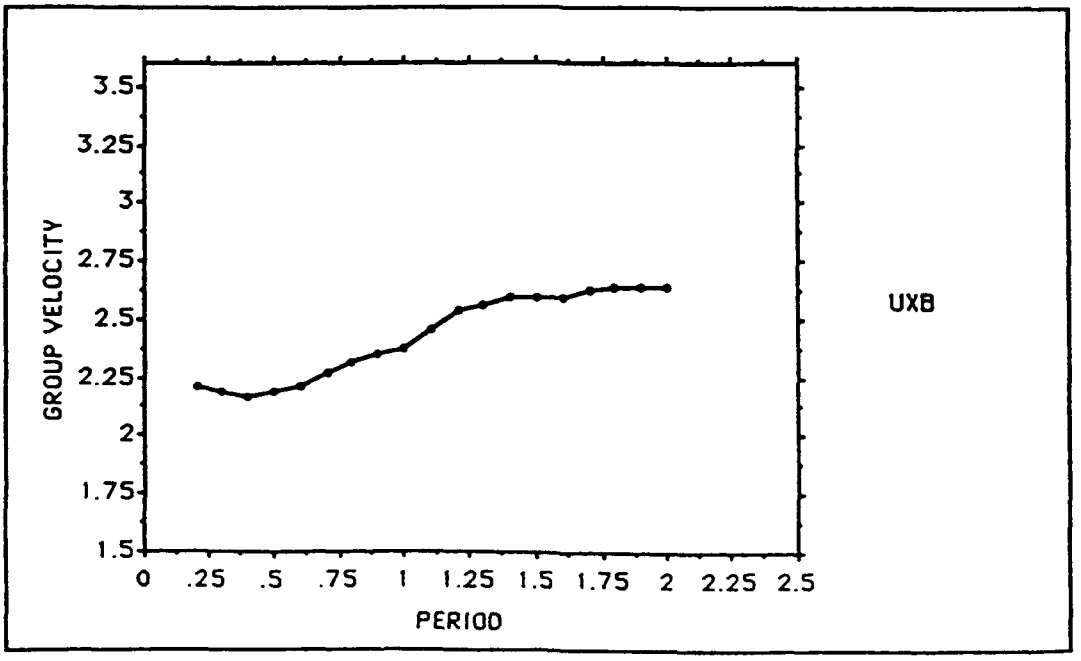
GROUP VELOCITY
3.5
3.25
3
2.75
2.5
2.25
2
1.75
1.5
0 .25 .5 .75 1 1.25 1.5 1.75 2 2.25 2.5
PERIOD
UXB

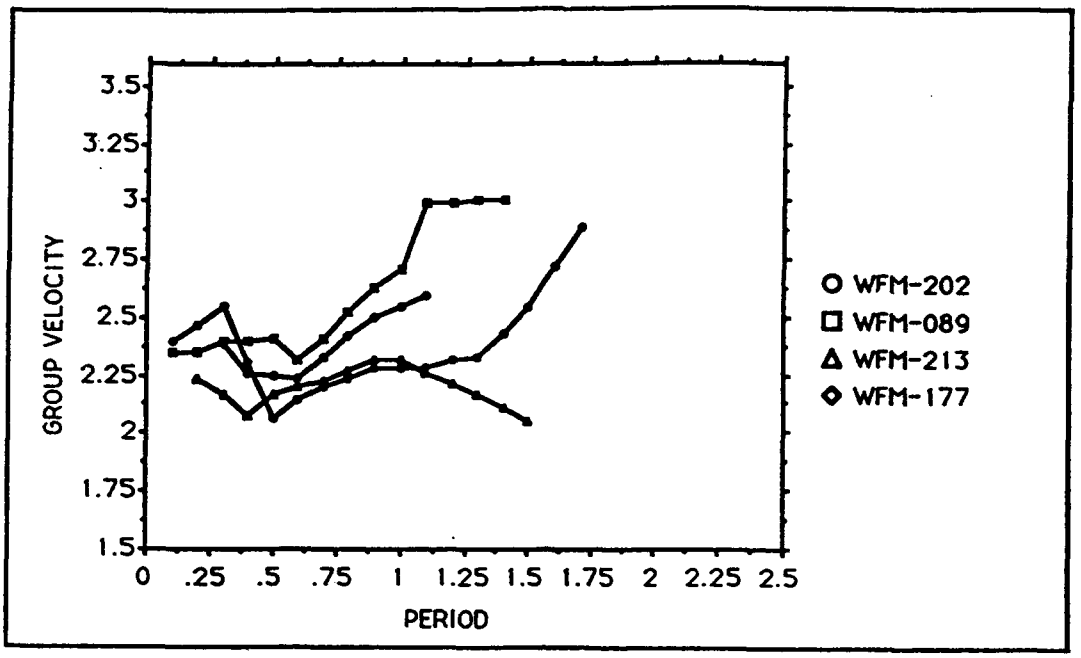
GROUP VELOCITY
3.5
3.25
3
2.75
2.5
2.25
2
1.75
1.5
0 .25 .5 .75 1 1.25 1.5 1.75 2 2.25 2.5
PERIOD
WFM-202
WFM-089
WFM-213
WFM-177

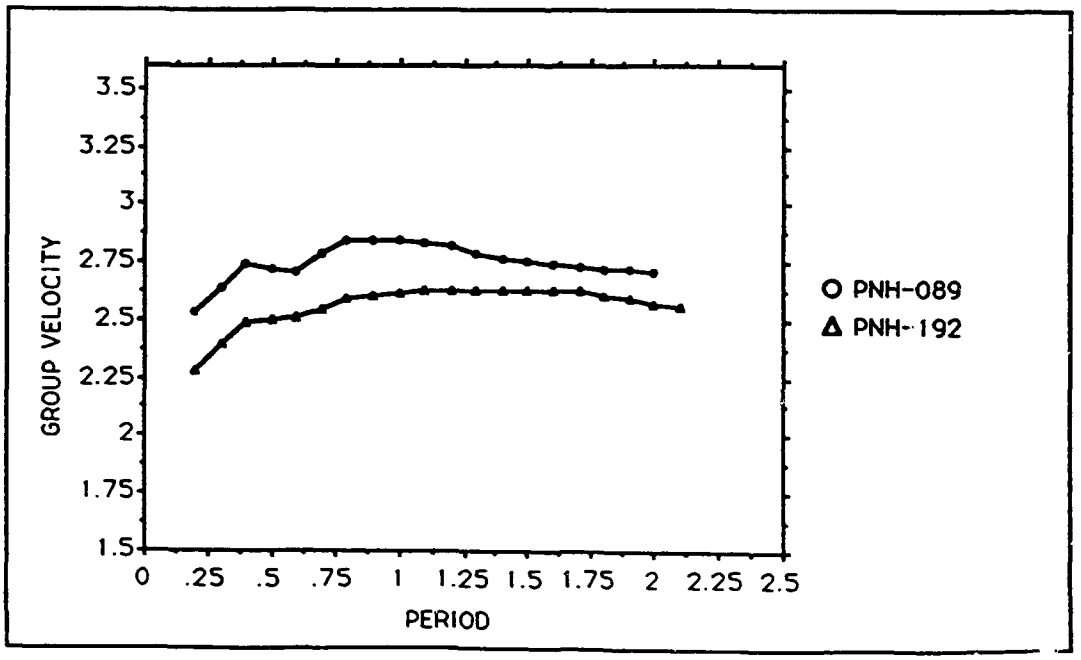
GROUP VELOCITY
3.5
3.25
3
2.75
2.5
2.25
2
1.75
1.5
0 .25 .5 .75 1 1.25 1.5 1.75 2 2.25 2.5
PERIOD
PNH-089
PNH-192

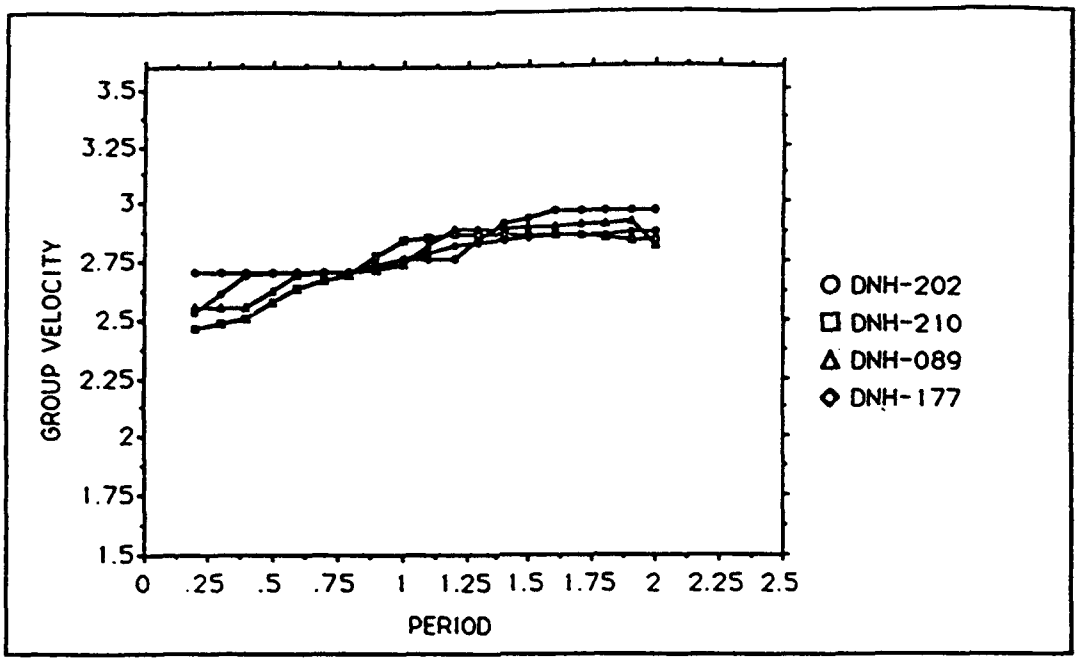
GROUP VELOCITY
3.5
3.25
3
2.75
2.5
2.25
2
1.75
1.5
0 .25 .5 .75 1 1.25 1.5 1.75 2 2.25 2.5
PERIOD
O DNH-202
□ DNH-210
△ DNH-089
◇ DNH-177

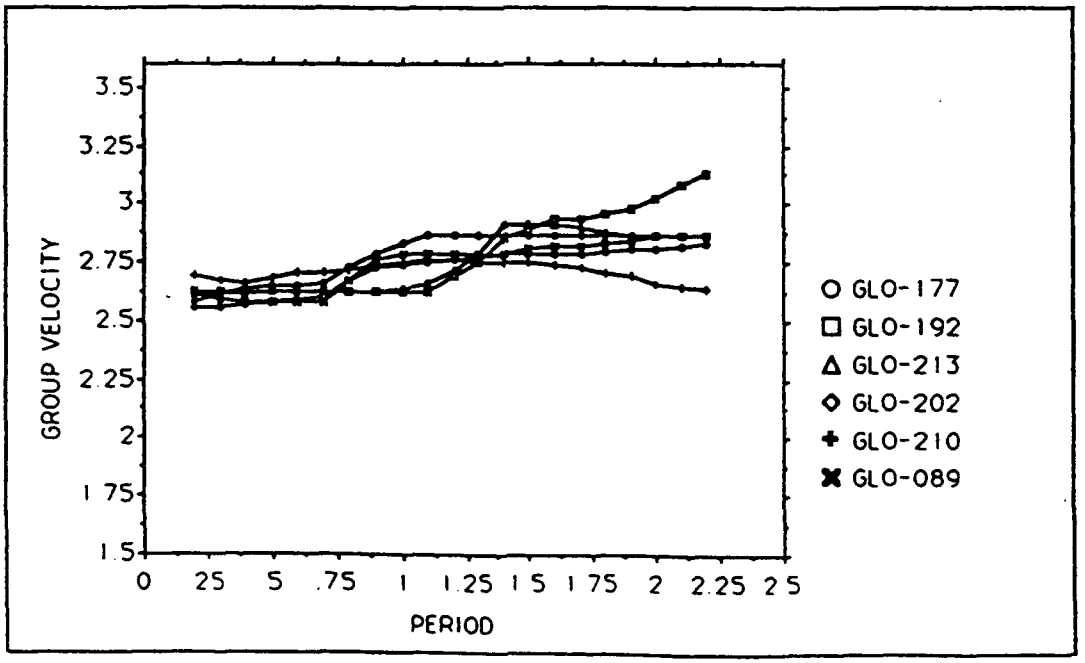
GROUP VELOCITY
3.5
3.25
3
2.75
2.5
2.25
2
1.75
1.5
0 25 5 .75 1 1.25 1 5 1 75 2 2.25 2 5
PERIOD
O GLO-177
□ GLO-192
△ GLO-213
◇ GLO-202
✚ GLO-210
✖ GLO-089

Prof. Thomas Ahrens
Seismological Lab, 252-21
Division of Geological & Planetary Sciences
California Institute of Technology
Pasadena, CA 91125

Prof. Keiiti Aki
Center for Earth Sciences
University of Southern California
University Park
Los Angeles, CA 90089-0741

Prof. Shelton Alexander
Geosciences Department
403 Deike Building
The Pennsylvania State University
University Park, PA 16802

Prof. Charles B. Archambeau
CIRES
University of Colorado
Boulder, CO 80309

Dr. Thomas C. Bache, Jr.
Science Applications Int'l Corp.
10260 Campus Point Drive
San Diego, CA 92121 (2 copies)

Prof. Muawia Barazangi
Institute for the Study of the Continent
Cornell University
Ithaca, NY 14853

Dr. Jeff Barker
Department of Geological Sciences
State University of New York
at Binghamton
Vestal, NY 13901

Dr. Douglas R. Baumgardt
ENSCO, Inc
5400 Port Royal Road
Springfield, VA 22151-2388

Dr. Susan Beck
Department of Geosciences
Building #77
University of Arizona
Tuscon, AZ 85721

Dr. T.J. Bennett
S-CUBED
A Division of Maxwell Laboratories
11800 Sunrise Valley Drive, Suite 1212
Reston, VA 22091

Dr. Robert Blandford
AFTAC/TT, Center for Seismic Studies
1300 North 17th Street
Suite 1450
Arlington, VA 22209-2308

Dr. Stephen Bratt
ARPA/NMRO
3701 North Fairfax Drive
Arlington, VA 22203-1714

Dr. Lawrence Burdick
IGPP, A-025
Scripps Institute of Oceanography
University of California, San Diego
La Jolla, CA 92093

Dr. Robert Burridge
Schlumberger-Doll Research Center
Old Quarry Road
Ridgefield, CT 06877

Dr. Jerry Carter
Center for Seismic Studies
1300 North 17th Street
Suite 1450
Arlington, VA 22209-2308

Dr. Eric Chael
Division 9241
Sandia Laboratory
Albuquerque, NM 87185

Dr. Martin Chapman
Department of Geological Sciences
Virginia Polytechnical Institute
21044 Derring Hall
Blacksburg, VA 24061

Prof. Vernon F. Cormier
Department of Geology & Geophysics
U-45, Room 207
University of Connecticut
Storrs, CT 06268

Prof. Steven Day
Department of Geological Sciences
San Diego State University
San Diego, CA 92182

Marvin Denny
U.S. Department of Energy
Office of Arms Control
Washington, DC 20585

Dr. Zoltan Der
ENSCO, Inc.
5400 Port Royal Road
Springfield, VA 22151-2388

Prof. Adam Dziewonski
Hoffman Laboratory, Harvard University
Dept. of Earth Atmos. & Planetary Sciences
20 Oxford Street
Cambridge, MA 02138

Prof. John Ebel
Department of Geology & Geophysics
Boston College
Chestnut Hill, MA 02167

Eric Fielding
SNEE Hall
INSTOC
Cornell University
Ithaca, NY 14853

Dr. Petr Firbas
Institute of Physics of the Earth
Masaryk University Brno
Jecna 29a
612 46 Brno, Czech Republic

Dr. Mark D. Fisk
Mission Research Corporation
735 State Street
P.O. Drawer 719
Santa Barbara, CA 93102

Prof Stanley Flatte
Applied Sciences Building
University of California, Santa Cruz
Santa Cruz, CA 95064

Dr. John Foley
NER-Geo Sciences
1100 Crown Colony Drive
Quincy, MA 02169

Prof. Donald Forsyth
Department of Geological Sciences
Brown University
Providence, RI 02912

Dr. Art Frankel
U.S. Geological Survey
922 National Center
Reston, VA 22092

Dr. Cliff Frolich
Institute of Geophysics
8701 North Mopac
Austin, TX 78759

Dr. Holly Given
IGPP, A-025
Scripps Institute of Oceanography
University of California, San Diego
La Jolla, CA 92093

Dr. Jeffrey W. Given
SAIC
10260 Campus Point Drive
San Diego, CA 92121

Dr. Dale Glover
Defense Intelligence Agency
ATTN: ODT-1B
Washington, DC 20301

Dan N. Hagedon
Pacific Northwest Laboratories
Battelle Boulevard
Richland, WA 99352

Dr. James Hannon
Lawrence Livermore National Laboratory
P.O. Box 808
L-205
Livermore, CA 94550

Prof. David G. Harkrider
Seismological Laboratory
Division of Geological & Planetary Sciences
California Institute of Technology
Pasadena, CA 91125

Prof. Danny Harvey
CIRES
University of Colorado
Boulder, CO 80309

Prof. Donald V. Helmberger
Seismological Laboratory
Division of Geological & Planetary Sciences
California Institute of Technology
Pasadena, CA 91125

Prof. Eugene Herrin
Institute for the Study of Earth and Man
Geophysical Laboratory
Southern Methodist University
Dallas, TX 75275

Prof. Robert B. Herrmann
Department of Earth & Atmospheric Sciences
St. Louis University
St. Louis, MO 63156

Prof. Lane R. Johnson
Seismographic Station
University of California
Berkeley, CA 94720

Prof. Thomas H. Jordan
Department of Earth, Atmospheric &
Planetary Sciences
Massachusetts Institute of Technology
Cambridge, MA 02139

Prof. Alan Kafka
Department of Geology & Geophysics
Boston College
Chestnut Hill, MA 02167

Robert C. Kemerait
ENSCO, Inc.
445 Pineda Court
Melbourne, FL 32940

Dr. Karl Koch
Institute for the Study of Earth and Man
Geophysical Laboratory
Southern Methodist University
Dallas, Tx 75275

Dr. Max Koontz
U.S. Dept. of Energy/DP 5
Forrestal Building
1000 Independence Avenue
Washington, DC 20585

Dr. Richard LaCoss
MIT Lincoln Laboratory, M-200B
P.O. Box 73
Lexington, MA 02173-0073

Dr. Fred K. Lamb
University of Illinois at Urbana-Champaign
Department of Physics
1110 West Green Street
Urbana, IL 61801

Prof. Charles A. Langston
Geosciences Department
403 Deike Building
The Pennsylvania State University
University Park, PA 16802

Jim Lawson, Chief Geophysicist
Oklahoma Geological Survey
Oklahoma Geophysical Observatory
P.O. Box 8
Leonard, OK 74043-0008

Prof. Thorne Lay
Institute of Tectonics
Earth Science Board
University of California, Santa Cruz
Santa Cruz, CA 95064

Dr. William Leith
U.S. Geological Survey
Mail Stop 928
Reston, VA 22092

Mr. James F. Lewkowicz
Phillips Laboratory/GPEH
29 Randolph Road
Hanscom AFB, MA 01731-3010(2 copies)

Mr. Alfred Lieberman
ACDA/VI-OA State Department Building
Room 5726
320-21st Street, NW
Washington, DC 20451

Prof. L. Timothy Long
School of Geophysical Sciences
Georgia Institute of Technology
Atlanta, GA 30332

Dr. Randolph Martin, III
New England Research, Inc.
76 Olcott Drive
White River Junction, VT 05001

Dr. Robert Masse
Denver Federal Building
Box 25046, Mail Stop 967
Denver, CO 80225

Dr. Gary McCartor
Department of Physics
Southern Methodist University
Dallas, TX 75275

Prof. Thomas V. McEvilly
Seismographic Station
University of California
Berkeley, CA 94720

Dr. Art McGarr
U.S. Geological Survey
Mail Stop 977
U.S. Geological Survey
Menlo Park, CA 94025

Dr. Keith L. McLaughlin
S-CUBED
A Division of Maxwell Laboratory
P.O. Box 1620
La Jolla, CA 92038-1620

Stephen Miller & Dr. Alexander Florence
SRI International
333 Ravenswood Avenue
Box AF 116
Menlo Park, CA 94025-3493

Prof. Bernard Minster
IGPP, A-025
Scripps Institute of Oceanography
University of California, San Diego
La Jolla, CA 92093

Prof. Brian J. Mitchell
Department of Earth & Atmospheric Sciences
St. Louis University
St. Louis, MO 63156

Mr. Jack Murphy
S-CUBED
A Division of Maxwell Laboratory
11800 Sunrise Valley Drive, Suite 1212
Reston, VA 22091 (2 Copies)

Dr. Keith K. Nakanishi
Lawrence Livermore National Laboratory
L-025
P.O. Box 808
Livermore, CA 94550

Prof. John A. Orcutt
IGPP, A-025
Scripps Institute of Oceanography
University of California, San Diego
La Jolla, CA 92093

Prof. Jeffrey Park
Kline Geology Laboratory
P.O. Box 6666
New Haven, CT 06511-8130

Dr. Howard Patton
Lawrence Livermore National Laboratory
L-025
P.O. Box 808
Livermore, CA 94550

Dr. Frank Pilotte
HQ AFTAC/TT
1030 South Highway A1A
Patrick AFB, FL 32925-3002

Dr. Jay J. Pulli
Radix Systems, Inc.
201 Perry Parkway
Gaithersburg, MD 20877

Dr. Robert Reinke
ATTN: FCTVTD
Field Command
Defense Nuclear Agency
Kirtland AFB, NM 87115

Prof. Paul G. Richards
Lamont-Doherty Geological Observatory
of Columbia University
Palisades, NY 10964

Mr. Wilmer Rivers
Teledyne Geotech
314 Montgomery Street
Alexandria, VA 22314

Dr. Alan S. Ryall, Jr.
ARPA/NMRO
3701 North Fairfax Drive
Arlington, VA 22203-1714

Dr. Richard Sailor
TASC, Inc.
55 Walkers Brook Drive
Reading, MA 01867

Prof. Charles G. Sammis
Center for Earth Sciences
University of Southern California
University Park
Los Angeles, CA 90089-0741

Prof. Christopher H. Scholz
Lamont-Doherty Geological Observatory
of Columbia University
Palisades, NY 10964

Dr. Susan Schwartz
Institute of Tectonics
1156 High Street
Santa Cruz, CA 95064

Secretary of the Air Force
(SAFRD)
Washington, DC 20330

Office of the Secretary of Defense
DDR&E
Washington, DC 20330

Thomas J. Sereno, Jr.
Science Application Int'l Corp.
10260 Campus Point Drive
San Diego, CA 92121

Dr. Michael Shore
Defense Nuclear Agency/SPSS
6801 Telegraph Road
Alexandria, VA 22310

Dr. Robert Shumway
University of California Davis
Division of Statistics
Davis, CA 95616

Dr. Matthew Sibol
Virginia Tech
Seismological Observatory
4044 Derring Hall
Blacksburg, VA 24061-0420

Prof. David G. Simpson
IRIS, Inc.
1616 North Fort Myer Drive
Suite 1050
Arlington, VA 22209

Donald L. Springer
Lawrence Livermore National Laboratory
L-025
P.O. Box 808
Livermore, CA 94550

Dr. Jeffrey Stevens
S-CUBED
A Division of Maxwell Laboratory
P.O. Box 1620
La Jolla, CA 92038-1620

Lt. Col. Jim Stobie
ATTN: AFOSR/NL
110 Duncan Avenue
Bolling AFB
Washington, DC 20332-0001

Prof. Brian Stump
Institute for the Study of Earth & Man
Geophysical Laboratory
Southern Methodist University
Dallas, TX 75275

Prof. *Jeremiah Sullivan*
University of Illinois at Urbana-Champaign
Department of Physics
1110 West Green Street
Urbana, IL 61801

Prof. L. Sykes
Lamont-Doherty Geological Observatory
of Columbia University
Palisades, NY 10964

Dr. David Taylor
ENSCO, Inc.
445 Pineda Court
Melbourne, FL 32940

Dr. Steven R. Taylor
Los Alamos National Laboratory
P.O. Box 1663
Mail Stop C335
Los Alamos, NM 87545

Prof. Clifford Thurber
University of Wisconsin-Madison
Department of Geology & Geophysics
1215 West Dayton Street
Madison, WS 53706

Prof. M. Nafi Toksoz
Earth Resources Lab
Massachusetts Institute of Technology
42 Carleton Street
Cambridge, MA 02142

Dr. Larry Turnbull
CIA-OSWR/NED
Washington, DC 20505

Dr. Gregory van der Vink
IRIS, Inc.
1616 North Fort Myer Drive
Suite 1050
Arlington, VA 22209

Dr. Karl Veith
EG&G
5211 Auth Road
Suite 240
Suitland, MD 20746

Prof. Terry C. Wallace
Department of Geosciences
Building #77
University of Arizona
Tuscon, AZ 85721

Dr. Thomas Weaver
Los Alamos National Laboratory
P.O. Box 1663
Mail Stop C335
Los Alamos, NM 87545

Dr. William Wortman
Mission Research Corporation
8560 Cinderbed Road
Suite 700
Newington, VA 22122

Prof. Francis T. Wu
Department of Geological Sciences
State University of New York
at Binghamton
Vestal, NY 13901

ARPA, OASB/Library
3701 North Fairfax Drive
Arlington, VA 22203-1714

HQ DNA
ATTN: Technical Library
Washington, DC 20305

Defense Intelligence Agency
Directorate for Scientific & Technical Intelligence
ATTN: DTIB
Washington, DC 20340-6158

Defense Technical Information Center
Cameron Station
Alexandria, VA 22314 (2 Copies)

TACTEC
Battelle Memorial Institute
505 King Avenue
Columbus, OH 43201 (Final Report)

Phillips Laboratory
ATTN: XPG
29 Randolph Road
Hanscom AFB, MA 01731-3010

Phillips Laboratory
ATTN: GPE
29 Randolph Road
Hanscom AFB, MA 01731-3010

Phillips Laboratory
ATTN: TSML
5 Wright Street
Hanscom AFB, MA 01731-3004

Phillips Laboratory
ATTN: PL/SUL
3550 Aberdeen Ave SE
Kirtland, NM 87117-5776 (2 copies)

Dr. Michel Bouchon
I.R.I.G.M.-B.P. 68
38402 St. Martin D'Heres
Cedex, FRANCE

Dr. Michel Campillo
Observatoire de Grenoble
I.R.I.G.M.-B.P. 53
38041 Grenoble, FRANCE

Dr. Kin Yip Chun
Geophysics Division
Physics Department
University of Toronto
Ontario, CANADA

Prof. Hans-Peter Harjes
Institute for Geophysic
Ruhr University/Bochum
P.O. Box 102148
4630 Bochum 1, GERMANY

Prof. Eystein Husebye
NTNF/NORSAR
P.O. Box 51
N-2007 Kjeller, NORWAY

David Jepsen
Acting Head, Nuclear Monitoring Section
Bureau of Mineral Resources
Geology and Geophysics
G.P.O. Box 378, Canberra, AUSTRALIA

Ms. Eva Johannisson
Senior Research Officer
FOA
S-172 90 Sundbyberg, SWEDEN

Dr. Peter Marshall
Procurement Executive
Ministry of Defense
Blacknest, Brimpton
Reading FG7-FRS, UNITED KINGDOM

Dr. Bernard Massinon, Dr. Pierre Mechler
Societe Radiomana
27 rue Claude Bernard
75005 Paris, FRANCE (2 Copies)

Dr. Svein Mykkeltveit
NTNT/NORSAR
P.O. Box 51
N-2007 Kjeller, NORWAY (3 Copies)

Prof. Keith Priestley
University of Cambridge
Bullard Labs, Dept. of Earth Sciences
Madingley Rise, Madingley Road
Cambridge CB3 OEZ, ENGLAND

Dr. Jorg Schlittenhardt
Federal Institute for Geosciences & Nat'l Res.
Postfach 510153
D-30631 Hannover , GERMANY

Dr. Johannes Schweitzer
Institute of Geophysics
Ruhr University/Bochum
P.O. Box 1102148
4360 Bochum 1, GERMANY

Trust & Verify
VERTIC
Carrara House
20 Embankment Place
London WC2N 6NN, ENGLAND